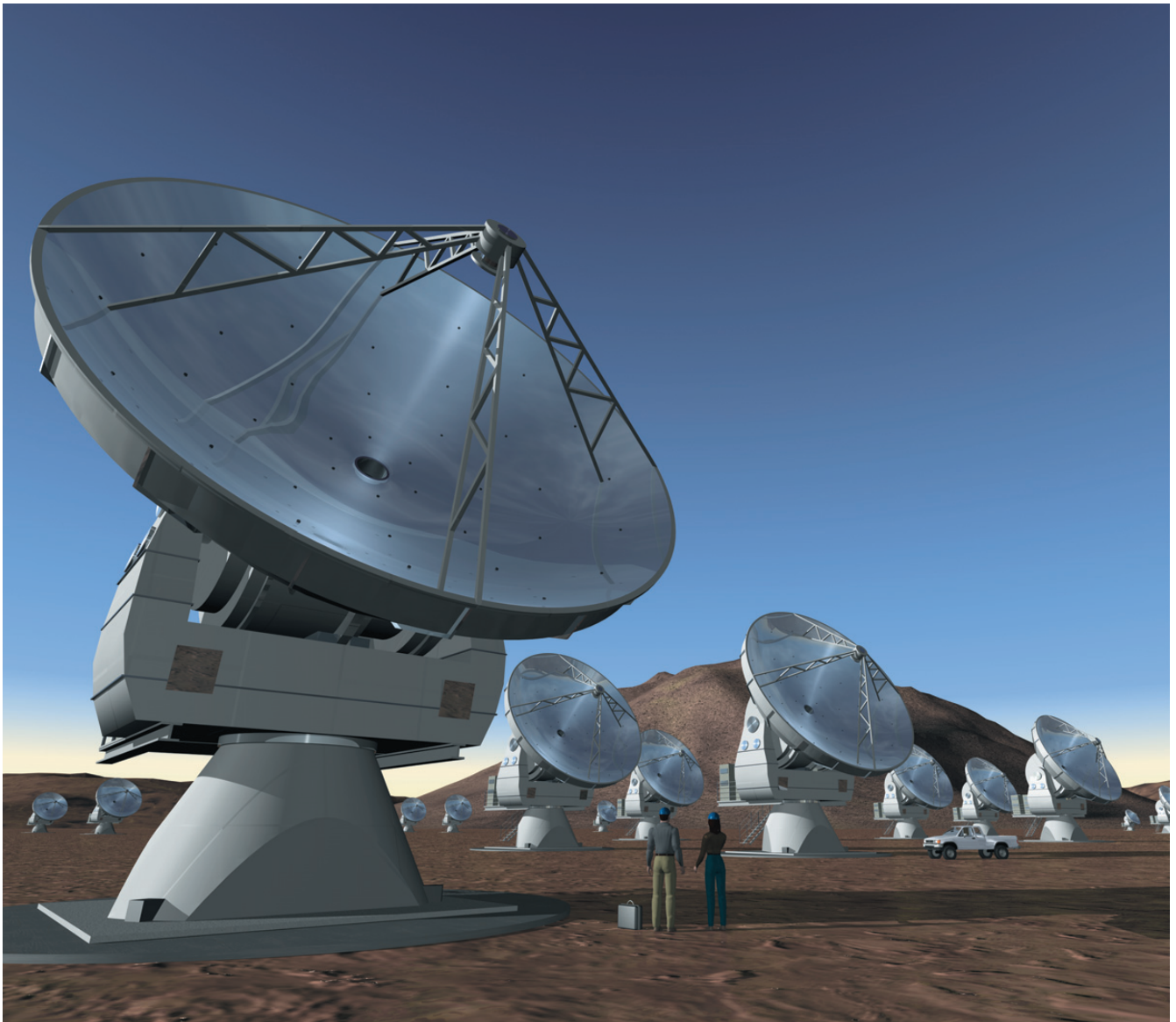


THE MESSENGER



EL MENSAJERO

No. 112 – June 2003



Computer simulation of the Atacama Large Millimeter Array (ALMA). Image created by Herbert Zodet.

Progress with the Atacama Large Millimeter Array (ALMA)

CATHERINE CESARSKY, Director General of ESO

The ALMA project has made remarkable progress over the last several months, as important agreements have been signed, the project structure finalized and prototype antennas moved from construction to testing.

The most important milestone, of course, was the signing in February of the Bilateral Agreement between ESO and the U.S. National Science Foundation for the construction and operation of ALMA, as reported in the last issue of *The Messenger*. Following the signature of the agreement with Spain for ALMA participation in January, this gave the final green light for the ALMA project. At the same time the ALMA Board was formally established, to oversee the realization of the project via the management structure; P. van der Kruit, President of ESO Council, is also the first ALMA Board Chairman. The Board has since approved the Project Plan that had been under development through the Phase 1 period, and has established the Joint ALMA Office with overall management responsibility under the Board. Massimo Tarenghi, who played such an important role in the

construction of the VLT, was named Director of the ALMA Project in April.

The European ALMA Board (EAB) was also established by ESO Council, to oversee the European side of the project, and the European Scientific Advisory Committee (ESAC) was expanded. Both have representation from all ESO member states and Spain. An ALMA Division within ESO was formally established at the beginning of the year, and key personnel continue to be hired.

Negotiations with the Chilean government have been proceeding rapidly and successfully. In October 2002, an agreement between Chile and ESO was signed authorizing ESO to establish a new centre for astronomical observation in Chile – the ALMA Observatory on the Plateau of Chajnantor, near San Pedro de Atacama. This agreement has been ratified by the Chilean parliament.

An important aspect in the development of ALMA is the manufacture and testing of two prototype antennas. The first prototype, produced by VertexRSI, is under test at the ALMA Test Facility in New Mexico, and the second prototype, produced by Alcatel/EIE, is being as-

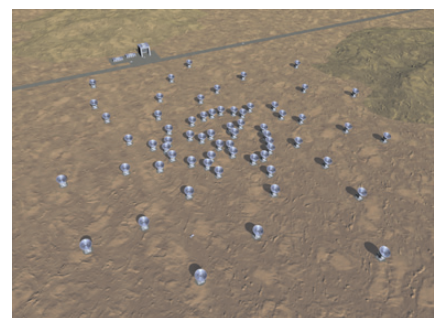
sembled at the site. These tests will be critical in deciding on the 64 production antennas.

Work on the many other aspects of the project continues at an accelerating pace, with several contracts being awarded or in preparation. The work covers all aspects of the project, including system engineering, the layout and development of the site infrastructure, the antenna transporters, the receivers and associated hardware and electronics, the backend subsystems, software development, calibration, and many others.

In parallel with all this activity, discussions with Japan continue concerning the possibility of its becoming a major partner, with the enhancements that this would bring to the project. A decision by the Japanese government may be made this year, for possible entry into the project early next year.



On 16 May 2003, at the airport of Milano Malpensa, the receiver cabin and reflector backup structure (BUS) of the Alcatel/EIE Antenna prototype were loaded on the special Airbus A 300 transporter ("Beluga") for shipment to Albuquerque airport (NM, USA) en route to their final destination, the VLA site in Socorro. Both cabin and BUS were manufactured in Italy and are made of carbon fibre reinforced plastic (CFRP) based on a design by the European Industrial Engineering (I) under the supervision of Alcatel Space Industries (F).



Computer simulation illustrating the "zoom array" of ALMA.

The Science Verification of FLAMES

FRANCESCA PRIMAS, User Support Group, ESO

After a new VLT instrument has been commissioned and thoroughly tested¹, a series of scientific and technical check-ups are scheduled in order to test the front-to-end operations chain before the official start of regular operations. Technically speaking, these are the so-called *Dry Runs*, part of which are usually devoted to the Science Verification (SV for short) of that specific instrument.

A Science Verification programme includes a set of typical scientific observations with the aim of verifying and demonstrating to the community the capabilities of a new instrument in the operational framework of the VLT Paranal Observatory. Though manifold, its goals can be summarised in two main points: from the scientific point of view, by demonstrating the scientific potential of the new instrument, these observations will provide ESO users with first science-grade data, thus fostering an early scientific return. From the technical point of view, by testing the whole operational system (from the preparation of the observations to their execution and analysis), it will provide important feedback to the Instrument Operation Teams (both in Paranal and in Garching), to the Instrument Division, and to the Data Flow groups. More details about the concept(s) behind a Science Verification can be found in the "Science Verification Policy and Procedures" document (available at <http://www.eso.org/science/vltsv/>).

Science Goals and Achievements

The Fibre Large Array Multi-Element Spectrograph (FLAMES) is the new multi-object, intermediate- and high-resolution spectrograph of the VLT (Pasquini et al. 2002). Mounted at the Nasmyth A platform of Kueyen (Unit Telescope #2), FLAMES can access targets over a large corrected field of view (25 arcmin diameter). It consists of three main components: a Fibre Positioner (OzPoz) hosting two plates (while one plate is observing, the other is positioning the fibres for the next observation); a link to the Red Arm of UVES (the high-resolution Ultraviolet and Visible Echelle Spectrograph) via 8 single fibres of 1 arcsec entrance aperture; a medium-high resolution optical spectrograph, GIRAFFE, equipped with three types of feeding fibre systems: 130 MEDUSA fibres, 15 deployable integral field units (IFU), and 1 large, fixed integral field unit (ARGUS). A special Observing Software (OS) coordinates the operation of the different subsystems, also allowing simultaneous acqui-

sition of UVES and GIRAFFE observations.

The FLAMES Dry Runs took place successfully between the end of January and the beginning of February (Jan 24 – Feb 03, 2003). Nine science programmes, proposed and assembled by the FLAMES SV Team (which included the VLT Programme Scientist, the Instrument PI, the Paranal Instrument Scientist, the User Support Astronomer, and Science Advisory Teams and representatives of the FLAMES Consortia), were executed. More than 5200 spectra were collected during the ten observing nights, and publicly released on March 3, exactly one month after the last observing night. This one-month time lag was necessary to visually inspect the quality of the frames (both raw and reduced), to make the correct association between raw and calibration frames to be distributed, and to prepare a detailed set of summaries and technical explanations. Any user from one of the ESO Member States and with an active registration to the ESO/ST-ECF Archive (see <http://archive.eso.org/register/new> for more information), can download the FLAMES SV datasets, whose scientific justifications are briefly described below. The interested reader is reminded that a wealth of details (such as colour-magnitude diagrams - to check which targets were observed, Field Charts and README files - two of the main user requirements) are available from the FLAMES SV web page (<http://www.eso.org/science/vltsv/>). The following SV programmes were selected based on their scientific weight (they must be interesting for the ESO com-

munity at large) and the proposed exploitation of the instrument capabilities:

- *The Chemical Signature of Different Stellar Populations in the LMC*: although it is considered an intermediate-age galaxy, the LMC is characterised by a large range of stellar ages, from a genuine old to a prominent young population. The main goal of this project was to investigate further its metal enrichment history by measuring the abundances of several elements for a statistically significant sample of Red Giant Branch stars ($17 < V_{mag} < 18$). Two complementary projects were combined: (1) the first spectroscopic metallicity determination of the LMC Clump to verify its influence (if any) on the intrinsic luminosity of the stars (by allocating 1/4 of the Medusa fibres to Clump stars); (2) the chemical analysis of LMC Long Period Variables in order to investigate the connection (if any) among their chemical composition, pulsation mode, and evolutionary phase (the UVES fibres were used for this purpose). Figure 1 shows the H- α region for one RGB, one Clump, and one LPV star.

- *Massive Kinematic Study of NGC 5128 using its Planetary Nebulae and Globular Clusters as Test Probes*: planetary nebulae (PN) are emission line objects, the systemic velocities of which can be probed using the brightest emission lines (see Figure 2). The 785 PN found and catalogued by Hui et al. (1993), over a large area (40×46 arcmin, EWxNS) of NGC 5128 (Centaurus A) were targeted in order to verify the initial findings that PN kinematics trace a triaxial potential,

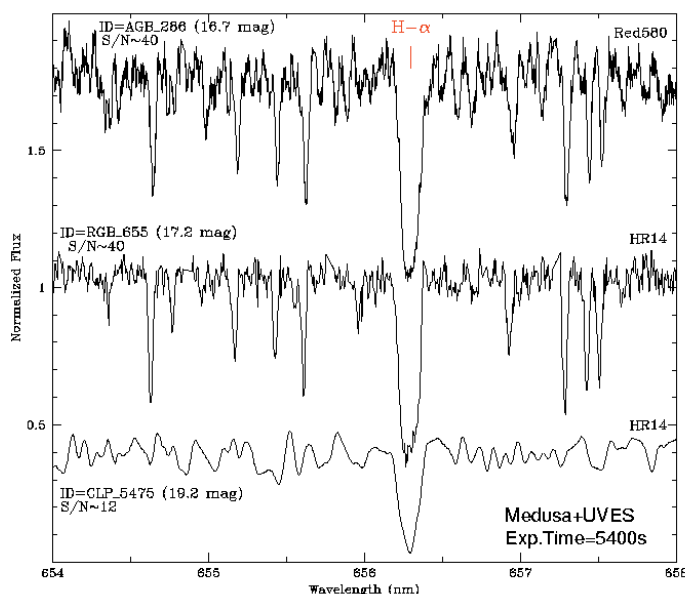


Figure 1: The H- α region as observed with Medusa and UVES (top spectrum) in three stars representative of the different stellar populations probed in the Large Magellanic Cloud.

¹Please note that all commissioning data are now available from http://www.eso.org/science/flames_comm/

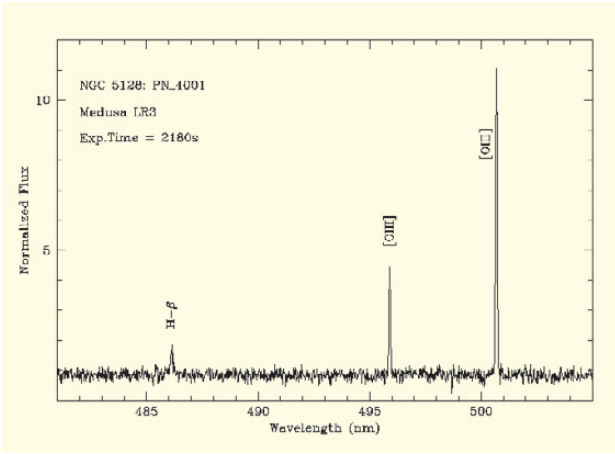


Figure 2: H- β and two [O III] lines in emission (the 495.9 and 500.7 nm), as detected in one of the planetary nebula observed with one Medusa fibre, at low resolution. More than 500 PN were observed in total.

with the mass-to-light ratio increasing with radius (thus suggesting the presence of a dark matter halo). Some MEDUSA and all UVES fibres were allocated to the brightest globular clusters of this giant elliptical galaxy in order to compare their kinematics and to derive their metallicity.

• **Mass Loss in Red Giant Stars of the Globular Cluster NGC 2808:** about 100 stars of the Red Giant Branch, in the magnitude interval $V=13.2-16.5$ mag, within a radius of about 7 arcmin from the cluster centre, were targeted, with the aim of measuring shifts of the CaII-K3, NaD and H- α core line profiles that are major diagnostics of mass outflow, hence mass loss. In order to observe the Ca H and K lines, this programme made use of one of the bluest settings available on FLAMES, HR#2, which covers the spectral range between 385 and 405 nm (see Figure 3). The brightest stars of the cluster were observed simultaneously with UVES, to obtain a larger spectral coverage (480–680 nm) for chemical abundance purposes.

• **Geometric Distances of the Galactic Globular Cluster NGC 2808:** the main idea behind this science case was to observe a very large number of stars (1000), and derive their radial velocities, in order to obtain the first determination of the cluster geometric distance (with an uncertainty of 2–3%, i.e. an age with an error less than 1 Gyr) via a direct comparison of the radial velocities to the (already available) proper motions. One GIRAFFE set-up (HR#5), together with the simultaneous allocation of UVES-fibres, was also used to obtain spectra of horizontal branch stars, thus increasing by one order of magnitude the size of the present sample.

• **Elemental Abundances in NGC 2243:** a complete chemical analysis of sub-giant stars and membership information for the fainter, turn-off stars in this open, metal-poor, intermediate-age (~ 2 Gyr) cluster were the main goals of the programme, which used two contiguous (hence slightly overlapping) high-resolution Medusa set-ups (Figure 4). The main scientific interest of this cluster lies in two aspects: its metallicity, which is comparable to the halo cluster 47 Tucanae, and its age which is instead remarkably smaller (47 Tuc formed some 10–12 Gyrs earlier). A direct abundance comparison between these two clusters (47 Tucanae has been extensively observed with UVES in the past) will shed light not only on their chemical history, but also on the formation and evolution of our own Galaxy.

• **Probing Activity and Angular Momentum Evolution of Low-Mass Members of the Orion Nebular Cluster:** surface rotation is a key observational parameter for stellar evolution, being tightly linked to the internal angular momentum transport, hence to mass loss. The main goal of this programme was to determine the $v \sin i$ distribution for a large number (120 targets, selected from the low-resolution survey of Hillenbrand 1997) of low-mass ($0.2-0.06 M_{\odot}$), relatively cold ($\log T_{\text{eff}} < 3.5$), M5–M7 type stars in the Orion Nebular Cluster (~ 1 Myr old, 430 pc away), for which only little information is available. Recent observations in Orion have shown that while the majority of low-mass pre-main sequence stars are rotating at rates approaching 30% of breakup, late-type

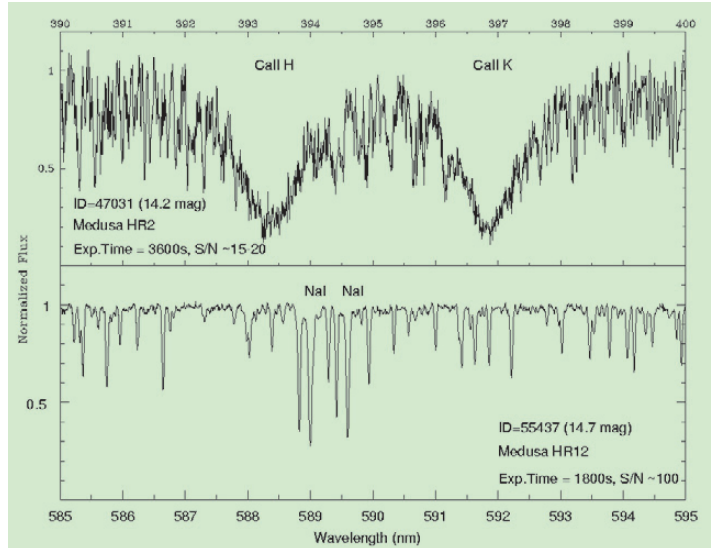


Figure 3: Two mass-loss diagnostics: the Ca H,K and the NaD lines, as observed in two different RGB stars of NGC 2808.

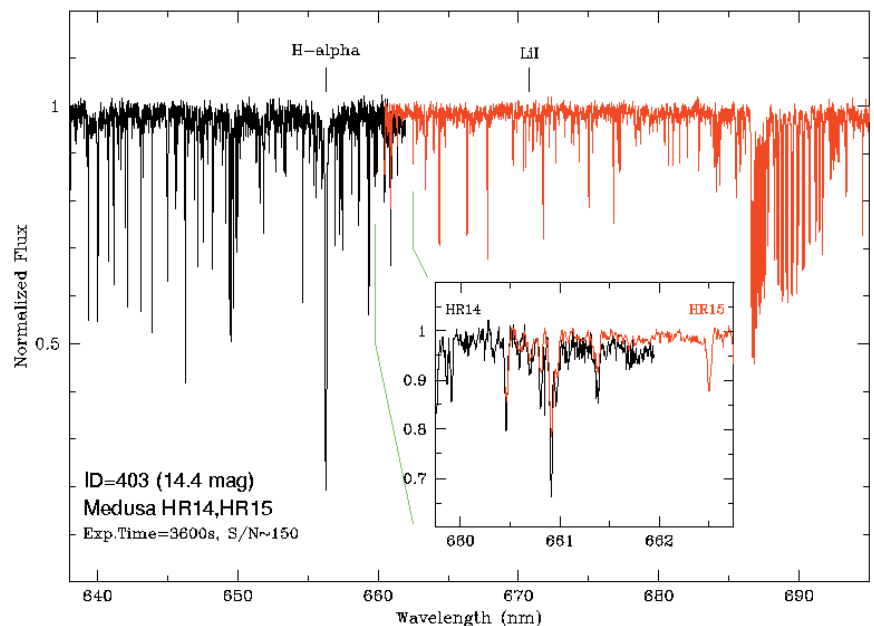


Figure 4: The same NGC 2243 sub-giant star, as observed in two contiguous high resolution Medusa settings: the total spectral coverage is from 638 to 697 nm.

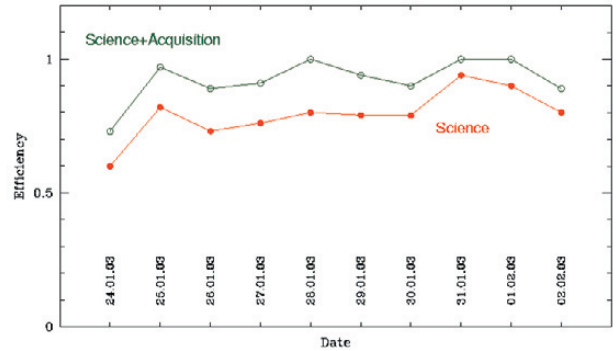
stars in older clusters appear to be slow rotators (e.g. Stassun et al. 1999, and Queloz et al. 1998, respectively).

- **Kinematics of Distant Galaxies from FLAMES-GIRAFFE IFU Mode:** the main goals of this programme were a) to derive, from spatially-resolved spectroscopy and HST images, velocity fields and rotation curves of galaxies with emission lines at moderately high redshift; b) to kinematically map merging systems, in order to quantify the number of perturbed galaxies and the merging rate; c) to study the evolution of the Tully-Fisher relation in order to complement the study of the mass and M/L functions. The chosen target was the well-known cluster of galaxies, MS 1054-03, at redshift $z = 0.83$. FLAMES was used in combined mode: the 15 Integral Field Units were mainly allocated to late-type galaxies Sc-Sd, merger systems and post-starburst spiral galaxies, whereas UVES fibres were devoted to four elliptical galaxies and one merging system, all brighter than 21 mag in I -band.

- **Dark and Stellar Mass in Late-type Dwarfs:** even if the existence of dark matter in spiral galaxies is well established, there are large uncertainties regarding its distribution inside the optical disc. The aim of this programme was to measure the (stellar) vertical velocity dispersion, from which one can directly measure the product $M/L \times q_0$, where M/L is the stellar mass-to-light ratio of the stars and q_0 the thickness of the disc. Observationally, this requires high spectral resolution: the selected target, NGC 1310, is less massive than the Milky Way; it rotates at 110 km/s, thus requiring a velocity resolution of the order of 10–20 km/s. The target was selected to fulfil the following criteria: preferably late-type, close to face-on, and not barred. The observations were carried out with 5 IFU placed at a radius of 1 scale length and the remaining 10 at a radius of 2 scale lengths.

- **Dynamical Study of Elliptical Galaxies:** the scientific objective was to accurately determine the velocity dis-

Figure 5: The efficiency rate achieved during the FLAMES Dry Runs: “Science” means the time spent on target, with respect to the “astronomical” length of each night, whereas the values on the “Science+Acquisition” curve also include the time spent on acquiring the target fields and the set-up of the instrument.



person and infer some constraint on the ellipsoid of velocity dispersions in the central part of the galaxy NGC 3585. This programme made use of one high- and one low-resolution setting (HR#12 and LR#05, respectively) using the same fibre configuration.

The time spent on each of these programmes and their completion rate (given in percentage), together with the chosen instrument modes and set-ups, are summarised in Table 1.

A Success

Three important factors are behind the success of the FLAMES SV : a stable instrument, very cooperative atmospheric conditions, and a set of well prepared science observations. The combination of the first two points made it possible to achieve a very high efficiency over the entire window of the observing run, as shown in Figure 5, where the time spent on “science targets” and normalised to the total number of hours available per night (as defined by the astronomical twilights) is shown for the entire run. On the third aspect, i.e. the preparation of the science observations, a more extensive and detailed description is needed.

In the very early organisational phases of the FLAMES SV, it was decided to try and implement a real (although for many aspects anomalous) Phase 2. With this term, familiar to all those astronomers who have had their observations carried out in “Service Mode” (cf Silva 2001), we usually identify that par-

ticular phase during which a user, with advice (if needed) from a pre-assigned support astronomer, submits a set of Observation Blocks (i.e. logical units of exposures to be executed at the telescope to obtain a coherent set of data) and detailed information on how her/his own programme should be carried out. This process requires the availability of software tools, documentation, and a list of generic and instrument-dependent requirements that need to be fulfilled.

In the case of a SV Phase 2, this process must be anomalous, by definition: the instrument has not yet been released for official operations, and all software tools, user documentation and user manuals are still in the final stages of revision. These uncertainties clearly require some flexibility on the side of the SV Team while preparing the observations (this is also why a SV Team mainly includes people who have been already exposed to the instrument, during its development, assembling, and commissioning phases).

In the case of FLAMES SV, Phase 2 took place over the Christmas break. All the required material was delivered to ESO in mid January, then checked and verified by the FLAMES user support astronomer, and made available to the team of night- and day-time astronomers present on Paranal for the execution of the observations. During this phase, a thorough assessment of the quality of the available tools and manuals was made, which proved to be very useful for the official Period 71 Phase 2, that started at the beginning of February

Table 1: FLAMES SV Science Programmes

Programme	Instr. Mode	Instr. Set-Up	Invested Time hours	Completion Rate %
NGC 5128: PN and GC	Medusa+UVES	LR3+R580	7	75
LMC: Stellar Populations	Medusa+UVES	HR13,14+R580,R860	21	76
NGC 2808: Mass loss	Medusa+UVES	HR2,11,14+R520	4	100
NGC 2808: Geometric Distance	Medusa+UVES	HR5,9+R520	7	100
NGC 2243: Abundances	Medusa+UVES	HR14,15+R580,R860	4	100
ONC: Low-mass Stars	Medusa	HR14,15	5	62
MS 1054-03: Kinematics	IFU+UVES	LR6+R860	9	75
NGC 1310: Dark and Stellar Mass	IFU	LR4	5.5	100
NGC 3585: Dynamics	IFU	HR12,LR5	5	100

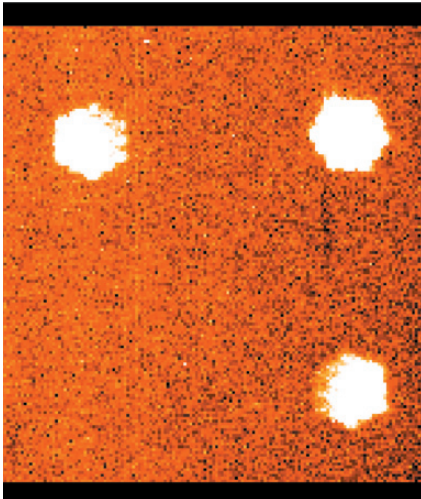


Figure 6: The centring of the reference stars on the Fibre Acquisition Coherence Bundles, as seen at the telescope console.

(see next section). Passing the Phase 2 verification usually offers the user and the operations team some confidence that the execution of a given programme should go smoothly. However, should the user have mistyped some crucial information (like the target coordinates), this will be detected only at the telescope. Because of the multiplex capability of FLAMES, target coordinates are even more important for successful observations. One needs very precise relative coordinates of several hundreds of targets in the field to be observed - technically speaking, one needs very accurate astrometry (< 0.3 arcsec). As FLAMES does not have a pre-imaging option, there is only one parameter/tool available to evaluate the quality of the astrometry: Figure 6 shows an image of the Field Acquisition Coherence Bundles (as seen at the telescope console) for one set of observations that were carried out during the FLAMES SV. These bundles (normally four, but at the time of the SV run the fourth one was not available) show how well centred the reference stars are, which must be chosen in the same astrometric solution as the science targets.

Lessons Learned

As stated at the very beginning of this presentation, one of the main goals of a Science Verification run is the important technical feedback that can be given to the teams directly involved in the front-to-end operations of that instrument, i.e. the Paranal Science Operation team (responsible for its operations), the User Support Group (the operational-interface between the users community and the Observatory), the Data Flow groups (i.e. those behind the development of instrument-specific data-reduction recipes, the implementation of quality-control and monitoring checks, the archival and distribution of the data-

packages to the users), and the Instrument Division in Garching (which has been responsible for developing, building and commissioning the instrument).

The FLAMES SV has been a very positive experience, also from the operational point of view. The lessons learned during the implementation, execution, and quality assessment of these FLAMES observations have proven to be very valuable, for the instrument support teams and also for the first FLAMES users (i.e. those with FLAMES programmes approved for P71), who benefited from more robust and user-friendly instrument-related tools.

The first positive outcome came from the (SV) Phase 2 exercise, which turned out to be a thorough testing of the FLAMES Fibre Positioner Observation Support Software (FPOSS) on real and different science cases (for which the user wants to allocate one specific group of fibres to one specific group of targets). This revealed a series of shortcomings in the FPOSS tool, which was revised and further tested as SV observations were taking place. Among the technical problems encountered at the telescope, the most recurring one was the “non-validity” of some UVES+Medusa fibre configurations, which had instead been validated by FPOSS during Phase 2. The need for solving this type of problem in real-time gave us a deeper understanding of how fibre-collisions were handled and treated, both at FPOSS and OzPoz levels. A quick recovery procedure at night time (by “manually” de-allocating the colliding fibres) was then followed by the debugging phase at software level during day-time operations, perfectly in time to test the newly revised version during the following night.

As SV observations are carried out in Service Mode, the presence or absence of difficulties during the execution of a given programme (based on the information provided by the Principal Investigator) gave us an idea of how complete the preliminary list of user requirements (set up during the SV Phase 2) was. Because of the presence at the telescope of most of the persons involved in the FLAMES operations, it was possible to revise in real time all the user-related documentation (e.g. User Manuals) and the software tools, like FPOSS, thus solving and implementing all the “bugs and wishes” we had assembled after Phase 2, and to prepare all FLAMES operations-related Web pages.

As the observations were being carried out, we also tried to reduce all the frames in a semi-automatic way, with the reduction recipes available at that time. This was done on a best-effort basis, as it was a low priority item on the FLAMES SV team “to-do” list. However, it was decided to invest the effort in or-

der to have a quick-look at the spectra quality, while observing. All these “quick-look” reduced spectra were publicly distributed together with the raw science and calibration frames, so that the entire ESO community could benefit equally from this set of observations. Those observations for which no quick-look spectrum could be extracted, were promptly made available to the Data Flow System group, in order to test the robustness and repeatability of the pipeline-reduction framework against different sets of science data.

The End of the Adventure

In retrospect, as the FLAMES SV coordinator, I must say that the very positive and successful experience of the FLAMES Science Verification Dry Runs has undoubtedly resulted from the hard work of several people, who deserve to be properly acknowledged. First of all, the FLAMES SV Team members (led by A. Renzini, and including M. R. Cioni, N. Cretton, A. Kaufer, C. Melo, L. Pasquini, M. Rejkuba, M. Romaniello J. Walsh, M. Zoccali, and myself - at ESO - and A. Blecha, C. Cacciari, V. Cayatte, and V. Hill, as representatives of the FLAMES Consortia) for having proposed and developed the science cases in a very flexible and timely manner. The Paranal FLAMES SV Team (A. Kaufer, J. Smoker, R. Schmutzer, C. Melo, M. Rejkuba and myself) played a fundamental role in securing an excellent set of first-grade science data (considering all the debugging, fixes and revisions implemented in real time at the telescope). One of the main strengths of this group was its very positive, friendly, and constructive team spirit. Among the ESO Fellows, the extra workloads undertaken at different stages of the FLAMES SV adventure by M. Rejkuba, M. Zoccali, and N. Cretton need to be recognised. Finally, the cooperation offered by the ESO/ST-ECF Science Archive (in particular, B. Pirenne and N. Rainer) made it possible to release all the data packages on a very compressed timescale. Thank you all!

Acknowledgements

The author would like to thank Pamela Bristow for a careful reading of the manuscript.

References

- Hillenbrand, L. A., 1997, *AJ*, **113**, 173
- Hui, X., Ford, H. C., Ciardullo, R., Jacoby, G. H., 1993, *ApJS*, **88**, 423
- Pasquini, L. et al., 2002, *The Messenger*, **110**, 1-9
- Queloz, D., Allain, S., Mermilliod, J.-C., Bouvier, J., Mayor, M., 1998, *A&A*, **335**, 183
- Silva, D., 2001, *The Messenger*, **105**, 18-24
- Stassun, K. G., Mathieu, R. D., Mazeh, T., Vrba, F. J., 1999, *AJ*, **117**, 2941

MACAO-VLTI First Light: Adaptive Optics at the Service of Interferometry

R. ARSENAULT¹, J. ALONSO², H. BONNET¹, J. BRYNNEL¹, B. DELABRE¹, R. DONALDSON¹, C. DUPUY¹, E. FEDRIGO¹, J. SPYROMILIO³, T. ERM³, J. FARINATO⁴, N. HUBIN¹, L. IVANESCU¹, M. KASPER¹, S. OBERTI¹, J. PAUFIQUE¹, S. ROSSI¹, S. TORDO¹, S. STROEBELE¹, J.-L. LIZON¹, P. GIGAN⁴, F. POUPLARD⁵, F. DELPLANCKE¹, A. SILBER¹, M. QUATTRI¹, R. REISS¹

¹European Southern Observatory, Garching, Germany; ²ESO, La Silla, Chile; ³ESO, Paranal, Chile; ⁴Astronomical Observatory of Padova, Italy; ⁵LESIA, Observatoire de Paris, France

The Multiple Application Curvature Adaptive Optics (MACAO) programme was initiated by ESO in 1998 to fulfil the high angular resolution requirements of the VLT Interferometer (Glindemann et al., 2002) and also instruments like SINFONI (Bonnet et al., 2002) and CRILES (Moorwood et al., 2002). After a learning phase of two years with the laboratory Curvature prototype delivered by Laplacian Optics, the ESO Adaptive Optics Department set up a project team at the beginning of 2000 for the line production of seven MACAO systems (Donaldson et al., 2000): four for VLTI, one for SINFONI, one for CRILES and one spare. Although the AO key components are similar for these seven systems, the opto-mechanical implementations are different for the VLTI, SINFONI and CRILES. In the following we will concentrate on the VLTI implementation.

The main aim of MACAO-VLTI is to feed the VLTI with a corrected wavefront, to improve light injection efficiency in the monomode fibres. The existing Coudé mirror train M8 is replaced by the corrective optics. The MACAO-VLTI Wave Front Sensor (WFS) is located just below M9 on the Coudé platform (Figure 1). M9 is a dichroic that allows the wavefront sensing in the visible (transmits 0.45–0.9 μm) and reflects the wavelengths 1 to 13 μm to the recombination laboratory.

Simulations done for the design reviews show that MACAO-VLTI will reach a Strehl ratio of 0.58 at 2.2 μm on bright stars ($V < 10$) with a seeing of 0.65" and this has been confirmed by tests in the laboratory. Limiting magnitude is evaluated at $V \sim 18$ which would result in a Strehl ratio slightly under ~ 0.1 . MACAO will also operate with worse seeing (1.0") but the correction is less spectacular (expected Strehl ratio of 0.39).

The first MACAO-VLTI system was delivered to Paranal on UT2 in April 2003, and results from the first light are shown further down in this article. The other three systems will follow at 6 month intervals. By the end of 2003 the first two systems will be available and will allow wavefront corrected beam recombination at the VLTI.

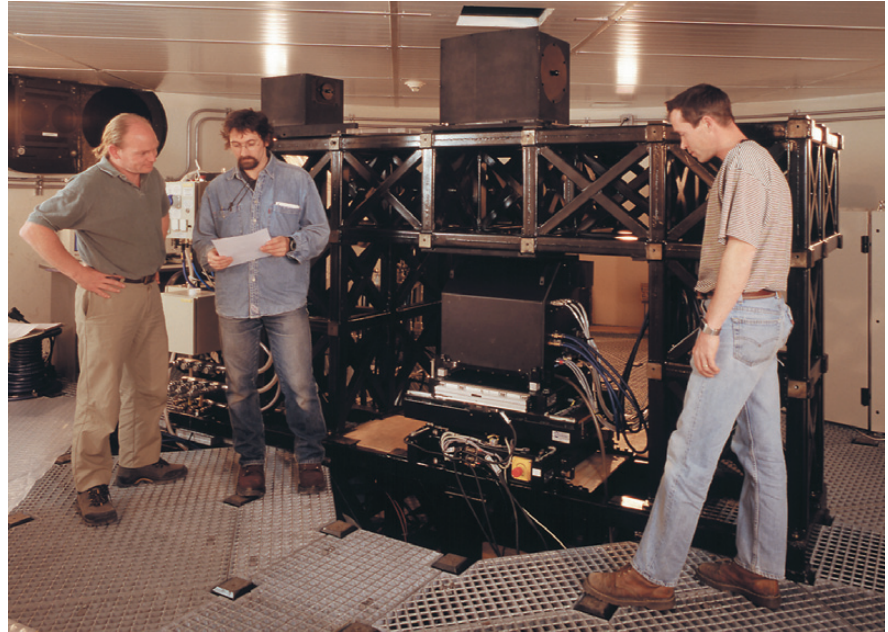


Figure 1: The location of the Coudé focus where the MACAO-VLTI systems are installed. MACAO is the black box under the M9 tower (arch) shown on the photograph.

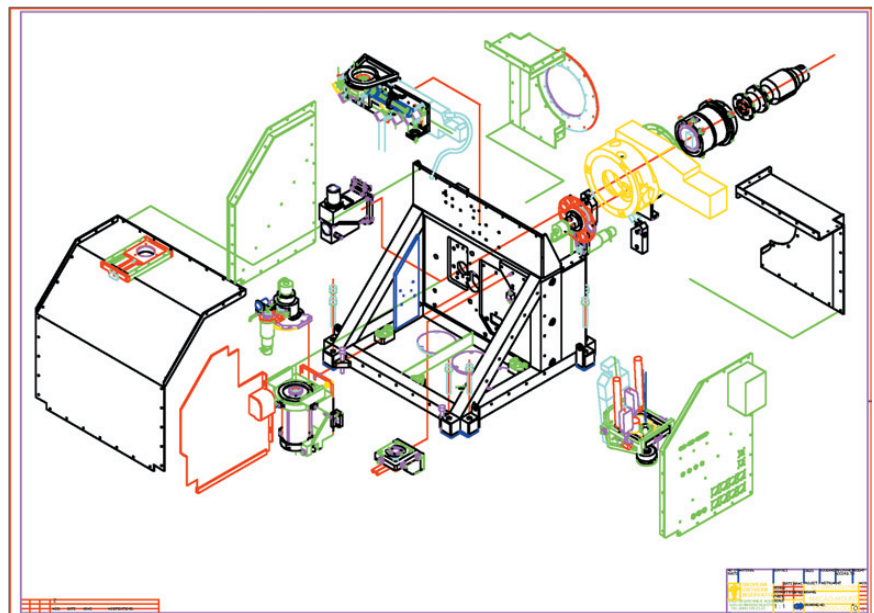


Figure 2: MACAO exploded view. The T-Mount, at the centre, is the main structure holding all components. On the front side one can see the shutter and BSD (top), the WFS optics (just below) and STRAP with its density filters wheel (at the lower-left). The TCCD (centre-bottom) and the membrane mirror on its gimball mount (lower-right) complete the equipment mounted on the front side of the T-Mount. On the back side are installed the last elements in the optical path namely: the density filter wheel, the rotating unit and the derotator prism and finally the micro-lens mount (upper right).

Figure 3: Opto-Mechanical setup of MACAO-VLTI on the XY table in the Coudé room during installation. The BSD can be seen in the uppermost part; the very crowded area on the left-hand side hosts the WFS optics and the membrane mirror gimball mount. Water pipes can be seen on the right side and are used for the cooling of the TCCD and STRAP units (if not helping in recognizing the components, this picture has at least the benefit of showing the complexity of the setup!).



MACAO-VLTI design

Opto-mechanical design

The existing Coudé mirror train feeds the delay lines of the VLTI before beam recombination; this constitutes the “science path” of the system. M8, which coincides with a pupil plane, is replaced by a 60 element bimorph mirror coupled with a curvature Wavefront Sensor (WFS). The WFS detectors are 60 Avalanche Photo-Diodes (APDs) from Perkin-Elmer (Canada).

The whole MACAO-VLTI assembly sits on the Coudé platform under a structure called the “M9 tower”. Figure 2 shows an exploded view of all MACAO components. The whole assembly is contained in a $650 \times 770 \times 850$ mm volume (including the XY table, not shown in this view). MACAO-VLTI provides acquisition mode with TCCD plus two main observing modes:

- Adaptive Optics image correction (curvature 60-element)
- Tip-Tilt correction (STRAP-M2 loop) on faint stars

The so-called “XY Table”, based on an ESO design, fulfils the field selector function of the AO system. It positions the MACAO assembly in the 240 mm (2 arcmin) field of view of the Coudé focus. It has been proven to provide a $2 \mu\text{m}$ relative positioning accuracy. All axis motions are linear to better than 20 arcsec (pitch, roll and yaw). Figure 3 shows a picture of the inside (front) of the MACAO-VLTI “box”. The XY table can be seen under the opto-mechanical assembly. Despite the small volume, one can see that space is scarce and integration/alignment definitely requires some skill.

The WFS box is composed of the following components. The Membrane Mirror, an aluminised pellicle mounted on a loudspeaker to be set in vibration at 2.1 kHz. It is located in the image plane and produces the defocus need-

ed in the pupil plane for curvature analysis. The WaveFront Sensor Optics, a set of four diamond turned mirrors in a single mount, can be changed as a unit. A Derotator Prism is needed to compensate the rotation between the DM (rotates with azimuthal axis) and the lenslet array (at rest on the Coudé platform). Figure 4 depicts the lenslet array unit which consists of two arrays with 60 subapertures each and 60 optical fibres. The purpose of this assembly is essentially to gather the light in the individual sub-apertures and inject it into the corresponding optical fibres. The telescope pupil image is divided in 60 sub-apertures, distributed in 5 rings of

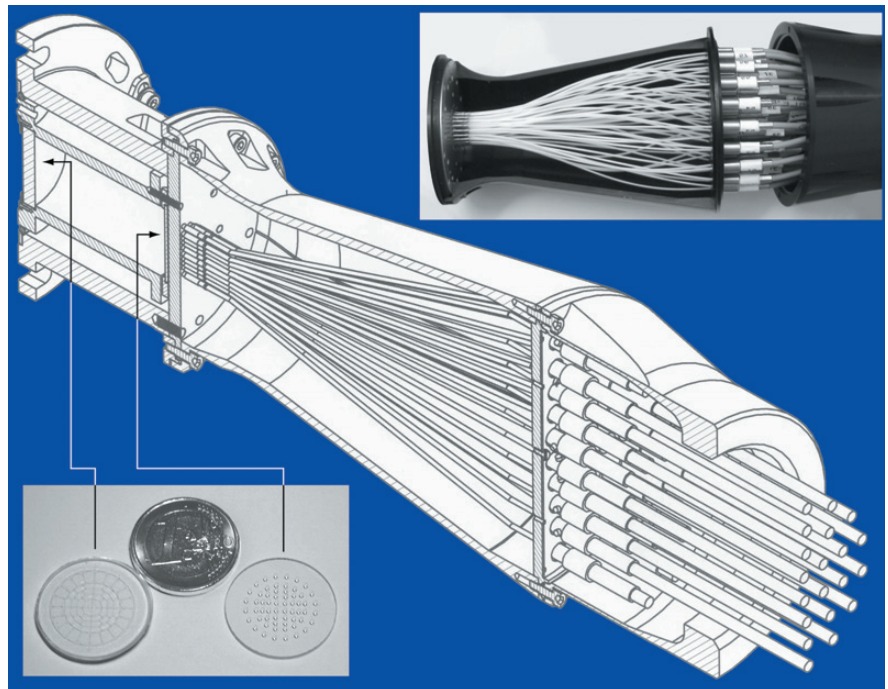


Figure 4: MACAO Lenslet array unit: The MACAO lenslet array unit is an original design and production of ESO. It uses two lenslet arrays in cascade. The first curvature lenslet array dissects the telescope pupil and focuses the light on the second ball lenslet array which concentrates and injects the light into the optical fibres connected at the other end to the 60 APDs.

varying number of lenslets: 4, 8, 12, 16 and 20. The Fibre Optic Bundle is made of the lenslets and 60 optical fibres terminated by FC connectors. It brings the light to the 60 APD WFS Detectors.

Corrective optics

The Deformable Mirror is fabricated by CILAS (France) and is of the bimorph type. Five such mirrors have been ordered (four units plus one spare) and a prototype for development and tests. The surface quality with voltage applied can reach 10 nm RMS. Less than 60 Volts are required to flatten the DM which leaves ample reserve for seeing correction (range of -400 to $+400$ V can be applied). The reflectivity is on average 99% in the IR ($\lambda > 1 \mu\text{m}$) and larger than 97% in the visible. It has been dimensioned to provide AO correction for seeing values up to $1''$.

The Tip-Tilt Mount is a custom design from the Observatoire de Paris (LESIA). It is based on a gimball mount in which the DM is inserted. The assembly is controlled by a dedicated electronics with its own internal 1 kHz control loop which makes tests and integration trouble-free. The bandwidth of the system has been tuned at 100 Hz for both axis and the stroke is 240 arcsec PV mechanical which corresponds to 6 arcsec on the sky.

Figure 5 shows the bimorph DM inserted into the Tip-Tilt mount. It also shows how this assembly replaces the conventional glass M8 mirror of the Coudé train.

An important property of this is the coincidence of the centre of gravity of

the DM and its supporting ring with the intersection of the X and Y tilt axis. This insures a better close-loop performance of the TTM. Furthermore, the surface of the DM is made coincident with the tilt axis (at centre) in order to have no optical path difference produced when tilts are applied.

Software

MACAO-VLTI is considered a telescope system and therefore is relatively transparent to the astronomer. In the end, the AO loop will be closed as part of the interferometric source acquisition procedure. The so-called VLT-ISS (VLT Interferometer Supervisor Software) sends command to the MACAO-VLTI OS (Observing Software) which coordinates the operations of the MACAO RTC (Real-Time Computer), ICS (Instrument Control Software), STRAP and TCCD subsystems.

In addition the MACAO OS supports the following observing modes:

- Staring: a single acquisition in which the AO loop remains closed during the entire observation.
- Chopping: an observation in which M2 is used to shift the field from object to sky and back again. The AO loop is synchronized (using the TIM board) with the frequency of M2 and the loop is opened during the chop on sky cycles.
- Nodding: an observation in which the telescope is used to shift from object to sky and back again. The ISS informs the MACAO OS of the nod to sky and nod to object cycles, the AO loop is opened during the nod to sky cycles.

An engineering interface of the OS has been designed and allows full control of the functions during integration and tests.

Electronics

The MACAO-VLTI electronics is composed of 4 cabinets containing all the required electronics. Three of them are installed in the Coudé room: the RTC-VLTI cabinets, the IC cabinet and the APD cabinet. The fourth one is located on the VLT azimuth platform for its proximity to the corrective optics. All electronics conforms to the ESO standard.

For the RTC hardware, an effort was made to select commercially available component to insure a smooth integration into the VLT environment. Two PowerPC 2604 (400 MHz) boards are used, one as LCU controller (controls VME rack and communication with outside world) and the second totally dedicated to the RTC calculation. A custom made APD Counter board (Shaktiware, Marseille, France) is used to acquire the flux from the APD.

The membrane mirror is set in vibration at 2.1 kHz; this function is managed by the APD counter board, a solution chosen because a single board manages the counter read rate and membrane driving signal which need to be well synchronized. The counts from the APD's (intra-focal and extra-focal) transit on the VME bus and are acquired by the RTC. They are processed (contrast calculation and multiplication by control matrix) and commands to the corrective optics are sent at a frequency of 350 Hz, hence 6 membrane mirror cycles. The time delay of the calculation has been measured to 310 μ sec.

The VLTI LCU controls the STRAP and TCCD operation for MACAO-VLTI while the IC cabinet (Instrument Control) contains a VME rack controlling all motorized functions. The two cabinets are identical in size and cov-

ered by a wooden-insulated "coffin"-type enclosure that reduces to a minimum heat radiation in the Coudé room and acoustic noise. Each cabinet's heat exchanger is connected to the SCP (Service Connection Point) which provides the cooling fluid. No fans have been implemented for the APD cabinet and all 60 APDs are mounted on cooling "plates" in which the cooling fluid circulates. The azimuth platform cabinet contains the DM voltage amplifier and the TTM servo-unit plus the usual cooling fans and heat exchanger.

The HV amplifier has been designed and built by 4D Engineering (Germany) and uses a VME architecture. This rack is controlled by a PowerPC CPU and signals are sent via a fast optical fibre communication link. The rack contains 4 boards which provide each 16 HV channels for a total of 64. It is upgradeable up to 15 boards (240 channels). The 10 V signals to be sent to the TTM servo-unit also transit through the fast optical fibre link.

Close loop & curvature

A curvature system was chosen because it offers a good performance for relatively low degrees of freedom, allowing lower costs for components (DM, RTC, lenslet, etc. (Roddier, 1988)). It uses the curvature principle which is that wavefront analysis is performed by measuring the intensity in 60 different sections of the pupil (sub-apertures). Measurements are performed with the pupil defocused – so-called intra or extra-focal images. This is produced by the vibrating membrane set in vibration at 2.1 kHz and the flux is then sampled at twice this frequency. The contrast value, $(I_{in}-I_{out})/(I_{in}+I_{out})$, is proportional to the Laplacian, hence the curvature of the wavefront.

Close loop control

The commands are applied to the corrective optics at a frequency of 350 Hz. The APD counter board provides the RTC with one set of intra/extra-focal counts every 0.48 msec. These counts are integrated by the RTC for 6 cycles and then multiplied by the command matrix to produce a command vector to be sent to the corrective optics. Besides acquiring WFS data, processing and sending commands to the correction optics (CO), the RTC also produces on-line diagnostic information and controls, a few electro-mechanisms (membrane mirror, neutral density filter and diaphragm). Systematic aberrations sent to the CO can be off-loaded to the Telescope Control System (tilt & focus at 0.2 Hz).

A watchdog is implemented to average the number of APD counts over a tunable number of cycles to determine whether they are over-illuminated. There are two safety levels aiming at

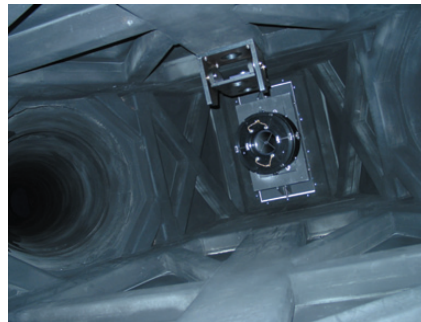


Figure 5: Bimorph deformable mirror in its tip-tilt mount. On the left one can see the protected silver coating 100 mm in diameter. The bimorph mirror is held by a spring loaded radial 3 points support in a dural ring. The assembly is inserted in the Tip-Tilt Mount (TTM) which can tilt the DM during close loop. To the right is a picture of the DM mounted at the M8 location of the VLT Coudé train. The hole on the left side leads up to M6.

protecting the APDs from an over-illumination. The routine which sends commands to the DM is also responsible for monitoring the voltages sent to the electrodes. It clips values in excess of + or -400 Volts, the maximum voltage.

There is provision for a modal optimisation, in which sensor data can be projected in another space where variable gains can be used for the different modes. Circular buffers can be generated to post-process sensor signals or mirror commands off-line.

Piston free AO system

For imaging purpose the piston produced by the deformable mirror in an AO system is not critical and the main concern is usually to avoid an accumulation of piston applied on the DM which would cause saturation of the electrodes. One of the main challenges of MACAO-VLTI is to insure that the corrective optics on 2 different UT's do not introduce phase delay between the recombined beams during close loop operation, which would limit fringe contrast. This is extremely critical if it occurs at high frequency, where the VLTI delay lines are no longer able to detect and correct for it. This is the reason for the strict piston specification: 25 nm RMS in 48 msec windows.

The strategy has been described by Vérinaud & Cassaing (2001) and involves defining a set of piston free influence functions. A special set-up using a commercial Shack-Hartman WFS and a capacitive sensor allows one to measure accurately (better than 1%) the optical piston averaged over the DM pupil for each electrode. The piston-free influence functions are built by adding a pure piston to the original influence function equal but opposite in sign. These are used to command the DM. The so-called tilt electrodes of the bimorph mirror (outside the pupil) contribute mostly to the production of a pure piston.

Integration & test

Test bench & facilities

A special effort was made to develop all necessary tools for a straightforward assembly and integration of the MACAO systems. This has turned out to be justified since all together five systems plus two Tip-tilt boxes (TTB) will have to be (have been) assembled and integrated in the life of this project.

For AO integration and test aspects, a complete Test bench has been designed and fabricated. This bench reproduces an f/46.7 optical beam, identical to a Coudé focus. The source module provides alignment sources (laser) and various set of target for the alignment of MACAO-VLTI with respect to the bench. A turbulence generator using phase screens produces a turbulent wavefront.

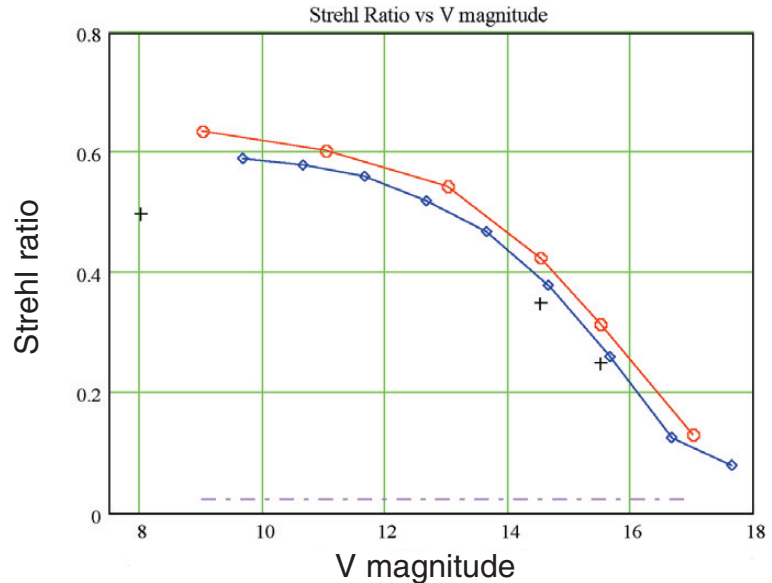


Figure 6: The blue curve shows the simulated Strehl ratio versus guide star V magnitude. The red curve shows the measured Strehl ratio in the laboratory (in K-band 2.2 μm). The simulated values include an error budget which probably explains why the laboratory curve shows better performance. The straight dashed-dot line shows the Strehl ratio in open-loop. The crosses are the specifications issued by VLTI.

A dedicated infrared camera working in K-band is installed permanently on the Test bench for characterization of the resulting image quality and evaluation of the Strehl ratio.

A second infrared test camera has been fabricated for commissioning the four MACAO-VLTI and SINFONI as well. The design is simple and uses three spherical mirrors. It uses a Hawaii 1K chip and is controlled by an IRACE system.

Simulations & test results

A whole set of simulations has been carried out in order to predict the performance of the system. The various assumptions were a model of the atmosphere with three main layers, matching what is agreed to be the standard average atmosphere in Paranal. The three layers are chosen to match a seeing condition of 0.65" at 500 nm, $t_0 \sim 4$ ms, wind speed ~ 11 m/s and $r_0 \sim 16$ cm. We have also tested one case of worse conditions, characterized by a seeing of 1" at 500 nm, $t_0 \sim 3$ ms and $r_0 \sim 10$ cm. Two different values for the sky background have been considered: $m_V = 20.7$ mag/arcsec² (average dark sky) and $m_V = 19$ mag/arcsec² (bright sky).

The reference flux for the simulations is $4 \cdot 10^5$ detected photons/second at magnitude 15 in the overall 8.2 m aperture. We chose a value of 250 cps for the APDs' dark current, from the Perkin-Elmer commercial list. The membrane stroke used is 0.25 m minimum (focal length) and a 500 μsec computing delay was assumed. Different configurations of sub-apertures and electrodes geometry have been envisioned. The one adopted minimizes the total noise variance and the variance of noise on the tilt correction.

In Figure 6 the blue curve shows the results of the simulations. The red curve shows the values measured in the laboratory in Garching with simulated turbulence. This shows a slightly higher Strehl ratio, but the most interesting feature is that a trend very similar to the simulations is seen versus star magnitude. The curve may slightly shift left if the whole system throughput (including telescope) is less efficient than what has been assumed (right if more). The plot is for a 0.65" seeing. The crosses show the specifications issued by VLTI.

Project organisation & future

Tip-tilt boxes

The milestone "Tip-Tilt Boxes Delivery" was a partial delivery of the MACAO systems to accommodate the VLTI planning. These are composed of the MACAO-VLTI opto-mechanical structure, including the XY tables, but without high order wavefront sensing and wavefront correction capability. The TTB allows the observer to acquire stars, to track stars off-axis and performs a tip-tilt correction of the source (closed loop between STRAP & M2 mirror). This set-up was delivered to UT1 and UT3 in November 2001 and has been in use since then. They will ultimately be replaced by full-fledged MACAO systems. Tests carried out on an 11.7 mag star show a ~ 10 mas tilt residual after correction.

Project aspect

It is worth mentioning that, in addition to MACAO-VLTI, SINFONI and CRIFES also use similar AO components. The implications are that several components can be ordered in several copies (usually 7 up to 10) leading to a

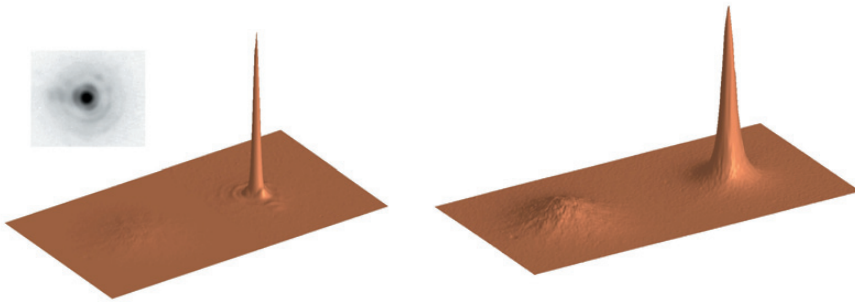


Figure 7: On the left is a K-band image of a bright star ($V \sim 10$) obtained in average seeing conditions ($0.8''$). Three diffraction rings can clearly be seen with a Strehl ratio larger than 50% and a FWHM of 60 mas. The plot on the right demonstrates the faint guide star performance. Using a $V = 16.5$ star, a K-band Strehl ratio of 10% and a FWHM of 140 mas were achieved in $0.55''$ seeing. The three dimensional plots also show the open loop images for comparison.

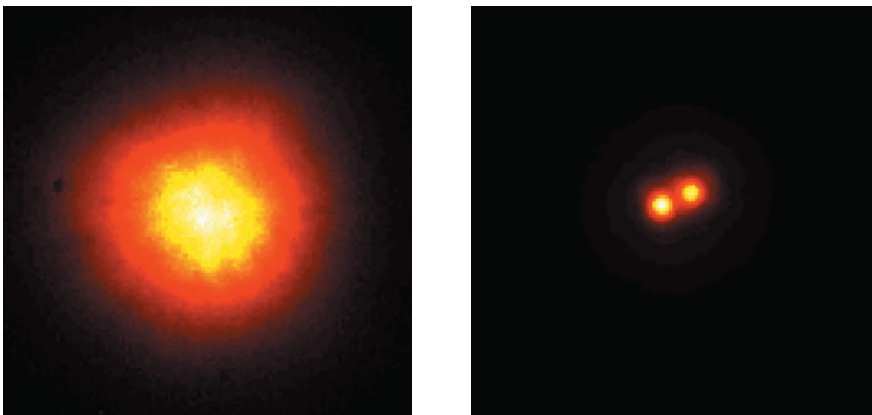


Figure 8 shows K-band images of a $V=10$ star obtained – before (left) and after (right) the adaptive optics was switched on. The separation of the binary is $0.12''$ and the seeing at the time of observation was $\sim 0.75''$ (see the text).

substantial cost reduction but also creating some motivation in industry. Besides, work or tasks accomplished on a particular project often benefit the other which leads to a non-negligible gain in development.

Schedule

The fast-track nature of the project is illustrated by the fact that Tip-tilt boxes delivery took place in November 2001, barely 7 months after the final design review. Then the first MACAO-VLTI system was delivered last April, and the second will be delivered in August 2003. Shortly afterwards, a joint team of the AO dept. and VLTI will perform a joint commissioning to obtain fringes with two MACAO-VLTI systems. The last two MACAOs will be delivered not before spring 2004 and winter 2004.

The interval between the successive MACAO-VLTI deliveries is dictated by the manpower available to perform the integration and optimisation of the systems. However, the commissioning schedule in Paranal is extremely busy in 2004 and this may add further constraints on the actual delivery dates.

Sky observations

Goal

The main goal of the April 2003 commissioning was to test the functioning of the whole system in the telescope environment and evaluate the AO performance on the sky. These were voluntarily decoupled from any interferometric functions and aim at assessing the performance of MACAO-VLTI in stand-alone mode. Further commissioning runs will take care of the interferometric aspects.

Strehl ratio & resolution

After we were re-assured on the basic functions of the system like source acquisition, closing of the loop, and stability, the performance evaluation activities started. This constituted an important part of this run and consisted in observing a star (point source) while varying the parameters of the system in order to obtain the highest possible Strehl ratio. The parameters that can be adjusted are the closed-loop main gain and the stroke of the vibrating membrane. These are known to depend on source extent and brightness. A set of

absorbing filters was used to simulate fainter stars.

Figure 7 shows a diffraction-limited K-band image of a bright star $V = 9.86$ (HIC 69495) obtained in April. Three diffraction rings can clearly be seen and the FWHM image resolution achieved in $0.8''$ seeing was 60 mas with a Strehl ratio above 50%. Also shown is the moderate image improvement achieved using a faint ($V = 16.5$) guide star. In $0.55''$ seeing, the corrected K-band image resolution was 140 mas with a Strehl ratio of 10%.

Figure 8 shows images of HIC 59206 ($V = 9.9$) taken in $0.75''$ seeing conditions, illustrating the improvement of the image resolution when using MACAO-VLTI. The left image was taken in open-loop (seeing limited), while the adaptive optics loop was closed during the exposure shown on the right. The separation of the binary is $0.12''$.

Astronomical targets

A few interesting objects, from an astronomical point of view, were selected to illustrate the performance of MACAO-VLTI. It must be pointed out that the aim of MACAO is not to produce astronomical images (the Test Camera is by no means a high performance scientific instrument) but rather to feed light to the VLTI. The following images allow comparison with other instruments. Results are impressive and compare advantageously to other AO systems with higher number of actuators.

Frosty Leo

Frosty Leo is a post-AGB star surrounded by an envelope of gas, dust, and large amounts of ice (therefore the name) displaying a bipolar morphology. It is one of the best examples of the brief transitional phase between the asymptotic giant branch (AGB) and planetary nebulae (PNe). For a three solar mass object, this transitional phase is believed to last only a few

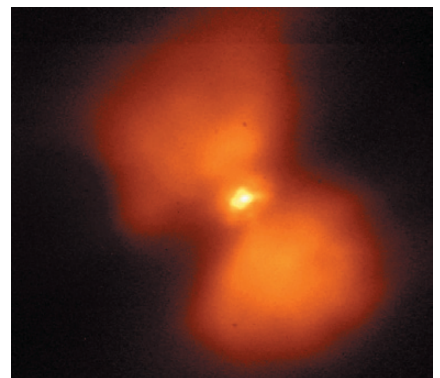


Figure 9 shows a $5'' \times 5''$ K-band image of Frosty Leo taken in $0.7''$ seeing. Although Frosty Leo is rather bright ($V=11$), it is a difficult AO target because of its extension of about $3''$ at visible wavelengths. The corrected image quality is about $0.1''$ FWHM.

thousand years, just a wink in the life of the star. Hence, post-AGB objects are very rare, and Frosty Leo is one of the nearest and brightest among them (see Figure 9).

NGC 3603

Among the first objects observed was the stellar cluster NGC 3603 located in the Carina spiral arm of the Milky Way at a distance of about 20,000 light-years (see Figure 10). With its central starburst cluster, it is one of the densest and most massive star forming regions in our Galaxy. Some of the most massive stars - with masses up to 120 times the mass of our Sun - can be found in this cluster.

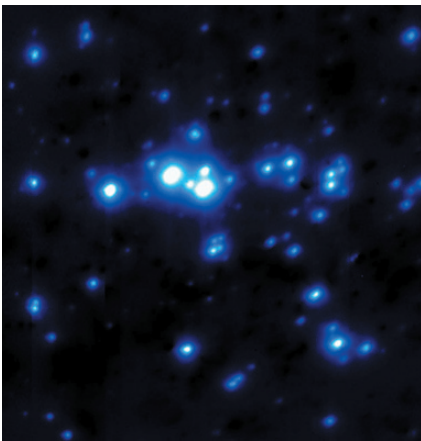


Figure 10 displays a K-band image of the starburst cluster NGC 3603. MACAO-VLTI compensated atmospheric disturbances by analyzing light from a star which was $30''$ separated from the field centre. The stellar images have a Full-Width-Half-Maximum (FWHM) diameter of 0.1 arcsec. The field measures 9×9 arcsec.

Eta Carinae

Eta Carinae (Figure 11) is one of the most massive stars in the Universe, probably more than 100 solar masses. It is about 4 million times brighter than the Sun, making it one of the most luminous stars known. As such massive stars have a comparatively short expected lifetime of roughly 1 million years, Eta Carinae must have formed recently in the cosmic timescale. Eta Carinae is also highly unstable and prone to violent outbursts caused by the fact that its high mass causes an extremely high luminosity. This leads to a high radiation pressure at the star's "surface", which blows significant portions of the outer layers off into space, in a slow but violent eruption. The last of these outbursts occurred between 1835 and 1855 and peaked in 1843, when, despite its distance (7,500 to 10,000



Figure 11 displays a K narrow-band image of the massive star Eta Carinae. The image quality is difficult to estimate because the central star saturated the detector, but the clear structure of the diffraction spikes and the size of the smallest features suggest a nearly diffraction limited performance. The field measures roughly 6.5×6.5 arcsec.

light years away), Eta Carinae briefly became the second brightest star in the sky with an apparent magnitude of -1 .

The Galactic Centre

The centre of our own galaxy (Figure 12) is located in the Sagittarius constellation at a distance of approximately 8 kpc from Earth. Recent AO observations using NACO at the VLT provide compelling evidence that a supermassive black hole with 2.6 million solar masses sits in the centre (Schödel, R., Ott, T., Genzel, R. et al., 2002; see also the March 2003 issue of *The Messenger*). This result, based on astrometric observations of a star orbiting the black hole at only 17 light hours minimum distance, could not have been obtained without imaging at diffraction limited resolution.

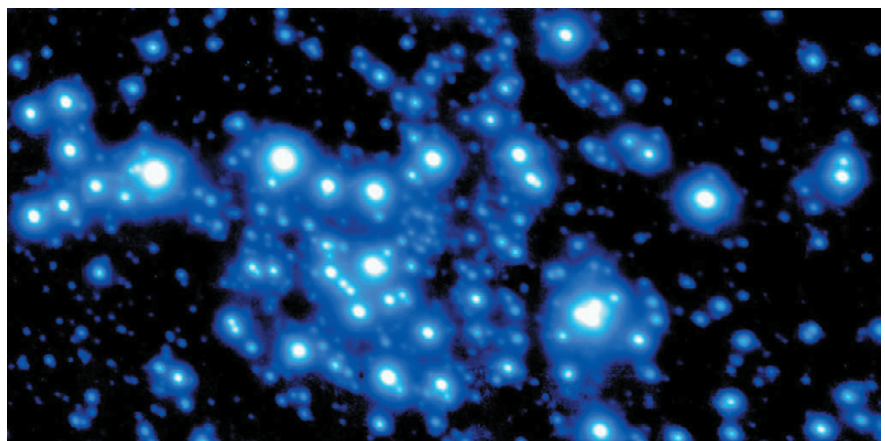


Figure 12 shows a 90 second K-band exposure of the central $6'' \times 13''$ around the Galactic Centre taken in $0.8''$ seeing, i.e., under average atmospheric conditions. Although the $V=14.6$ guide star is located roughly $20''$ from the field centre, leading to isoplanatic degradation of image quality, it is nearly diffraction limited with a point source FWHM of about $0.130''$.

Summary

The AO department of ESO has completed the design of an adaptive AO system for the VLT Interferometer. Ordering of components, manufacturing and integration took place in 2001 and 2002. The system is built in four copies, one for each VLT. It is installed at the Coudé room and the Coudé train is used as a "science path". Only one of the mirrors (M8, pupil conjugated) is replaced by the corrective optics. The 60 elements system should allow a Strehl ratio of ~ 0.6 on bright sources.

Commissioning activities started in April 2003 and the delivery of the 4th system is planned for late 2004. At the time of this writing the first commissioning of the first MACAO has been completed and results are encouraging. The integration and test phase of the 2nd system is in full swing.

References

- Bonnet, H., et al. 2002, Proc. SPIE 4839: Adaptive Optical System Technologies II, "Implementation of MACAO for SINFONI at the Cassegrain focus of VLT, in NGS and LGS modes"
- Donaldson, R. et al., 2000, Proc. SPIE 4007, p.82-93, "MACAO and its application for the VLT interferometer"
- Glindemann, A., et al., 2002, Proc. SPIE 4838: Interferometry for Optical Astronomy II
- Moorwood, A.F.M., et al., 2002, Proc. SPIE Astronomical Telescopes and Instrumentation, "CRIRES: a high-resolution infrared spectrograph for the VLT"
- Roddier, F., 1988, "Curvature sensing and compensation: a new concept in adaptive optics", *Appl. Opt.*, **23**, 1223-5
- Schödel, R., Ott, T., Genzel, R. et al., 2002, *Nature*, **419**, 694-696
- Verinaud, C., Cassaing, F., 2001, *A&A*, **365**, 314

MIDI Combines Light from the VLTI: the Start of 10 μm Interferometry at ESO

CH. LEINERT¹, U. GRASER¹, A. RICHICHI², M. SCHÖLLER², L. F. B. M. WATERS³, G. PERRIN⁴, W. JAFFE⁵, B. LOPEZ⁶, A. GLAZENBORG-KLUTTIG⁷, F. PRZYGODDA¹, S. MOREL², P. BIEREICHEL², N. HADDAD², N. HOUSEN², A. WALLANDER²

¹MPI für Astronomie, Heidelberg, Germany; ²ESO, Garching, Germany; ³Astron. Institute Univ. of Amsterdam, Netherlands; ⁴Obs. de Paris-Meudon, France; ⁵Sterrewacht Leiden, Netherlands; ⁶Obs. de la Côte d'Azur, Nice, France; ⁷ASTRON, Dwingeloo, Netherlands

When at the beginning of November 2002 the MIDI containers were opened up in Paranal and the team members together with ESO personnel started to assemble the instrument in the VLTI interferometric laboratory, nobody could be completely sure that their ambitious goal could actually be achieved: to bring together for the first time two beams of light from distant giant telescopes at the wavelength of 10 microns and obtaining stable, repeatable and accurate interference fringes. Although the instrument had been designed and built with the utmost care and all laboratory tests in Europe indicated that all specifications were met, going to the sky was another matter. The thermal infrared covers the wavelength range around the peak of the natural emission of a black body with a temperature about 300 K. This is close to the ambient temperature of the telescope mirrors and structure, of the two dozens of mirrors (in each arm) needed to bring the light into the tunnel and the interferometric lab, of all the mechanic structures, and of course of the sky. Therefore, at the wavelengths to which MIDI is sensitive, everything

glows brightly! There is no distinction between day and night, and even the brightest stars are just tiny speckles of light in an overwhelmingly bright background. For this reason, previous attempts to perform interferometry in the thermal infrared had to find other ways to combine the light (for example, like Bester et al. (1990), in the style of radiointerferometers, thereby however sacrificing sensitivity), or never achieved a real routine operation. Even the ambitious efforts being carried out at the Keck Interferometer, in spite of having started earlier than at ESO, are so far still confronted with difficulties in this special area.

It was indeed a big satisfaction when, after a few weeks of integration, MIDI achieved first fringes on the small siderostat telescopes first, and on the large Unit Telescopes immediately afterwards. This encouraging result was immediately reported in an ESO Press Release (25-02) and a press release by the MPIA in Heidelberg (02-12-19). After that, a First Commissioning run has also been completed in February 2003, with fringes being obtained rou-

tinely and reliably on several stars. This success might give the impression that things were relatively simple. In reality, it was quite the opposite.

Some history

When in January 1997 scientists at the Max-Planck-Institut für Astronomie in Heidelberg (MPIA) were sitting together to think about how to react to ESO's call for proposing interferometric instrumentation for the VLTI, it was not clear for which wavelength range they should propose to build an instrument. The near-infrared range around a wavelength of 2 μm had the advantage of being a proven high-quality observing method with detector arrays on many telescopes. Observing in the wavelength region around 10 μm , the main mid-infrared atmospheric transmission window, at first view appears laden with disadvantages: the thermal emission of the room temperature surroundings is at its maximum, about 10 $\text{W}/\text{m}^2/\text{sr}/\mu\text{m}$, by many orders of magnitude higher than the expected typical signal from a star, and the long wavelength of 10 μm will limit the spatial resolution achievable on the VLT Interferometer - and given by the ratio of $\lambda/\text{baseline}$ - to a value five times smaller than for near-infrared wavelengths. On the other hand, the mid-infrared wavelength range has its attractive sides, too. It is a tracer of material at temperatures of a few hundred K, at which 10 μm radiation is emitted most efficiently. Such material is intimately connected to young stars in the form of discs or circumstellar envelopes, to giant stars in dust shells formed from expulsion of surface layers and in Active Galactic Nuclei as tori confining the space around the central massive black holes - all of them areas of high current research interest. The higher penetrating power of the longer wavelength is an additional advantage in studying these often rather dense clouds of material. And a 10 μm interferometric instrument using the full available atmospheric transmission window from 8 μm to 12 μm would have been the first of its kind worldwide. In the end, the enthusiasm for a totally new field of observations won over the risks and challenges, and the acronym

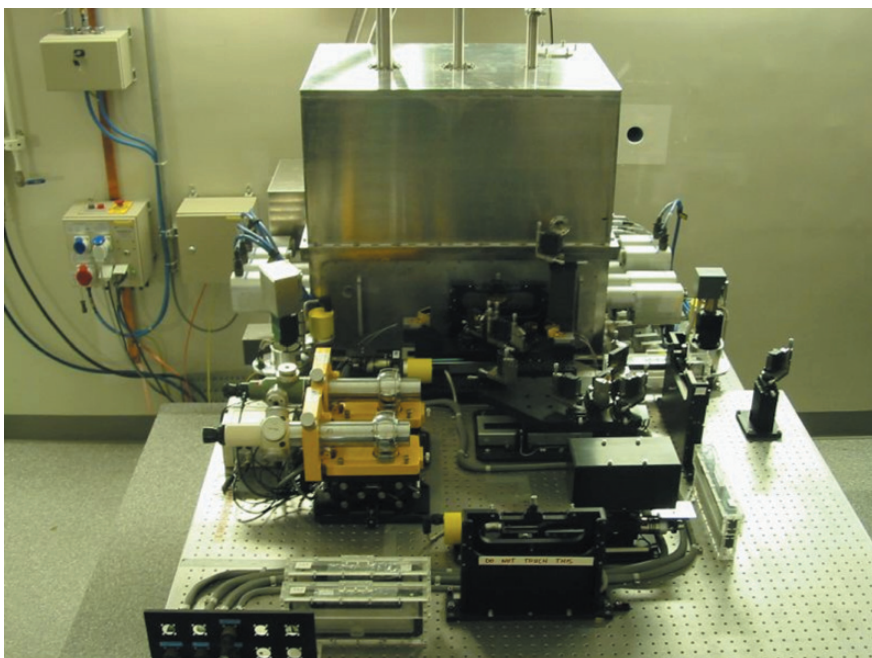


Figure 1: The fully assembled MIDI instrument in the interferometric laboratory on Paranal during commissioning in February.

“MIDI” (Mid-infrared Interferometric instrument) carries with it the chosen wavelength range.

Looking back, those days now seem history. MIDI was transported to Paranal in October 2002, packed in 34 boxes with a total weight of nearly 8 tons. The assembly and installation began on November 4, and from November 15 to 27, they were followed by an extensive alignment and verification phase in the interferometric laboratory. Finally MIDI went to the sky. After several nights of testing with the 40 cm siderostats MIDI eventually was connected to the Coudé beams of ANTU and MELIPAL and in the second of two nights, the 15th of December, MIDI detected its first fringes with the VLT telescopes.

This moment was full of emotion for the people present and all their colleagues back in Europe: it culminated an effort of over 5 years. Indeed, the first solid step of planning a mid-infrared instrument for the VLTI began at MPIA in summer 1997: it was the beginning of a road which led to the “Preliminary Acceptance Europe” (PAE) in September 2002.

Besides the MPIA, which is leading the effort with a PI team (project scientist and project manager) and providing cryogenics, mechanics, control and system software, detector including read-out electronics and associated software, major and important contributions came from the Netherlands, France, and other German institutes:

- the cold optics from ASTRON (Dwingeloo), the near-real-time software, the templates to run the instrument and the software management from NEVEC (Sterrewacht Leiden) as Dutch contributions,
- the data reduction software, management of the instrument science group (OCA, Nice) and efforts to provide MIDI with a 10 micron monomode fibre as spatial filter (Observatoire de Paris) from France,
- the warm optics from the Kiepenheuer-Institut für Sonnenphysik (Freiburg) and preparation of interferometric calibrators from the Thüringer Landessternwarte (Tautenburg).

Last but not least one should emphasize the crucial collaboration with ESO personnel both in Garching and Paranal in all areas of the project.

The work carried out by the consortium covered a very wide range of topics, from the design and realisation of optical and mechanical concepts, to the demanding task of providing the complex software needed to run the instrument as integral part of the VLTI. The importance and size of

this software work, not further described here, can hardly be overestimated. Mostly hidden to the outside and requiring intense cooperation between the instrument and the VLTI software teams, the development of specialized software is at the heart of the MIDI project.

It should be noted here that MIDI started off as a specialised PI-instrument and only after Concept Design Review was changed to a fully compliant VLT instrument, following ESO standards as far as possible and with the ambitious goal to be operated in a routine and user-friendly fashion like any other instrument on Paranal. This is a bold goal for an interferometric instrument. As a result of this history, unlike all other first generation ESO VLT instruments, in the MIDI project essentially all of the hardware was paid for by the MIDI consortium. ESO also developed and provided specialized hardware needed to integrate MIDI into the VLTI. The total cost of MIDI born by the consortium - not counting the necessary matching efforts on ESO's side - is of the order of 6 million Euros. Of this, 1.8 million Euros are for equipment, materials and optical parts, with the remaining for salaries during the extensive planning, construction and testing.

The instrument

Principle of measurement

The optical concept of the instrument is shown in Figure 2. From the left, the afocal beams from two telescopes of the VLTI are approaching the instrument. Their nominal diameter is 80 mm, and they are reduced to 18 mm diameter by a beam compressor provided as part of the VLTI infrastructure, represented here for simplicity by two lenses.

After the four folding mirrors of a small internal delay line, the compressed beams enter the cryostat (“Cold box”) through the entrance window (“Dewar window”). The telescope pupil is imaged by the VLTI delay line optics onto a cold pupil stop to provide the needed suppression of thermal emission from outside the beams. Next,

an intermediate focus is formed, where different slits or diaphragms (i.e. spatial filters) can be introduced for additional suppression of unwanted radiation. If no spatial filters are used, the detector pixels, which are much smaller than the Airy disc, still provide an alternative way to limit the spatial region admitted for the measurement. Then the beams are recollimated (again, reflective optics is represented by a lens for simplicity) and move on to combine on the surface of a 50-50 beam splitter, situated close to the reimaged pupil plane. The active coating is indicated in the Figure on the lower half of the back side of the ZnSe plate. This is the heart of the instrument.

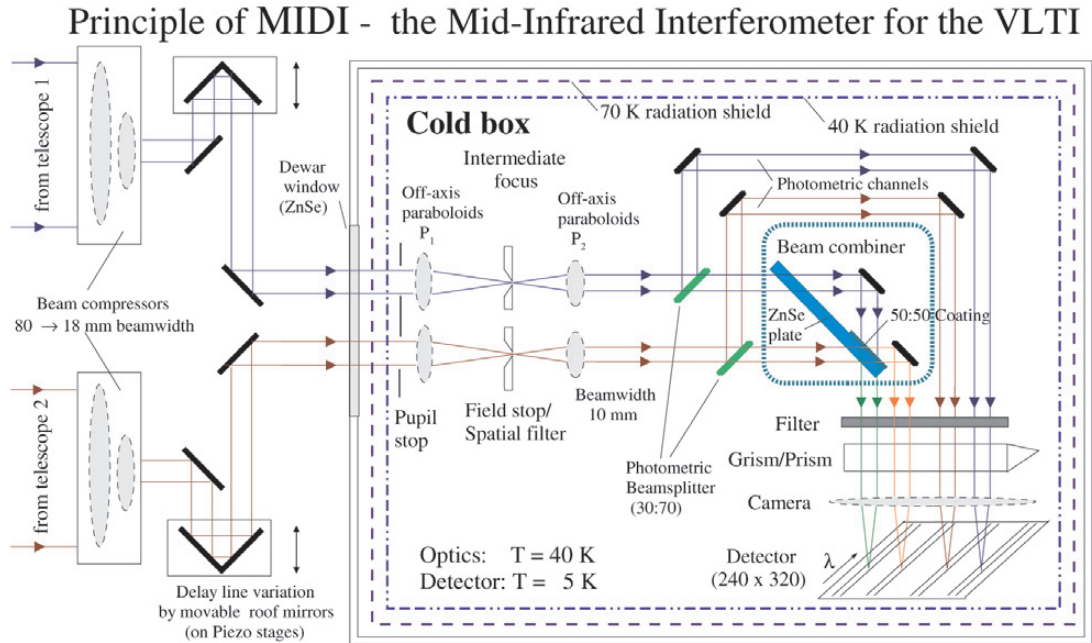
From the beam combiner onwards, the two interfering beams have a common optical axis. Actually, there are two such overlaid beams, one outgoing to each side of the beam combiner. These two outputs are modulated in flux depending on the optical path difference of the interfering beams, but with opposite sense because of energy conservation. Next, an image of the sky is formed for each of the two combined beams on the detector. Spectral information can be obtained by inserting filters or by spectrally dispersing the image using a prism for low or a grism for intermediate spectral resolution. If it is required to monitor the flux in the incoming telescope beams for high precision measurements, beam splitters can be inserted in front of the beamcombiner unit. The resulting additional monitoring beams are imaged onto the same detector.

MIDI measures the degree of coherence between the interfering beams (i.e. the object visibility at the actual baseline setting) by artificially stepping the optical path difference between the two input beams rapidly over at least one wavelength within the coherence time of ~ 0.1 s. This is done with help of the piezo-driven roof mirrors forming part of the small delay lines just outside the cryostat. The result in both channels is a signal modulated with time (“temporal fringe”), from which the fringe amplitude can be determined. The large

Table 1: Basic parameters of the instrument

Wavelength coverage	N band (8 - 13 μm)	expandable to Q (17 - 26 μm)
Resolution (λ/B for 100 m)	20 milli-arcsec	
Spectral resolution	up to 300	(prism, grism)
Airy disc (FWHM) at 10 μm	0.26" (for UTs) 1.14" (for ATs)	(FOV = 2")
Sampling time for fringe motion	100 ms ... 1 sec	average ... best conditions
Atmospheric stability for chopping	200 ms	
Detector	50 microns 320 x 240 pixels 2 x 10 ⁷ electrons 800 electrons	pixel size dimensions full well read noise
Background noise from sky from VLTI (at UT in Airy disc)	1.6 x 10 ¹⁰ photons/sec 1.23 x 10 ¹¹ photons/sec	
Limiting N-magnitude (without/with external fringe tracking)	at UTs 3-4 mag (1-2.5 Jy) at ATs 0-1 mag	/7-9 mag (0.1-0.6 Jy) /4-6 mag

Figure 2:
Schematic
diagram of the
instrument.
For explanation,
see text.



and not precisely known thermal background forces us to determine the total flux separately by a chopped measurement, chopping between the object and an empty region of the sky, and determining the source flux by subtraction. The raw normalised visibility is obtained by dividing the fringe amplitude by the total flux. As in standard interferometric practice, the calibrated visibility is obtained by dividing the raw visibility of an object by that of a known star.

Critical points and basic features

In the planning phase of MIDI three major technical fields were identified that could at the end turn out to become a show-stopper or at least create some constraints for the technical development of MIDI: vibrations, detector read-out, and alignment.

Vibrations are a natural consequence of the fact that MIDI had to apply a closed cycle cooler for cooling the optics to below 40 K and the detector to below 10 K. At the time when MIDI was planned this was the only option to guarantee the necessary cooling power. Over more than two years extensive tests were carried out with several dewar set-ups to find possibilities to damp these vibrations both in the MIDI instrument itself and in the environment where we had to avoid disturbing neighbouring instruments. Finally we ended up with a design that concentrates on a very heavy (650 kg) separate mount for the cold head and we connected it to the MIDI vacuum by a metallic bellow selected for its damping properties. Naturally, a number of additional technical measures such as special damping feet had to be applied until we came up with a solution where the internal jitter on the detector would not exceed 0.04 pixel.

Another critical point for MIDI concerns the necessary fast read-out times

introduced by the very high and variable background at 10 μm (see Table 1). With such a high background resulting mainly from all the warm optical elements in the VLTI chain the detector pixels would be saturated very quickly after several milliseconds. So, only dispersing of the signal over a number of pixels prevents saturation. The typical integration times for MIDI therefore are in the range of one to several hundreds of milliseconds. It is clear that this could lead to a very high data rate of up to some tens of Mbytes/sec. By windowing the frames during detector read-out the most important operating modes will not exceed a pure read-out time of 3 msec and a final data rate of 3 Mbyte/sec which is compliant with the current capabilities of the ESO archiving system. Developing this detector readout system with the real-time synchronisation capabilities needed for self-fringe tracking was one of the major tasks of instrument development (see Ligori et al. 2003).

Normally with instruments working in the mid-infrared regime the variability of

the high background is corrected for by chopping of the telescope and thus subtracting the background. This also holds for interferometry where the knowledge of the two beam intensities is needed for the accurate calculation of the object's visibility. In MIDI the two photometric channels (see Figure 2) were foreseen for delivering this information. However, when the external fringe-tracker and the adaptive optics are in operation, chopping will impose significant losses in time efficiency and additional synchronization constraints. This mode remains to be tested extensively in the next commissioning runs.

A third major concern was the accuracy of the alignment, and in particular how the alignment of the cold optical elements, which can only be performed in the warm when the devices are accessible for adjustment, is maintained during cooling. Two major steps have been taken to overcome this difficulty. First: the whole cold optical bench including its mountings have all been made out of parts of one single block of aluminium

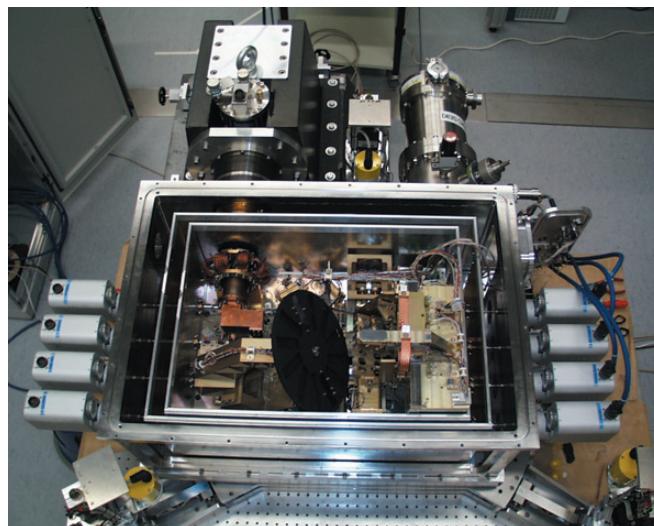


Figure 3: MIDI's Cold Optical Bench (COB) inside the open dewar. The two radiation shields are visible around the optical setup which is cooled down with the Closed Cycle Cooler (on the left side in the background) to a temperature of 40 K. The filter wheel (black), focus and other parts can be moved with the eight motors at the sides of the instrument.

alloy, and they were designed in a way that the shrinking of the material of 0.42% which comes from cooling down from 300 to 40 K is nearly homologous and should keep the optical characteristics (see Glazenborg-Kluttig et al. 2003). Second: A dewar mount was constructed which is movable around five of its six axes and thus provides for an accurate adjustment of the heavy (230 kg) MIDI dewar. During the integration and the first commissioning we were very glad to find the concept of the MIDI alignment to be fully confirmed. A view into the cold optics in the open dewar is given in Figure 3.

The outcome of all of these phases of planning, design and development has been presented recently (Leinert, Graser et al. 2003a, 2003b, Przygodda et al. 2003). Here is a summary description of the main characteristics of the instrument (see also Table 1):

- Two beam pupil-plane interferome-

ter at mid-IR-wavelengths (8–13 μm)

- Principle of measurement: The beams from two telescopes meet on a beam-combining beam splitter, where their pupils are superimposed “on axis”.

- The intensity of the two complementary outputs is modulated by stepping the optical path difference through one or more wavelengths by means of an internal piezo-driven delay line.

- a grism and a prism provide a spectral resolution up to 300.

- phase measurement will occur eventually by external referencing (when the dual beam capabilities of PRIMA become available on the VLTI).

MIDI on Paranal: first results and scientific programme

Currently the MIDI instrument is in a phase of extensive tests during the first commissioning runs at Paranal to verify the function of the instrument in all op-

erating modes. At present, the first commissioning has been completed and already encouraging results can be presented.

Figure 4 shows the signals of the two interferometric output channels obtained during an observation of Eta Carinae using the VLT unit telescopes ANTU and MELIPAL (UT1 and UT3). The circular fields are dominated by background radiation from the sky and the VLTI tunnels. Only because the object is very bright (flux more than 5000 Jy in the core, one of the brightest in the sky at 10 μm) is it identifiable in MIDI’s FOV of 2 arcsec. Usually an object becomes distinguishable only after the background is subtracted by chopping and nodding procedures. Chopping is performed by a modulation of the secondary mirror with a frequency of about 2 Hz and an amplitude of 3 arcsec. The resulting image in case of the observation of Eta Carinae is shown in Figure 5. One can clearly identify the complex structure of the object. The image, rivaling in sharpness the best mid-infrared images obtained with dedicated imaging instruments on Mauna Kea, demonstrates the excellent imaging capabilities of MIDI and the whole VLTI infrastructure which sends the light via 31 mirrors and 5 transmissive elements until it reaches the detector.

When searching for the fringe signal, the large delay line of the VLTI infrastructure is moved in steps of 30 micron over a range of a few millimetres, while MIDI’s internal piezo-driven delay line is performing additionally a few scans of 60 micron each at each of those steps. At the position where the optical path difference (OPD) between the two interferometric arms is almost zero, the fringe signal from the object becomes detectable in the subtraction of the two interferometric output channels. As an example, Figure 6 shows the superposition of five consecutively measured fringe packets, showing that fringe motion can be quite small under good seeing conditions. Fringe detection was performed also on a 9 Jansky source without problems, but finally the limiting magnitude of the instrument in self fringe tracking mode is not expected to be better than 1 Jansky, due to the fluctuations in the very strong background radiation. To increase the sensitivity it is necessary to apply external fringe tracking. This possibility will be given by FINITO, which will be installed on Paranal later this year. Together with the adaptive optics system MACAO, it is expected to dramatically increase MIDI’s sensitivity.

The scientific potential of MIDI has been discussed by the instrument science group and presented by Lopez et al. (2000). Further discussions led to a guaranteed time programme to fill the 300 hours of guaranteed observing time available to the instrument

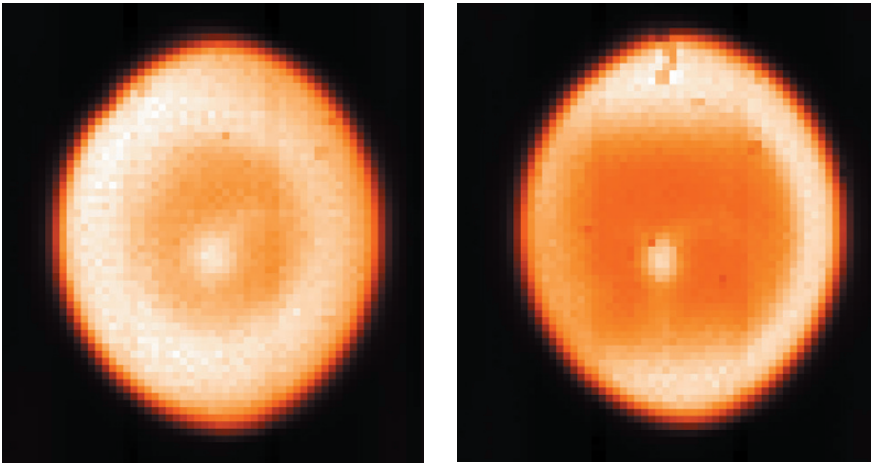


Figure 4: Raw images of the very bright infrared object η Car during telescope pointing. Left: beam from UT1, right: beam from UT3. On the detector the two beams are at top and at bottom, separated by unexposed parts of the array. In these exposures, no field limitation has been introduced except that given by the mechanical openings in the instrument. The outer, bright ring is thermal emission from the VLTI tunnel and outside the field-of-view. The field-of-view through the VLTI to the colder sky (about 2”) is seen as the darker inner circular structure. It is less pronounced for the beam from UT1 because at the time of this exposure there was some vignetting, increasing the contribution of unwanted thermal emission. η Car is bright enough to be seen already in these raw images.

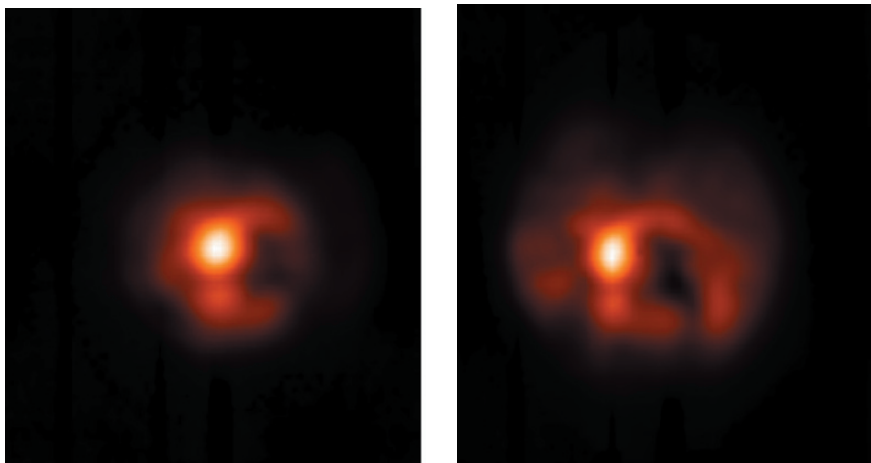
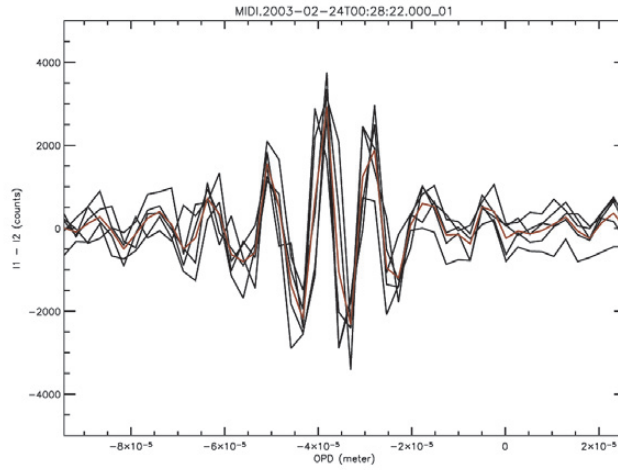


Figure 5: Chopped images of η Car obtained during the centring process. Left: beam from UT1, right: beam from UT3. The size of the blobs is close to the diffraction limit for 8-m telescopes, about 0.25”. Note the good optical quality.

Figure 6: The superposition of five fringe packets, measured at intervals of ~ 0.3 s and their average plotted against the optical path difference (OPD).

Here, the packets were obtained in the fringe searching mode. The fringe tracking mode allows one to adjust the delay lines automatically in order to compensate the atmospheric OPD variations. Then, the object visibility can be obtained with high accuracy by averaging the amplitude of hundreds of packets.



team on the UTs, which is shown in Table 2. This list gives an impression of what may be feasible to observe with the MIDI instrument. It has to be kept in mind that the objective of direct planet detection is atypical. It tries to detect the very small shift with wavelength of the centre of the combined image of star and planet. Requiring a differential accuracy of 10^{-4} , not guaranteed to be attainable by the instrument, it is a programme of extremely high risk for possibly high reward.

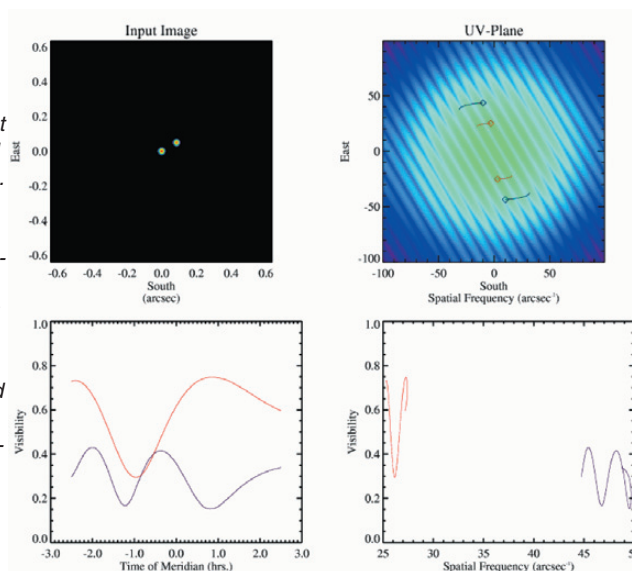
When planning observations with MIDI, a few constraints have to be kept in mind. For self-fringe tracking, not only must the source be bright enough but there must be sufficient flux in a very compact ($<0.1''$) central region, to which the interferometric measurements will refer. In general, the visual brightness should be at least 16 mag, in order to allow the operation of the tip-tilt and MACAO adaptive optics system. For observations with external fringe tracking, the *H*-band brightness should be at least 11 mag in order to drive the fringe tracker. In addition, one has to consider that interferometry with two telescopes

of the VLTI will provide only a few measured points of visibility, in a reasonable time of several hours, i.e. only a few points where the Fourier transform of the object image is determined. The scientific programme has to be checked in advance as to whether its main questions can be answered on this basis (e.g. to determine the diameter of a star one does not need to construct an image of its surface). As an example Figure 7 shows a prediction for the close young binary Z CMa. Here, the existence of circumstellar discs around the two components will show in a strong reduction with telescope separation of the sinusoidal visibility variations typical for a binary source. Such a signature can be clearly identified with a limited set of VLTI observations.

The near future

Now that MIDI is approaching routine observations as a science instrument on Paranal, have we exhausted the potential of $10 \mu\text{m}$ interferometry? Quite certainly not. A year from now, external fringe stabilisation by the fringe tracker

Figure 7: Simulation of an observation of the young binary Z CMa. The binary has been represented by two point sources at the observed separation of $0.1''$ at P.A. 300° , each surrounded by a circular disc with Gaussian brightness distribution and FWHM of 10 mas. From upper left to lower right we see: the image of the object; its Fourier transform and the tracks covered by the telescope pairs UT1-UT3 (outer lines) and UT1-UT2; the observed visibility as function of time (left) and of spatial frequency. Here, the curves with the lower visibility values correspond to the longer baseline UT1-UT3.



FINITO should increase the sensitivity of the highly background-limited instrument MIDI by at least a factor of 10 – even a factor of 80–100 appears possible. This will increase dramatically the number of interesting objects to be studied. Next, a proposal has been submitted to the funding agencies to allow an extension of MIDI operation into the $20 \mu\text{m}$ wavelength range. Also, the possibility is being studied to inject beams from more than two telescopes simultaneously into the MIDI instrument by means of an additional special external optics rearranging the geometry of the input beams (Lopez et al. 2003). This would allow one to derive from the interferometric measurements the so-called “closure phases” and thus enable the reconstruction of images. An alternative way for image reconstruction may open two years from now, when the VLTI will have installed the PRIMA “dual-beam” facility which will allow one to freeze the fringe motion at a particular position such that the phases necessary for image reconstruction can be obtained even in normal operation of MIDI with two-beam combination. Mid-infrared interferometry promises to become a field with much wider applications during the next decade. But the most exciting time for those having been involved in the instrument development is now: the first steps into new territory.

Acknowledgments

The dedicated efforts of a large number of colleagues from the institutes involved were necessary to bring the instrument MIDI to its present state of completion, in addition to the few who are honoured as authors of this article. We very much want to thank all of those for their important work and helpful cooperation and apologise if someone’s name should be missing in the following list of contributing persons:

- from MPIA Heidelberg: H. Baumeister, H. Becker, S.V.W. Beckwith (now STScI), A. Böhm, O. Chesneau, M. Feldt, A. Glindemann (now ESO), B. Grimm, T. Herbst, S. Hippler, W. Laun, R. Lenzen, S. Ligor, R. J. Mathar, K. Meisenheimer, W. Murr, R. Mundt, U. Neumann, E. Pitz, I. Porro (now MIT), M. Robberto (now STScI), R.-R. Rohloff, N. Salm, P. Schuller (now Harvard-Smithsonian Center for Astrophysics), C. Storz, K. Wagner, K. Zimmermann
- from Astronomical Institute of the University of Amsterdam: R. van Boekel
- from ASTRON, Dwingeloo: S. Damstra, J. de Haas, H. Hanenburg
- from Kapteyn Institute Groningen: J.-W. Pel
- from Sterrewacht Leiden: E. Bakker, W. Cotton (now NRAO), J. de Jong, J. Meisner, I. Percheron (now ESO), H. Rottgering
- from Observatoire de Paris Meudon:

Table 2: Proposed guaranteed time programme

Topic	Telescopes	
	UTs	ATs
Dust Tori in Nearby Active Galactic Nuclei	65 h	–
Inner discs of low-mass young stellar objects	65 h	90 h
Inner discs around intermediate-mass young and Vega-type stars	62.5 h	100 h
Massive young stars	52.5 h	305 h
The dusty environment of hot stars	2 h	68 h
Cool Late Type Stars and related objects	25 h	450 h
Extra-solar planets and brown dwarfs	25 h	–

- J. Bonmartin, G. Chagnon, V. Coude du Foresto, M. Nafati (now Nice)
- from Observatoire de la Côte d'Azur Nice: P. de Laverny, G. Niccolini
 - from Laboratoire d'Astrophysique Grenoble: A. Dutrey
 - from Kiepenheuer-Institut für Sonnenphysik Freiburg: L. Gantzert, O. von der Lühe, Th. Sonner, K. Wallmeier
 - from Thüringer Landessternwarte Tautenburg: B. Stecklum
 - from ESO: P. Ballester, B. Bouvier, C. Sabet, F. Derie, Ph. Gitton, A.

Glindemann, S. Guisard, B. Koehler, S. Levêque, J.-M. Mariotti (†), S. Menardi, F. Paresce, J. Spyromilio, M. Tarengi (now ALMA)

References

- M. Bester, W. C. Danchi, and C. H. Townes, "Long baseline interferometer for the mid-infrared" SPIE 1237, 40 - 48, 1990.
- A. W. Glazenberg-Kluttig, F. Przygodda, H. Hanenburg, S. Morel, J.-W. Pel, "Realization of the MIDI cold optics", SPIE

- 4838, 1171-1181, 2003
- C. Leinert, U. Graser et al., "Ten-micron instrument MIDI - getting ready for observations on the VLTI", SPIE 4838, 893-904, 2003a
- Ch. Leinert, U. Graser et al., "MIDI - the 10 μ m instrument on the VLTI", Conf. Proc., 11th EAS Meeting: "JENAM 2002: The Unsolved Universe", Porto, Portugal, Astrophys. Space Sci. 2003b
- S. Ligoří, U. Graser, B. Grimm, R. Klein, "Experiences with the Raethyon Si: As IBC detector arrays for mid-IR interferometric observations", SPIE 4838, 774-785, 2003
- B. Lopez, Ch. Leinert, U. Graser et al., "The astrophysical potentials of the MIDI VLTI instrument", SPIE 4006, 54 - 67, 2000.
- B. Lopez, Ph. Mathias, D. M'ekarnia et al., "APres-MIDI, APerture Synthesis in the MID-Infrared with the VLTI", SPIE 4838, 1011 - 1015, 2003.
- F. Przygodda, O. Chesneau, U. Graser, Ch. Leinert, S. Morel, "Interferometric observations at mid-infrared wavelengths with MIDI", Conf. Proc., 11th EAS Meeting: "JENAM 2002: The Unsolved Universe", Porto, Portugal, Astrophys. Space Sci. (2003)



L. GERMANY, *SciOps*

Danish 1.54m Handover

On September 30, 2002, ESO stopped offering the Danish 1.54 m telescope to its community. The Danish 1.54 m is now only available to the Danish community, and ESO continues to perform the maintenance of the telescope. The main repository of information regarding that telescope is now the "Ground-Based Astronomical Instrument Centre" (IJAF) at the CUO (<http://www.astro.ku.dk/ijaf/>).

Final Dishwalk at the SEST

March saw us witness the last ever dishwalk at the SEST telescope before its closure later this year. The SEST dish is inspected once a year for damage to the teflon coating. This may be caused by pebbles flying around in high wind (which cause small holes in the coating), high humidity, and from the coating peeling off at the edges of the panels. This damage is "fixed" by sticking small plastic patches over the affected area.

To do the inspection, the dish has to



Lars-Ake Nyman and Mikael Lerner make the final dishwalk on the SEST.
Photo by Lauri Haikala.

be pointed close to zenith (since only aliens can defy gravity to walk on the dish when it is at low elevations). The work has to be done bare foot (so as not to damage the delicate surface), and usually in the Chilean autumn, since the sun is high in the sky during summer

and the SEST has a 50 degree Sun avoidance zone. Pointing too close to the Sun will fry the secondary (as happened back in the 80's), and walking around with bare feet on a metal surface in the middle of summer is also probably going to fry the inspectors!

Studying High Redshift Galaxy Clusters with the ESO Distant Cluster Survey

G. RUDNICK¹, S. WHITE¹, A. ARAGÓN-SALAMANCA², R. BENDER^{3,4}, P. BEST⁵, M. BREMER⁶, S. CHARLOT^{1,7}, D. CLOWE⁸, J. DALCANTON⁹, M. DANTEL¹⁰, G. DE LUCIA¹, V. DESAI⁹, B. FORT⁷, C. HALLIDAY¹¹, P. JABLONKA¹⁰, G. KAUFFMANN¹, Y. MELLIER⁷, B. MILVANG-JENSEN⁴, R. PELLO¹², B. POGGIANTI¹¹, S. POIRIER¹⁰, H. ROTTGERING¹³, R. SAGLIA³, P. SCHNEIDER⁸, L. SIMARD¹⁴, D. ZARITSKY¹⁵

¹MPA, Garching, Germany; ²University of Nottingham, UK; ³Ludwig-Maximilian University, Munich, Germany; ⁴MPE, Munich, Germany; ⁵ROE, Edinburgh, UK; ⁶University of Bristol, UK; ⁷IAP, Paris, France; ⁸IAEF, University of Bonn, Germany; ⁹University of Washington, Seattle, USA; ¹⁰OPM, Paris, France; ¹¹Osservatorio Astronomico di Padova, Padova, Italy; ¹²OMP, Toulouse, France; ¹³Leiden Observatory, The Netherlands; ¹⁴HIA, Victoria, Canada; ¹⁵Steward Observatory, Tucson, USA

Galaxy clusters are the most massive quasi-equilibrium objects in the Universe and are the meeting places of the cosmos. Their deep potential wells are dominated by unseen dark matter, but contain a cosmologically representative baryon fraction in the form of galaxies and intergalactic gas. These are trapped in a virialized state, with the gas heated to tens of millions of degrees and the galaxies moving with *rms* velocities of ~ 1000 km/s.

The study of the evolution of galaxy clusters and of the galaxies within them has largely been driven by observation. Starting in the late 1970's a picture began to emerge in which cluster galaxies evolve towards redder colours with decreasing redshift (Butcher & Oemler 1978) and in which galaxy morphologies are biased towards ellipticals and bulge-dominated systems in denser environments (Dressler 1980). In the following years, imaging with the Hubble Space Telescope (HST) and spectroscopy with 4-meter class and larger telescopes confirmed and extended these early results, adding detailed information about the spectral and morphological properties of galaxies out to $z \sim 0.5$.

A theoretical framework has developed for interpreting these observations, based largely on simulations of dynamical effects on cluster galaxies. As galaxies fall into clusters along the filaments which define large-scale structure, the observed trends can be imprinted by a variety of processes: galaxy morphologies may be altered by repeated gravitational shocking through high speed encounters with other galaxies and with the global cluster potential (galaxy harassment; e.g. Farouki & Shapiro 1981; Moore et al 1996); hot gas envelopes around galaxies can be removed by the hot intra-cluster medium, eliminating the reservoir of gas

which can accrete onto the disc and form stars (strangulation; e.g. Larson, Tinsley & Caldwell 1980); the HI can be similarly stripped by motion through the intra-cluster medium (ram-pressure stripping; e.g. Gunn & Gott 1972) or may be used up in a brief star-burst triggered by the high pressure cluster environment (stimulated star formation; e.g. Dressler & Gunn 1983); and massive galaxies may merge into a central supergiant cD (cannibalism; White 1976). Theoretical treatments of these processes have improved dramatically as computer capabilities have advanced. Dark matter simulations can follow the formation of rich clusters, tracking the evolution of substructures as small as the halos of the faintest dwarf galaxies. The formation of the galaxies themselves can then be studied by adding simplified treatments of gas cooling, star formation, feedback, and stellar evolution (e.g. Springel et al. 2001).

The wealth of observations now available suggests that none of these processes dominates the transformation of galaxies; all appear to play some role, and they may have differing importance in different environments. Their interplay makes clusters ideal laboratories for studying galaxy evolution. This usefulness is enhanced by several practical advantages. Clusters contain many galaxies close together on the sky and at the same redshift, making efficient observation easy with a modest field of view and permitting the approximation that all cluster members are equidistant from the observer.

One of the limitations in using existing observations to constrain theoretical models is that most studies of clusters at $z > 0.3$ have concentrated on X-ray selected samples. This biases the samples towards the most massive and the densest systems. In addition, the

largest available sample at $z \sim 0.4-0.5$ has heterogeneous and poorly defined selection criteria, significantly complicating any comparison with theoretical predictions. Finally, few clusters have been observed *in detail* at $z \geq 0.5$ where evolutionary changes become dramatic.

The time is ripe to significantly advance our understanding of galaxy evolution in clusters. The basic theoretical paradigm for structure formation is now well established on the relevant scales, and many of the important physical processes can be calculated reliably. Even more importantly, improved instrumental capabilities allow quite precise data on the structure and stellar content of galaxies to be obtained out to redshifts where evolutionary effects are large — at $z \sim 0.8$ where the universe was less than half as old as it is today.

The ESO Distant Cluster Survey

We initiated the **ESO Distant Cluster Survey (EDisCS)**, an ESO Large Programme, to take the next step in surveying the evolution of clusters and cluster galaxies. We aim to make a systematic study of cluster structure and cluster galaxies out to $z \sim 0.8$ at a level of detail which will allow quantitative comparison with the large and statistically complete samples of nearby clusters being provided by the 2dF and, particularly, the SDSS projects. Our programme involves matched optical photometry from the VLT and near-IR photometry from the NTT, followed up by multi-object spectroscopy using FORS2 on the VLT. Science goals for the photometric part of the survey include: characterizing the absolute rest-frame ultraviolet (UV) to near infrared (NIR) spectral energy distributions (SEDs) of the galaxies; studying galaxy morphology as a function of SED; measuring the cluster luminosity functions as a func-

tion of redshift and of cluster properties; estimating cluster masses through gravitational lensing; and characterising cluster structure. In practice, this involves deep, high resolution imaging of a large enough cluster sample to span the (large) expected variance in cluster properties, the use of bulge-disc decomposition software to quantify galaxy morphology and of photometric redshifts to reject non-members, and the careful analysis of faint image shapes to measure the gravitational shear.

Our follow-up spectroscopy targets a second set of science goals: measuring the stellar and dynamical masses of cluster galaxies; characterizing their chemical abundances, star formation rates (SFRs) dust contents, and star formation histories (SFHs); comparing these with the properties of field galaxies at the same redshift; and studying the dynamical structure of the clusters. These require high quality spectra for many member galaxies in each cluster and with well understood sampling and completeness statistics. Only with a dataset of this quality is a realistic confrontation with theoretical models possible. Our consortium has already carried out suites of high resolution simulations of the formation of clusters and cluster galaxies which can be used to investigate whether the physical processes outlined above can, in some combination, account for the properties we observe for galaxies in our EDisCS sample.

ESO's suite of instruments and tele-

scopes is ideally suited for such a project, which requires optical and NIR imagers with excellent image quality and relatively wide fields, as well as an efficient multi-object spectrograph mounted on an 8-meter class telescope.

Survey Description and Progress

To ensure the most efficient use of telescope time, successive refinement steps were taken to arrive at a robust cluster sample. An original set of 30 cluster candidates, 15 with estimated redshifts $z \sim 0.5$ and 15 with $z \sim 0.8$, was drawn from the optically selected Las Campanas Distant Cluster Survey (LCDCS; Gonzalez et. al. 2001). Given that the spurious candidate rate in the LCDS can be as high as 50% by $z \sim 0.8$, we used four nights on VLT/FORS2 to obtain two-colour images of each field to confirm the presence of a galaxy overdensity with the expected elliptical-like colours. We then chose the 10 best cluster candidates at each estimated redshift for deeper imaging, followed by spectroscopy. These 20 clusters were observed at the VLT in *BVI* for the $z \sim 0.5$ candidates and *VRI* for the $z \sim 0.8$ candidates. In addition, 20 nights of NIR observations were scheduled at the New Technology Telescope (NTT) using the SOFI NIR camera. This time was used to get K_s -band data for the $z \sim 0.5$ candidates and JK_s for the $z \sim 0.8$ candidates. At the present time, all of the optical and all but one night of the NIR

imaging is complete. Most of the data were taken under excellent conditions with almost all combined images having $<1.0''$ FWHM seeing. In Figure 1 we show optical images for four of our clusters. *I*-band selected catalogues with multi-band photometry were then constructed using the SExtractor software (Bertin & Arnouts 1996). The optical and NIR imaging, including the construction of the catalogues, will be described in upcoming papers (White et al., in preparation; Aragón-Salamanca et al., in preparation).

An initial phase of spectroscopy consisted of a relatively short exposure of a single mask in each field to confirm the presence of a true cluster in the expected redshift range. This resulted in the elimination of one high-redshift candidate that appeared to be a superposition of several weak groups. We then began taking longer exposures of 3 or 4 masks per cluster with the aim of obtaining high quality spectra for ~ 50 members in each cluster. As of April 2003 we have observed for 19 of our total allocated 22 nights (the eight nights of data from Spring 2002 are fully reduced), confirming that all extensively observed clusters are indeed real. Our final sample will have 7 clusters with true redshifts in the range $0.6 \leq z \leq 0.8$. We now have 1240 redshifts for our high redshift clusters, and 554 for our low redshift clusters. We project, given our performance for the first eight nights, that we now have at least 380

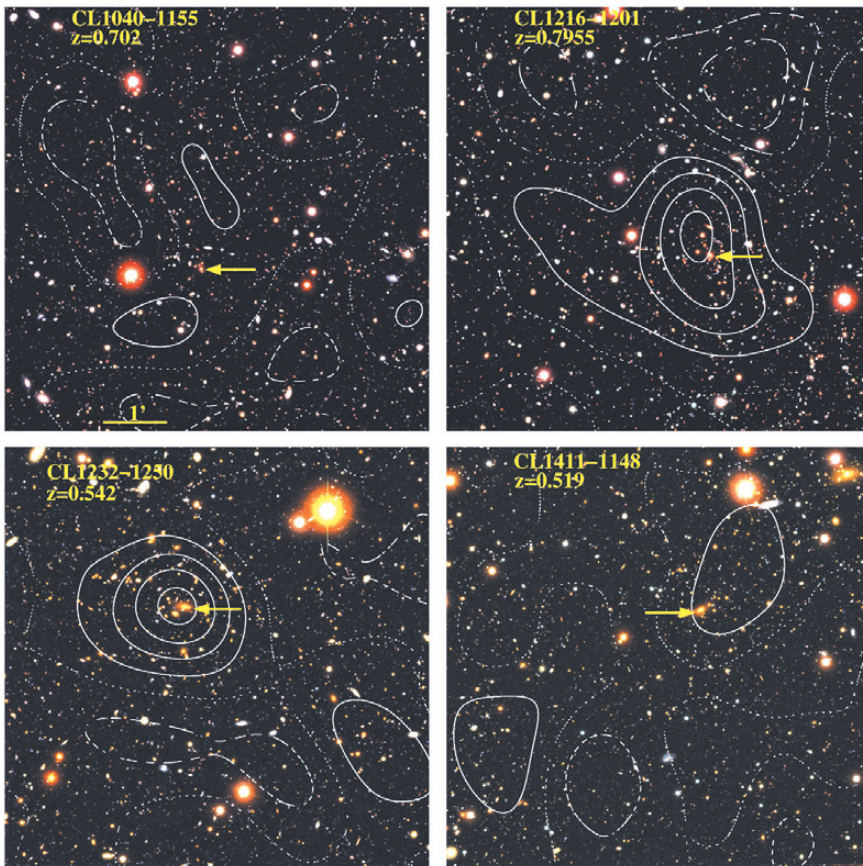


Figure 1: 3-colour images with overlaid weak lensing mass maps for four of the clusters in the EDisCS sample. The top two images, cl1040-1155 on the left and cl1216-1201 on the right, are from the high-redshift sample and were imaged in *I*, *R*, and *V*. The bottom two images, cl1232-1250 on the left and cl1411-1148 on the right, are from the intermediate-redshift sample and were imaged in *I*, *V*, and *B*. The yellow arrow in each frame indicates the location of the BCG. The weak lensing mass maps are normalized to have zero mean surface density at the edge of the images, with the solid contours indicating positive density, the dotted contour zero density, and the dashed contours negative density. Each contour represents a change in surface mass density of about $10^8 (h_{70})^{-1} M_{\odot}/\text{kpc}^2$ in an $\Omega_m = 0.3$, $\Lambda = 0.7$ cosmology. All of these clusters have been spectroscopically confirmed with many members, but some of them show no associated peak in their weak lensing mass distribution, demonstrating the diversity of the relation between light and mass in our cluster sample. Figure prepared by Douglas Clowe.

cluster members for the high redshift fields and at least 200 cluster members for the intermediate redshift fields. After the remaining three nights of our allotted spectroscopy, we should reach final numbers of 1290/410 at high redshift and 1000/350 at intermediate redshift. The spectroscopic data will be presented in Halliday et al. (in preparation).

At the present time we already have an impressive data set, with extensive photometry over a long baseline in wavelength, a set of 19 fully confirmed clusters at $0.4 < z < 0.8$ with a range in cluster richness, and fully reduced spectroscopy of about 920 galaxies (from our spectroscopy in 2002). We are, however, still far from being spectroscopically complete even at bright magnitudes. We remove non-members from our photometric samples in two steps, first by using photometric redshifts calculated with two independent codes (Rudnick et al. 2001; *Hyperz* - Bolzonella, Miralles, & Pelló 2000); then through statistical subtraction of the remaining background within a physical projected radius, $r_{clust} = 0.75 (h_{70})^{-1}$ Mpc, using the observed population density at larger clustercentric distance. Our photometric redshifts z_{phot} are quite accurate, with $\langle |z_{spec} - z_{phot}| \rangle = 0.06-0.08$ for both the $z \sim 0.5$ and $z \sim 0.8$ clusters. Using our photometric redshifts we reject $\sim 60\%$ of the field galaxies above the spectroscopic limit and $75-80\%$ of the field galaxies brighter than $I = 25$, while retaining $\sim 90\%$ of all confirmed cluster members, independent of rest-frame colour. The subsequent statistical subtraction removes $\sim 50\%$ of the remaining galaxies. The performance of these techniques will be evaluated in detail in Pelló et al. (in preparation).

The Cluster Luminosity Function and its Evolution

One important observational characteristic of a galaxy population is its luminosity function (LF), which describes the galaxy abundance as a function of absolute magnitude. Evolution of the LF encodes how the luminosity distribution of a galaxy population evolves as a result of star formation, of stellar aging, of obscuration, and of galaxy merging. Observations of the structure and kinematics of cluster ellipticals show that their stellar mass-to-light ratios have increased by about a factor of 2.5 in the B -band since $z = 1$, presumably a result of the aging of their stars. For mixed populations, however, the fading may be different because of dust, star formation, and differential age effects. In addition, it is important to realise that although the galaxies which populate $z = 0$ clusters *do* include those which populate $z = 1$ clusters, the majority would probably be considered “field” objects at the higher redshift. Both the

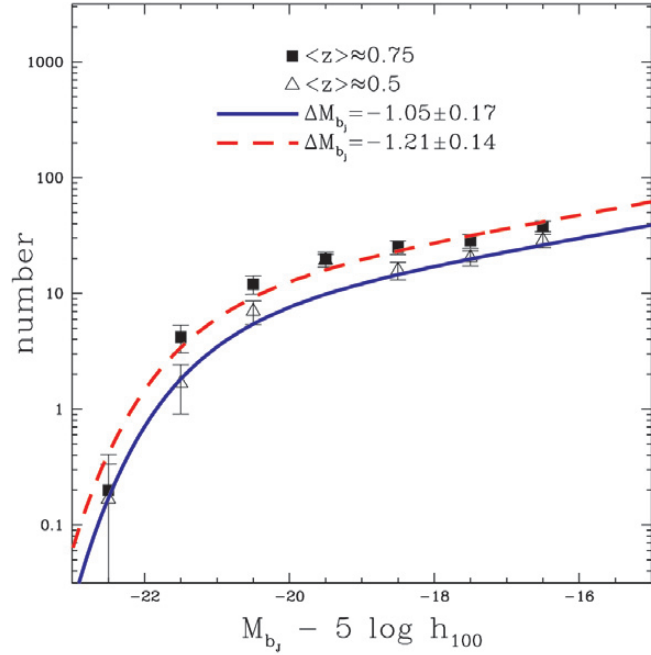


Figure 2: The mean rest-frame b_J -band galaxy luminosity function for all of our $z > 0.6$ clusters (solid points) and for all of our $z < 0.6$ clusters (open points). The blue solid line is the best fit Schechter function to the intermediate redshift sample with α fixed at the local value of -1.28 . The red dotted line is the best fit to the high redshift sample, also with $\alpha = -1.28$. The quoted brightening is with respect to the 2dF cluster luminosity function. Figure prepared by Gregory Rudnick.

newly accreted galaxies and the original cluster members may also have their luminosities altered by merging since $z = 1$. Thus, quite detailed modelling is needed in order to interpret the evolution of cluster LFs.

Observations of many local clusters from 2dF Galaxy Redshift Survey (2dFGRS) have shown that the LF of cluster galaxies is remarkably similar for clusters with many different properties (De Propris et al. 2002). We use this large local sample as a zero-point for studying evolution in our own dataset. Using the observed SED of each galaxy, normalized to its total I -band flux, and the spectroscopic redshift of the cluster in which it resides, we derive the rest-frame b_J luminosity. We then use our cleaned cluster galaxy samples to construct a LF for each cluster. To obtain a mean cluster LF in each redshift bin, we stack our clusters. We split our sample at $z = 0.6$ and plot the mean high and intermediate redshift LFs in Figure 2. We determine the brightening of our LFs with respect to the local mean cluster LF from 2dF by fitting with a Schechter function keeping α fixed at the 2dF value of -1.28 and marginalising over the normalization. This results in derived brightenings of $\Delta M_{b_J} = -1.05 \pm 0.17$ at $\langle z \rangle \approx 0.5$ and $\Delta M_{b_J} = -1.21 \pm 0.14$ at $\langle z \rangle \approx 0.75$. This can be compared to the brightening predicted by changing M/L values of ellipticals (van Dokkum & Stanford, 2003), $\Delta M_{b_J} = -0.57 \pm 0.05$ at $z = 0.5$ and $\Delta M_{b_J} = -0.86 \pm 0.08$ at $z = 0.75$. It is interesting that we see a fading of the LF which appears *larger* than expected just from the aging of stars in early-type galaxies. It is unclear whether this is due to the inclusion of later types in our sample, or to the fact that recently added galaxies are

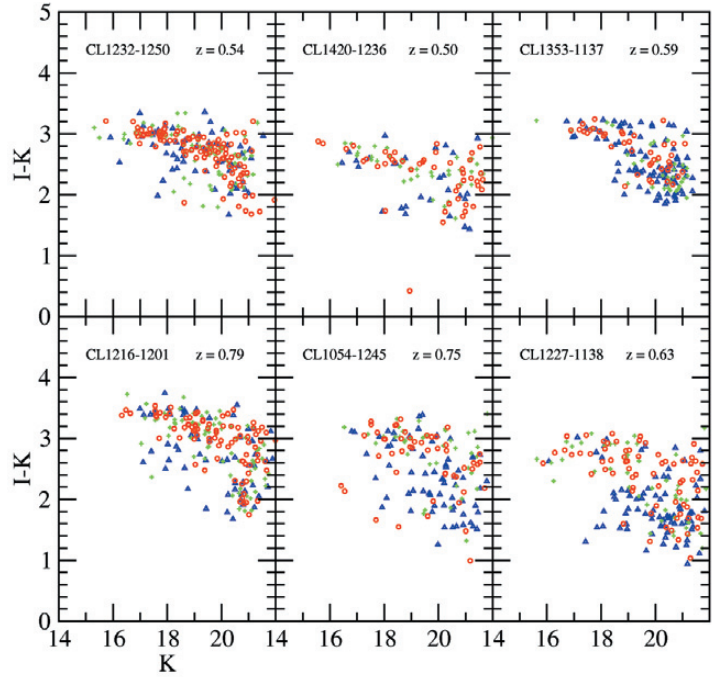
systematically fainter than those already present in clusters at high z .

The Colour-Magnitude Relation and Galaxy Morphology

One powerful characterization of the galaxy population is the joint luminosity-morphology-colour distribution. Different morphological components are thought to have different formation mechanisms and the colour of a galaxy results from a combination of its dust content, its SFH, and its metallicity. Most clusters in the local universe have a dominant population of red galaxies which appear uniformly old. These “red sequence” galaxies are spheroid-dominated, but many of them also have a significant red disc. These may be the transformed remnants of infalling spirals. There is also a small population of blue galaxies in clusters, whose fractional contribution to the cluster light increases with increasing redshift (the so-called “Butcher-Oemler effect”) and whose low redshift descendants are uncertain.

To study how galaxies are affected by the environments in which they reside, it is necessary not only to go backwards in time, but also to probe a range of environments at each epoch. It is in this area where EDISCS excels. Using our “cleaned” cluster samples we can construct optical/NIR colour-magnitude diagrams with galaxies classified by morphology. Examples are shown in Figure 3. Immediately obvious is the large variation in the red sequence strength. The clusters with a strong red sequence still have significant numbers of blue galaxies, however, although the most luminous galaxies are almost always red. These blue galaxies reflect the Butcher-Oemler effect, and we see its cluster-to-

Figure 3: Colour-Magnitude morphology diagrams for six of our intermediate and high redshift clusters. For each cluster, the colour coding of the points indicates bulge-to-total ratio. Blue triangles are galaxies with $B/T < 0.3$, green plus marks are those with $0.3 \leq B/T < 0.6$, and the red circles are those with $B/T > 0.6$. Note the large cluster-to-cluster variation in red sequence strength as well as the large and variable number of disc-dominated galaxies which lie on the red sequence. Figure prepared by Luc Simard.



cluster variation clearly. Another striking trend is for the relative strength of the red sequence to decrease with increasing redshift, along with the ratio of red to blue galaxies at the bright end. Our spectroscopy will show whether these bright blue galaxies are still actively forming stars or if they are “post-starburst” systems, devoid of current star formation. Either way, these blue galaxies must redden with time so that, by lower redshift, the galaxy populations in these clusters resemble those seen in the local universe.

The excellent quality of our deep VLT images makes it possible to undertake detailed morphological studies. Using the GIM2D code we perform bulge-disc decompositions for all galaxies by fitting seeing-convolved models directly to the 2D images. Extensive Monte Carlo simulations (e.g., Simard et al. 2002) have allowed us to assess where the estimated morphological parameters can be trusted and we should robustly determine the bulge-to-total ratios (B/T) and disc scale lengths for the brighter galaxies in all our clusters. First results

are shown in Figure 3, where the different points correspond to different B/T values. At all redshifts, the blue galaxies are predominantly disc-dominated. The red sequence, however, shows a large number of disc-dominated galaxies, even in some of our richest clusters. In a few clusters, the disc-dominated galaxies even dominate the red sequence. What are these galaxies? At the bright end, our spectroscopy should tell us whether they are dominated by an old stellar population or by a dusty

starburst.

Even with the high quality of our FORS2 data, detailed morphological classification at $z \sim 0.6-0.8$ is difficult, especially for structural parameters of the bulge. To improve the quality of our morphological classification at high redshift, we have obtained 80 orbits of Hubble Space Telescope (HST) F814W data using the Advanced Camera for Surveys (ACS) for 10 of our higher redshift clusters. These data are comprised of four one-orbit tiles that cover the

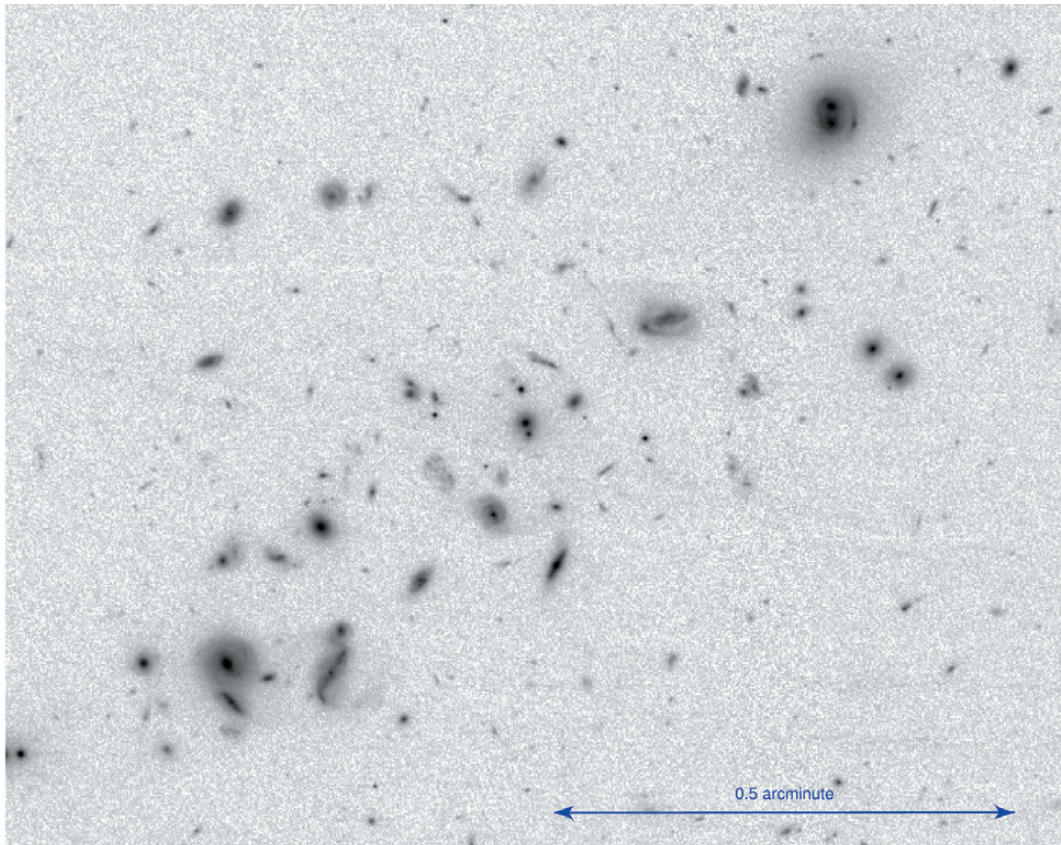
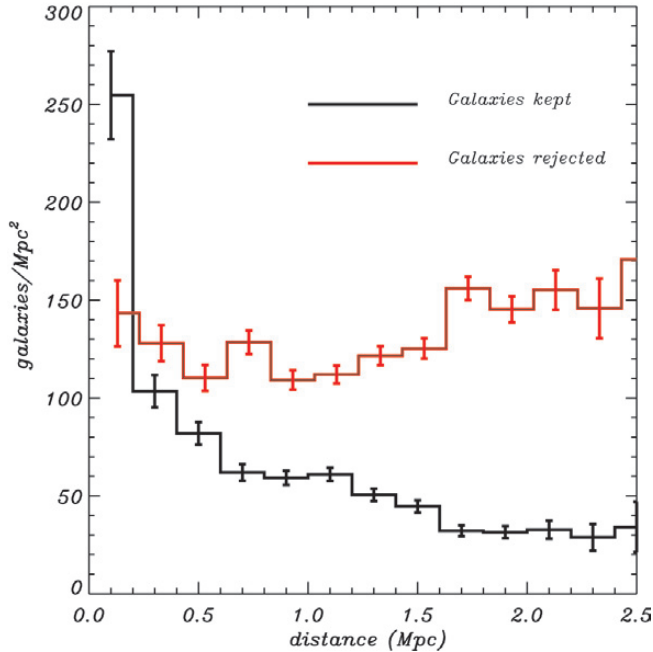


Figure 4: A 5-orbit F814W image of the cluster cl1037-1243 ($z = 0.580$) taken with the Advanced Camera for Surveys (ACS) on board the Hubble Space Telescope (HST). This is one of our lowest redshift candidates imaged with ACS and therefore demonstrates the maximum image detail which we will obtain. The high spatial resolution afforded by these images allows us to measure bulge scale lengths and bulge ellipticities for our highest redshift clusters, as well as to see small-scale structure in many galaxies. By using the ground-based and HST data to constrain the outer and inner regions respectively, we will be able to build a detailed picture of galaxy morphology in our highest redshift clusters. Figure prepared by Vandana Desai.

Figure 5: Stacked radial profile for four clusters with $\langle z \rangle = 0.75$. The black line counts all retained galaxies with $I < 24$, while the red line counts galaxies rejected using photometric redshifts. Note that the rejected galaxies show no concentration to the cluster centre (the residual non-flatness is caused by large-scale structure unassociated with the clusters) while the mean cluster profile is detected significantly to 1.5 Mpc. Figure prepared by Gabriella De Lucia.



same field of view as the deep VLT images, with an additional four orbit central exposure.

A reduced image of the centre of one of the lowest redshift clusters with HST imaging, the cluster cl1037-1243, ($z = 0.58$) is shown in Figure 4. This image, which comprises five orbits of exposure time, already illustrates the wealth of structure visible, including spiral structure and bars. The apparent lack of bright galaxies with elliptical morphology is also quite striking. With these data, we will be able to derive bulge scale lengths and bulge ellipticities even for our highest redshift clusters.

Cluster Structure

In addition to studying the galaxy populations within our clusters, our large dataset also allows us to study the structure of the clusters themselves. To mitigate cluster-to-cluster variations we stack the clusters in a given redshift range and calculate their mean radial profile. Such an average profile can meaningfully be compared to a similarly stacked profile of simulated clusters to evaluate whether the physical processes which influence galaxy properties as a function of clustercentric distance are correctly modelled in the sim-

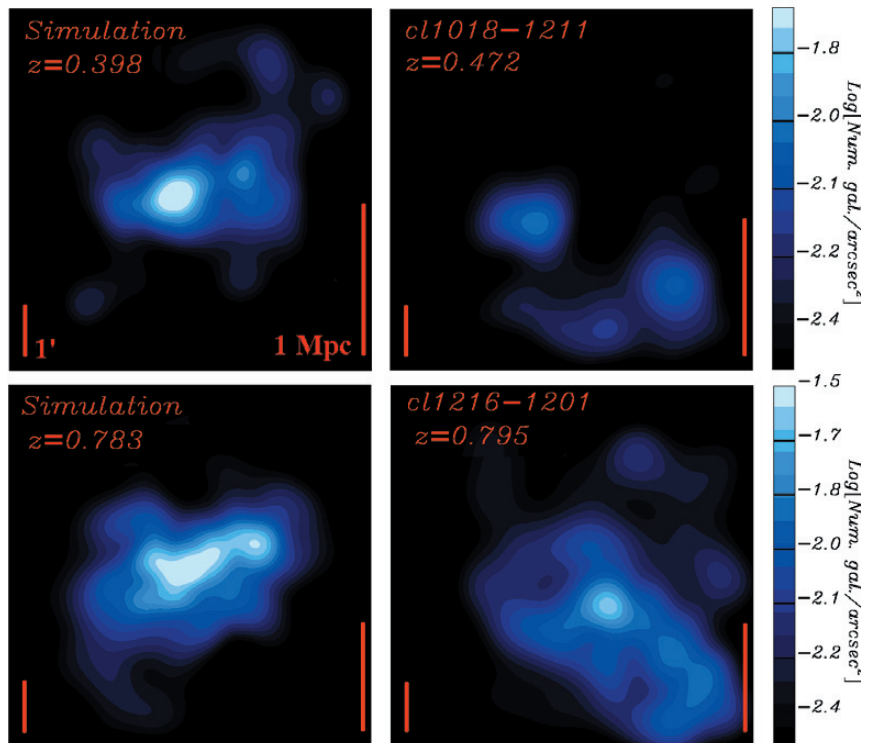
ulations. In Figure 5 we show the stacked density profile from four clusters with $\langle z \rangle = 0.75$. Although the individual cluster profiles can be quite noisy, we clearly detect the mean cluster profile out to 1.5 Mpc.

Our study of cluster structure will not, however, be limited to radial profiles. Using our suite of high-resolution simulations of cluster and cluster galaxy formation, we can compare models and observations statistically in the full, three-dimensional space of observables (projected position on the sky + radial velocity). In Figure 6 we compare the projected galaxy density distribution in two observed clusters with simulations. All density maps were similarly constructed by smoothing the discrete galaxy distribution with an adaptive kernel. The input catalogues correspond to a magnitude-limited sample, and, in the observational case, contain only those galaxies which survived our photometric redshift cut. It is obvious from these plots that the detail of the simulations now matches that of the observations, allowing us to compare the two directly using such “mock” catalogues.

Weak Lensing

The depth and image quality of our VLT imaging is so high that we can detect and measure the shapes of many faint background galaxies lying behind our clusters. Gravitational lensing effects due to the matter within the clusters distort these background images causing a weak but measurable tendency for the principal axes of nearby images to align. Measurements of this effect across an image can be inverted

Figure 6: Projected galaxy density maps smoothed using an adaptive kernel technique. The bottom right panel shows our highest redshift cluster cl1216-1201 ($z = 0.795$) and the top right panel shows the cluster cl1018-1211 ($z = 0.472$). All cluster members at $I < 25$ are used. In both clusters, many non-members have been excluded based on photometric redshifts. The panels on the left show projections of two of our high resolution simulations at similar redshifts to the observed clusters. The galaxies in the simulations are selected over the same projected area, accepting only objects within ± 2000 km/s from the brightest cluster galaxy and applying the same I -band magnitude limit as in the observations. Figure prepared by Gabriella De Lucia.



to obtain a smoothed map of the projected total mass distribution. This can be compared with the projected distribution of cluster light and with the cluster mass inferred using the Virial Theorem and the observed motions of galaxies within the cluster. The precision of such mass estimates from gravitational lensing can be enhanced by using photometric redshifts or colour cuts to isolate galaxies which lie behind the cluster. In Figure 1 we show mass surface density contours derived from a weak lensing analysis overlaid on optical images of four of our clusters. At each redshift we show two clusters, both spectroscopically confirmed to have many members, but only one of which shows a clear lensing signal. These results demonstrate yet again the diversity of our sample, highlighting the need for large datasets to correctly characterize the cluster population. When our spectroscopy is fully reduced we will be able to compare the equivalent “velocity dispersion” derived from lensing to that measured from the galaxy velocities, allowing us to check if the clusters are in a relaxed dynamical state. Deviations from such a state are to be expected, given the evident asymmetry of many of our clusters. Comparison with our simulations will check whether deviations from a relaxed state are at the theoretically predicted level.

Spectroscopic Science

The EDisCS project is also distinguished by the abundance of high quality spectroscopy it is assembling. With these data we will explore in detail the physical characteristics of the ~800 cluster members, together with a greater number of field galaxies. As shown in Figure 7, our data are good enough to measure the internal kinematics of galaxies down to at least $I = 21.5$. With such spectra we will make field-to-cluster comparisons for fundamental plane and Tully-Fisher evolution, we will determine how the stellar populations in elliptical galaxies evolve with time, we will identify active galactic nuclei, star-forming galaxies and “post-starburst” systems, and we will see how the abundance of all such systems varies with redshift and environment. Because our spectroscopic selection samples all morphological types, we can examine the relations between luminosity, mass, and size for disc galaxies and compare these relations in the cluster environment to those in the field at similar redshift, again providing important constraints for models of galaxy evolution. In combination with our photometric SEDs, the spectral range of our observations will allow us to characterize the stellar populations, SFRs, heavy element abundances, and SFHs of our galaxies. In combination with detailed

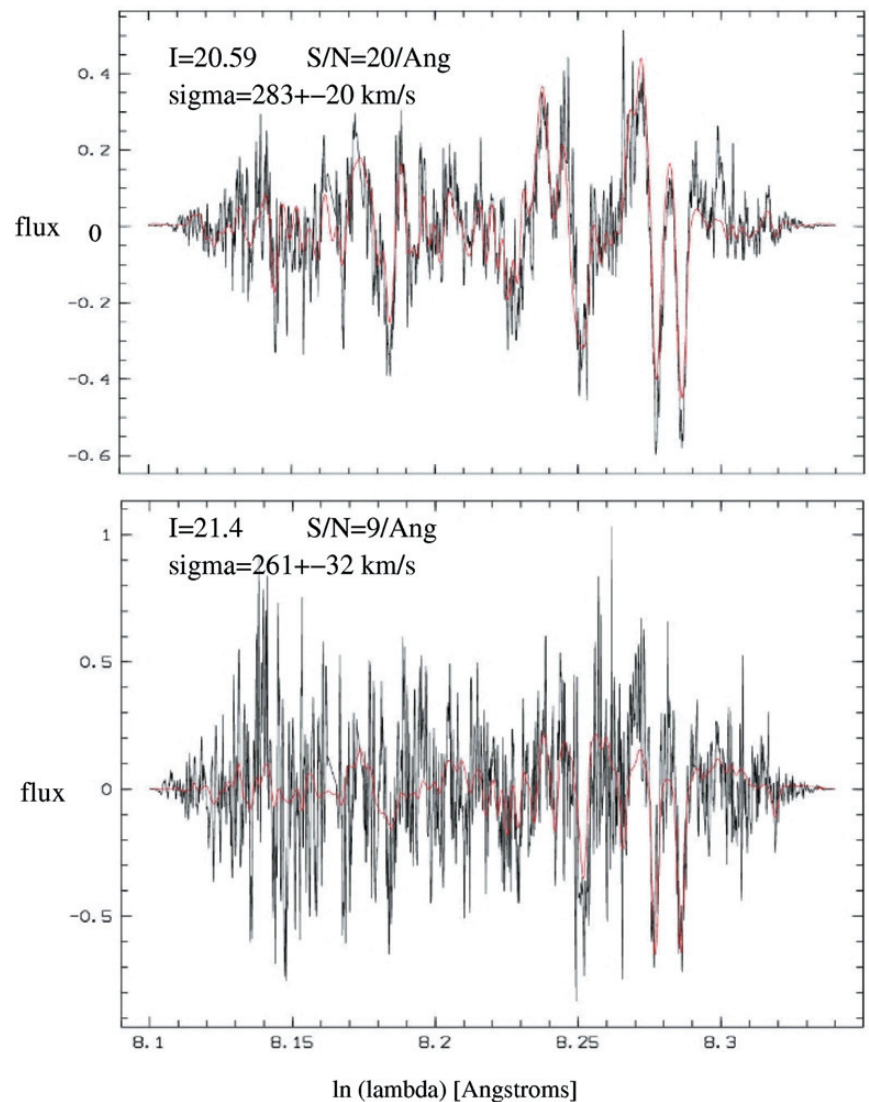


Figure 7: Measures of velocity width for two galaxies in cl1216-1201 at $z = 0.795$. The dark line is the galaxy spectrum with the continuum removed. The red line is the best fit stellar template convolved with the instrumental resolution and a Gaussian velocity dispersion. Using our spectra, we are able to obtain precise velocity dispersion measurements from absorption lines down to $I \sim 21.5$. The instrumental resolution is approx 110 km/s. Figure prepared by Roberto Saglia.

modelling, we will then be able to build up a much clearer picture of how galaxy evolution is driven by internal and environmental processes.

Our programme has shown that the cluster-to-cluster variance in many cluster properties is large. To obtain a picture of the typical clusters as a function of redshift and environment, and to study the scatter in their properties, it is necessary to study many objects in detail. Thanks to our large and homogeneously selected sample and the high quality of the imaging and spectroscopic data provided by ESO facilities, a comparison of the EDisCS dataset to nearby large cluster samples and to detailed theoretical models will substantially improve our understanding of how galaxies have evolved since the universe was half its present age.

References

- Butcher, H. & Oemler, A. 1978, *ApJ*, **219**, 18
- De Propris et al. 2002, submitted to *MNRAS*, astro-ph/0212562
- Dressler, A. 1980, *ApJ*, **236**, 351
- Dressler, A. & Gunn, J. E. 1983, *ApJ*, **270**, 7
- Dubinski, J. 1998, *ApJ*, **502**, 141
- Farouki, R. & Shapiro, S. L. 1981, *ApJ*, **243**, 32
- Gonzalez, A. H., Zaritsky, D., Dalcanton, J. J., & Nelson, A. 2001, *ApJS*, **137**, 117
- Gunn, J. E. & Gott, J. R. I. 1972, *ApJ*, **176**, 1
- Larson, R. B., Tinsley, B. M., & Caldwell, C. N. 1980, *ApJ*, **237**, 692
- Moore, B., Katz, N., Lake, G., Dressler, A., & Oemler, A. 1996, *Nature*, **379**, 613
- Simard, L. et al. 2002, *ApJS*, **142**, 1
- Springel, V., White, S. D. M., Tormen, G., & Kauffmann, G. 2001, *MNRAS*, **328**, 726
- van Dokkum, P. G. & Stanford, S. A. 2003, *ApJ*, **585**, 78
- White, S. D. M. 1976, *MNRAS*, **174**, 19

SPY – The ESO Supernovae Type Ia Progenitor Survey

R. NAPIWOTZKI¹, N. CHRISTLIEB², H. DRECHSEL¹, H.-J. HAGEN², U. HEBER¹,
 D. HOMEIER⁴, C. KARL¹, D. KOESTER³, B. LEIBUNDGUT⁵, T.R. MARSH⁶,
 S. MOEHLER³, G. NELEMANS⁷, E.-M. PAULI¹, D. REIMERS², A. RENZINI⁵,
 L. YUNGELSON⁸

¹Dr. Remeis-Sternwarte, Universität Erlangen-Nürnberg, Bamberg, Germany; ²Hamburger Sternwarte, Hamburg, Germany; ³Institut für Theoretische Physik und Astrophysik, Universität Kiel, Germany; ⁴Department of Physics & Astronomy, University of Georgia, USA; ⁵European Southern Observatory, Garching, Germany; ⁶Department of Physics & Astronomy, University of Southampton, UK; ⁷Institute of Astronomy, Cambridge, UK; ⁸Institute of Astronomy of the Russian Academy of Sciences, Moscow, Russia

Supernovae and their progenitors

Supernovae (SNe) mark the violent termination of a star's life in an explosion. They are classified according to their light curve as type I or II, with the type I SNe producing very similar light curves, while the SNe type II are more diverse. Spectroscopic observations reveal the presence of hydrogen in SNe type II, while no hydrogen lines are detectable in SNe type I. According to their spectral appearance the type I class can be further subdivided into Ia, Ib, and Ic.

SNe type II and Ib,c are observed only in spiral galaxies and irregular galaxies containing young stellar populations. This indicates that their progenitors are short-lived massive stars (masses above $8 M_{\odot}$). Indeed, the occurrence of SN explosions and the formation of a neutron star remnant at the end of the nuclear lifetime of a massive star are now relatively well understood processes.

However, the question of SN Ia progenitors is not yet settled (e.g. Livio

2000). SN Ia are observed in all types of galaxies, including elliptical galaxies containing only old stellar populations. The light curves of SN Ia are dominated by the decay of the radioactive material synthesized in the explosion (mainly nickel). The ^{56}Ni isotope sits at the top of a decay chain leading to ^{56}Co (half-life 6.1 days) and to stable ^{56}Fe (half-life 77 days). The rapid evolution of SN Ia light curves indicates that the precursors of these supernovae must be compact objects of small mass with very little mass holding back the gamma-rays produced by the radioactive decay. The only candidate, which can fulfill the observational constraints, is the thermonuclear explosion of a white dwarf.

Since type Ia supernovae were identified as excellent distance indicators for cosmology and have provided indications of cosmic acceleration, it is extremely important to have a better understanding of their explosions and the systems that lead up to them. While it is possible to test the quality of the distance indicator in the nearby universe by checking the linear Hubble expansion, one has to rely on the accuracy of the distance indicator to go beyond the linear Hubble flow and probe the redshift regime, where the cosmological models differ in their predictions. At this point, other signatures of the reliability of the distance indicator have to be secured. With lookback times of about half

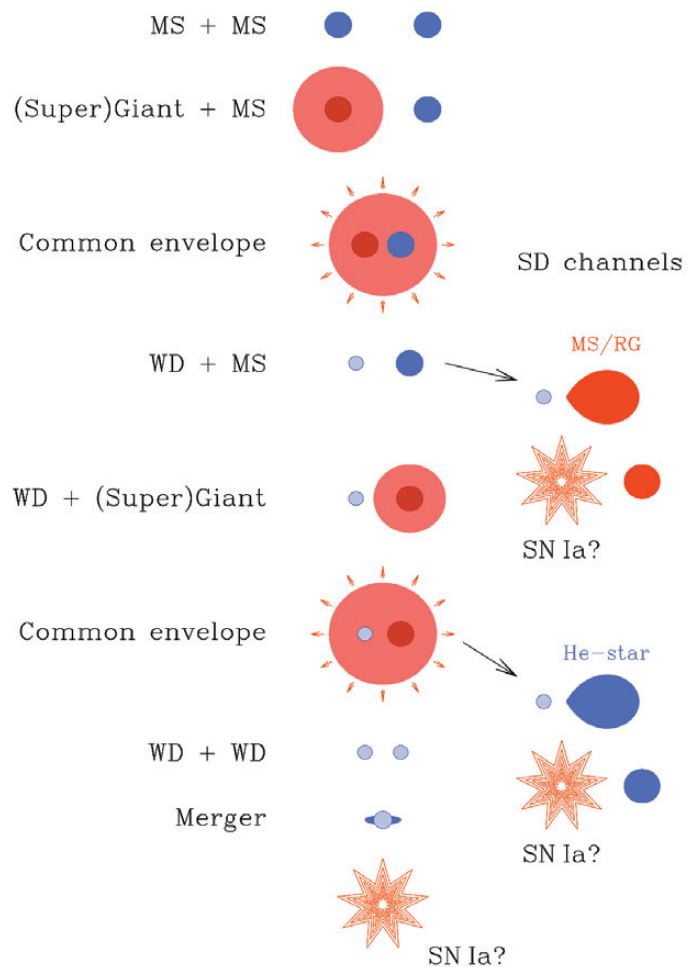


Figure 1: Possible evolutionary channels for the formation of a SN Ia progenitor via the double degenerate (DD) and the single degenerate (SD) scenarios. In both scenarios the evolution starts with a binary of two main sequence (MS) stars. The more massive star becomes a red giant and its envelope is ejected in a common envelope event. In the DD scenario the second MS star evolves to a red giant with a second common envelope event and the formation of a close binary of two white dwarfs (WD). If the DD system is close enough and massive enough, gravitational wave radiation will cause it to merge and explode as a SN Ia. In the two variants of the SD scenario the secondary fills its Roche lobe while i) close to the main sequence or as red giant (RG) or ii) as a He-star after another common envelope phase. Mass is transferred onto the WD star and increases the WD mass until the Chandrasekhar limit is reached. Note that the SD scenarios predict the survival of the companion star.

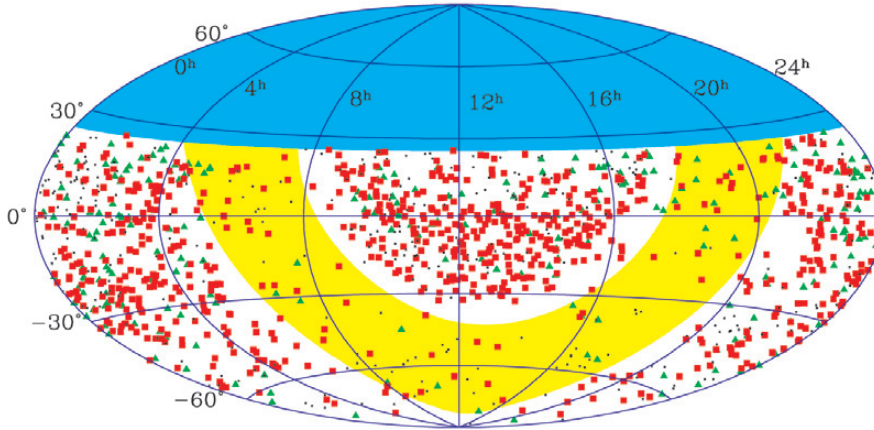


Figure 2: Distribution of all known white dwarfs south of $\delta = +25^\circ$ and brighter than $V = 16.5$. Red squares indicate white dwarfs with two spectra taken by SPY. A second spectrum remains to be collected for the green triangles, while the black dots are the remaining objects without a SPY observation. The yellow band indicates the position of the Galactic disk ($|b| < 20^\circ$).

the current age of the universe, one has to make sure that evolution of the distance indicator is not mimicking a cosmological effect. To do this reliably one has to try to understand the distance indicator in as many aspects as possible. One of the shortcomings of type Ia supernovae is our ignorance of the progenitor systems and the exact explosion mechanism. By identifying these progenitors we should be able to constrain possible evolutionary effects on the cosmological result.

While the cosmic microwave background experiments have provided a phenomenal accuracy of the integrated cosmological parameters, they cannot provide the more detailed measurements to explore the expansion history of the universe, i.e. the equation of state parameter. Only distance indicators, like type Ia supernovae, can yield this information. But the systematics of these derivations have to be assessed as precisely as possible. The knowledge of the precursor state and the physics of the transformation to the supernova are hence vital ingredients for our understanding of cosmology.

Most stars (i.e. all stars with a mass below about 8 solar masses) will end their lives as white dwarfs. These are small cooling bodies consisting mainly of carbon and oxygen with thin layers of hydrogen and/or helium on top, supported by degenerate electron gas. They will cool for billions of years and disappear as small cold clumps into the cosmic background without signs of their once glorious lives. Some white dwarfs will, however, destroy themselves in a gigantic thermonuclear explosion. To do so, they have to be forced into a density and temperature regime, where carbon and oxygen burn explosively and disrupt the star. Above the Chandrasekhar mass ($1.4 M_\odot$) the electron degeneracy can no longer support white dwarfs. At this point the white dwarf either has to collapse to a neutron star or explode as a supernova. Since

no physical process is known which leads to such conditions in a single white dwarf, a companion star has to help. This general picture of binary white dwarfs as the progenitor stars for type Ia supernovae is the most commonly held view today.

The growth of a white dwarf to Chandrasekhar mass is a long-standing problem of observational astrophysics. Several channels have been identified as possibly yielding such a critical mass (Fig. 1). They can broadly be grouped into two classes (e.g. Livio 2000). The single degenerate (SD) channel in which the white dwarf is accompanied by a regular star, either a main se-

quence star, a (super)giant, or a helium star, as mass donor and the double degenerate (DD) channel where the companion is another white dwarf. Close DDs radiate gravitational waves, which results in a shrinking orbit due to the loss of energy and angular momentum. If the initial separation is close enough (orbital periods below 10 h), a DD system could merge within a Hubble time, and if the combined mass exceeds the Chandrasekhar limit the DD would qualify as a potential SN Ia progenitor.

The double degenerate scenario for the progenitors was proposed many years ago. So far, no SN Ia progenitor has been identified, which is not really

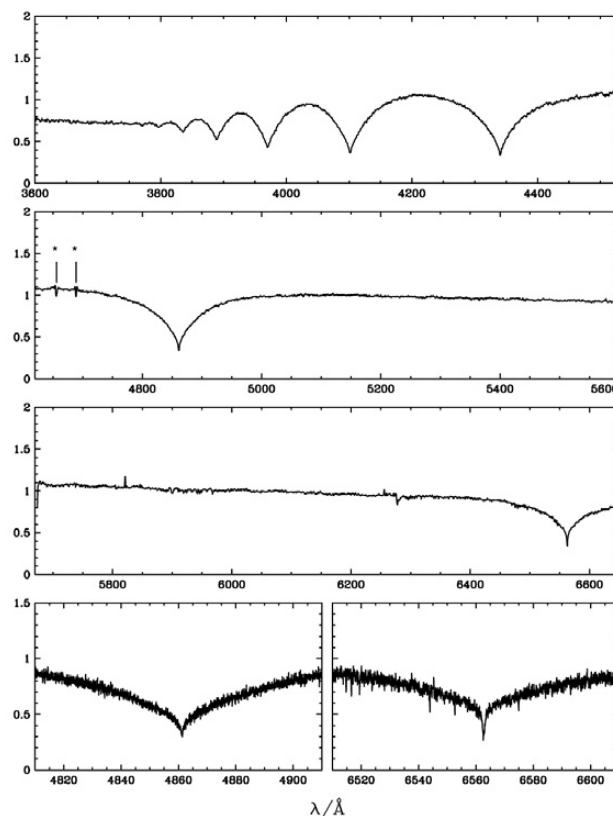


Figure 3: UVES spectrum of the DA white dwarf WD 1026+023. The upper three panels correspond to the blue channel and to both parts of the red channel covered by different CCDs. The spectra were smoothed to a resolution of 1 \AA . Two reduction artifacts are indicated by asterisks. The lower panel shows the unbinned spectra of the $H\alpha$ and $H\beta$ line cores.

surprising considering the rareness of SNe Ia and the small volume that can be surveyed for white dwarfs. The orbital velocity of white dwarfs in potential SN Ia progenitor systems must be large (>150 km/s) making radial velocity (RV) surveys of white dwarfs the most promising detection method. Several systematic RV searches for DDs were undertaken starting in the mid 1980's. Before 2001, combining all the surveys, ~ 200 white dwarfs were checked for RV variations with sufficient accuracy yielding 18 DDs with periods $P < 6.3$ d (Marsh 2000 and references therein). None of the 18 systems seems massive enough to qualify as a SN Ia precursor. This is not surprising, as theoretical simulations suggest that only a few percent of all DDs are potential SN Ia progenitors (Iben, Tutukov & Yungelson 1997; Nelemans et al. 2001). It is obvious that larger samples are needed for statistically significant tests.

The surveys mentioned above were performed with 3–4-m class telescopes. A significant extension of the sample size without the use of larger telescopes would be difficult due to the limited number of bright white dwarfs. This situation changed after the ESO VLT became available. In order to perform a definitive test of the DD scenario we have embarked on a large spectroscopic survey of more than 1000 white dwarfs using the UVES spectrograph at the UT2 telescope (Kueyen) of VLT to search for RV variable white dwarfs (ESO SN Ia Progenitor survey – SPY). SPY will overcome the main limitation of all efforts so far to detect DDs that are plausible SN Ia precursors: the samples of surveyed objects were too small.

The survey

As outlined above, we need a very large input sample of white dwarfs, which are bright enough ($B \leq 16.5$) to take high-resolution spectra with a sufficiently high signal-to-noise ratio. The most complete catalogue of spectroscopically confirmed white dwarfs is the actual version of the McCook & Sion (1999) catalogue. However, it contains “only” 918 white dwarfs brighter than $B = 16.5$ south of $\delta = +25^\circ$. Since we needed a larger input sample, we added more objects from recent surveys: the *Hamburg-ESO survey (HES)*, the *Hamburg-Quasar survey (HQS)*, the *Montreal-Cambridge-Tololo survey (MCT)*, and the *Edinburgh-Cape survey (EC)*. A map of all known white dwarfs (observed and unobserved by SPY) fulfilling our criteria is shown in Fig. 2. A striking feature is a lack of white dwarfs in the Galactic plane. This cannot be explained by interstellar extinction, because bright white dwarfs are nearby objects. However, all major surveys during the last decades (including the surveys mentioned above) were aimed at

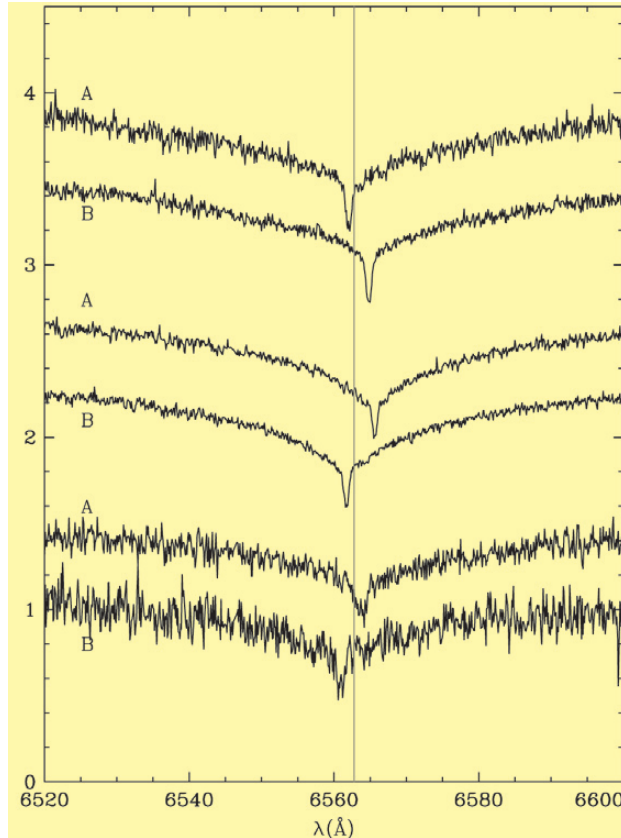


Figure 4: Three single-lined RV variable DDs from our VLT survey. The vertical line marks the rest wavelength of $H\alpha$. The spectra are slightly rebinned (0.1 \AA) without degrading the resolution.

the detection of galaxies and quasars and restricted to high Galactic latitudes.

Spectra were taken with the UV-Visual Echelle Spectrograph (UVES) of the UT2 telescope (Kueyen) of the ESO VLT. UVES is a high resolution Echelle spectrograph, which can reach a resolution of 110,000 in the red region with a narrow slit. Our instrument set-up (Dichroic 1, central wavelengths 3900 Å and 5640 Å) uses UVES in a dichroic mode. Nearly complete spectral coverage from 3200 Å to 6650 Å with only two roughly 80 Å wide gaps at 4580 Å and 5640 Å is achieved.

Our programme was implemented as a large programme in service mode. It takes advantage of those observing conditions, which are not usable by most other programmes (moon, bad seeing, clouds) and keeps the VLT busy when other programmes are not feasible. A wide slit (2.1") is used to minimize slit losses and a 2×2 binning is applied to the CCDs to reduce read out noise. Our wide slit reduces the spectral resolution to $R = 18,500$ (0.36 \AA at $H\alpha$) or better, if seeing discs were smaller than the slit width. Depending on the brightness of the objects, exposure times between 5 min and 10 min were chosen. The S/N per binned pixel (0.03 \AA) of the extracted spectrum is usually 15 or higher. Due to the nature of the project, two spectra at different, “random” epochs separated by at least one day are observed.

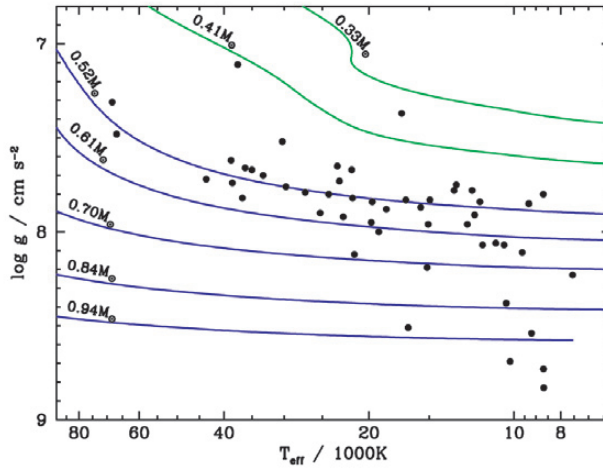
ESO provides a data reduction pipeline for UVES, based on MIDAS procedures. The quality of the reduced

spectra is in most cases very good; especially the removal of the interorder sensitivity variation and merging of the orders works very well. Sometimes the reduction pipeline produces artifacts of varying strength, e.g. a quasiperiodic pattern in the red region similar in appearance to a fringing pattern. In a few cases either the blue or the red part of the spectrum has extremely strong artifacts of unknown origin. This pipeline reduction was extremely useful for a fast selection of RV variable DDs for follow-up observations (described below). In the meantime we have produced a semi-automatic set of procedures for the reduction of our UVES spectra. A reduction of the survey data is already completed and yielded a large set of good quality white dwarf spectra.

As an example of the quality achievable the spectrum of a hydrogen-rich DA white dwarf is shown in Fig. 3. A characteristic feature of white dwarfs are the very broad spectral lines caused by the high densities in their atmospheres. Obviously, broad lines are very ill-suited for RV measurements. However, deviations from local thermal equilibrium (LTE) produce sharp NLTE cores of the $H\alpha$ lines in the atmospheres of hydrogen-rich DA white dwarfs (Fig. 3), which allow accurate RV measurements. This feature is not present in non-DA white dwarfs (spectral types DB, DO) with hydrogen-poor atmospheres, but the use of several helium-lines enables us to reach a similar accuracy.

Since SPY produces a large number

Figure 5: Mass determination of (single and binary) DA white dwarfs. Temperature and gravity, determined from a model atmosphere analysis of the UVES spectra (Koester et al., 2001) are compared to cooling sequences of white dwarfs (Blöcker et al., 1997) for a range of white dwarf masses.



of spectra, which have to be checked for RV variations, a fast and reliable algorithm to measure RV shifts is necessary. We apply a “cross-correlation” routine based on a χ^2 test (description in Napiwotzki et al. 2001). The RV shift is evaluated from the minimum χ^2 . Error margins can be estimated from the χ^2 statistics as well. One great advantage of our procedure is its flexibility and that it can easily be applied to measure RV shifts in stars of different spectral types (Balmer lines of DA white dwarfs, H α lines of DBs, H α and metal lines of hot DO white dwarfs). We routinely measure RVs with an accuracy of about 2 km/s, therefore running only a very small risk of missing a merger precursor, which have orbital velocities of 150 km/s or higher.

The large programme was finished at the end of last semester. A total of 1014 stars were observed (Fig. 2). This corresponds to 75% of the known white dwarfs accessible by VLT and brighter than $B=16.5$. A second spectrum is still lacking for 242 white dwarfs, but time has been granted to complete these observations. Currently we could check 772 stars for RV variations, and detected 121 new DDs, 16 are double-lined systems (only 6 were known before). The great advantage of double-lined binaries is that they provide us with a well determined total mass. Since it is likely that the SPY sample contains even more double-lined systems (with a faint secondary), we will check follow-up observations of apparently single-lined systems for the signature of the sec-

Figure 6: Periods (P) and system masses (M_{total}) determined from follow-up observations of DDs from SPY. Results for double-lined systems (black circles) are compared to previously known systems (green circles). The other DD systems are single-lined (triangles: WD primaries; diamonds: sdB primaries). The masses of the unseen companions are estimated from the mass function for the expected average inclination angle ($i = 52^\circ$).

ondary. Our sample includes many short period binaries (some examples are discussed in the next section), several with masses closer to the Chandrasekhar limit than any system known before. In addition, we detected 19 RV variable systems with a cool main sequence companion (pre-cataclysmic variables; pre-CVs). Some examples of single-lined and double-lined DDs are shown in Fig. 4 and 7. Our observations have already increased the DD sample by a factor of seven. After completion, a final sample of about 150 DDs is expected.

Follow-up observations of this sample are mandatory to exploit its full potential. Periods and white dwarf parameters must be determined to find potential SN Ia progenitors among the candidates. Good statistics of a large DD sample will also set stringent constraints on the evolution of close binaries, which will dramatically improve our understanding of this phase of stellar evolution. During our follow-up observa-

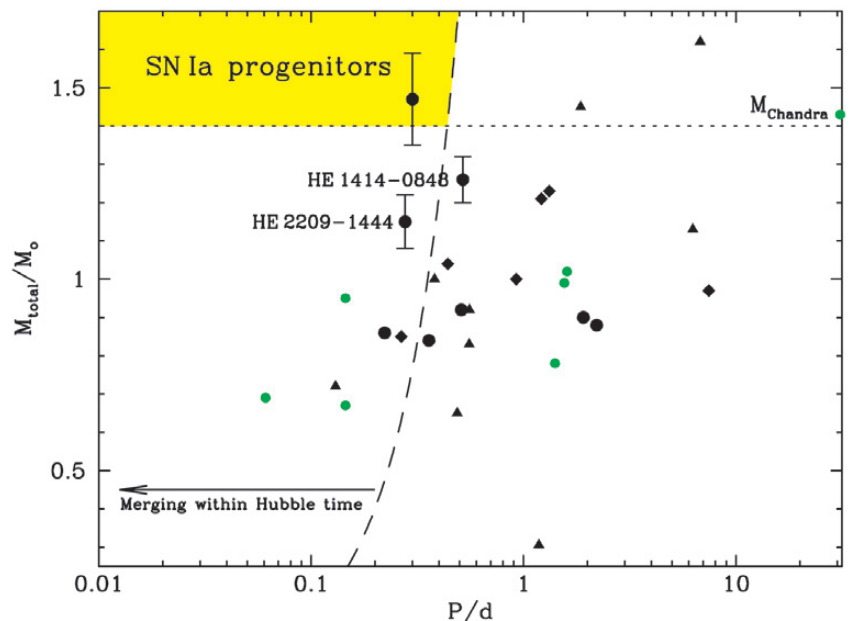
tions we have detected a very promising potential SN Ia precursor candidate. However, some additional observations are necessary to verify our RV curve solution.

Although important information like the periods, which can only be derived from follow-up observations, are presently lacking for most of the stars, the large sample size already allows us to draw some conclusions. (Note that fundamental white dwarf parameters like masses are known from the spectral analysis described below). One interesting aspect concerns white dwarfs of non-DA classes (basically the helium-rich spectral types DB, DO, and DZ, in contrast to the hydrogen-rich DAs). SPY is the first RV survey which performs a systematic investigation of both classes of white dwarfs: DAs and non-DAs. Previous surveys were restricted to DA white dwarfs. Our result is that the binary frequency of the non-DA white dwarfs is equal to the value determined for the DA population within the statistical accuracy.

Parameters of double degenerates

Once the binaries in the white dwarf sample have been revealed, follow-up observations are necessary to determine the system parameters of the DDs. We concentrated on candidates with high RV variations, indicating short periods, because the probability to find potential SN Ia candidates is highest among these systems. However, let us note that probably some of the “small RV” DDs could be short period systems (possibly even SN Ia progenitors) with low inclination angles and/or unfavourable phase differences of the SPY observations.

The secondary of most DD systems



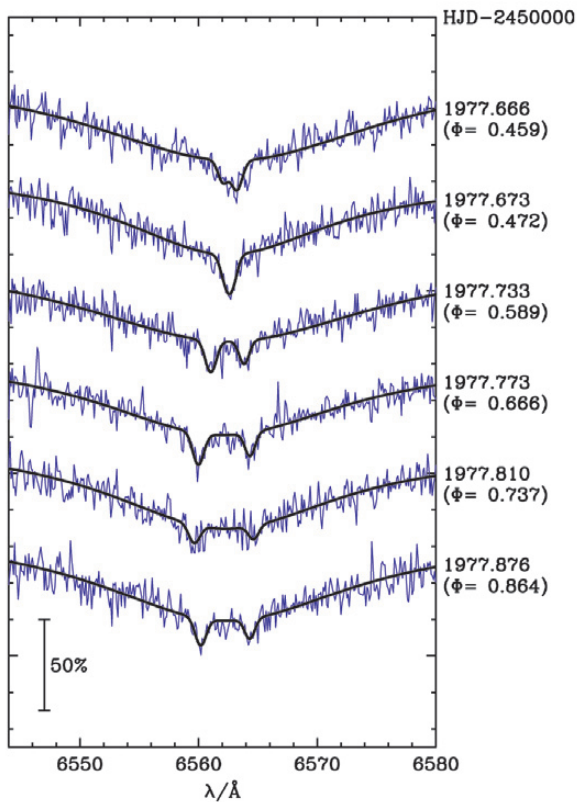


Figure 7: $H\alpha$ spectra of HE 1414-0848 covering 5 hours during one night together with a fit of the line cores. The numbers indicate the Julian date of the exposures and the orbital phase ϕ .

has already cooled down to invisibility. These DDs are single-lined spectroscopic binaries (SB1). Our spectroscopic follow-up observations allow us to determine the orbit of the primary component (i.e. the period P and the radial velocity amplitude K_1). The mass of the primary M_1 is known from a model atmosphere analysis (Fig. 5). Constraints on the mass of the secondary M_2 can be derived from the mass function: $M_2^3 \sin^3 i / (M_1 + M_2)^2 = K_1^3 P / (2\pi G)$. (1)

For a given inclination angle i the mass of the secondary can be computed. However, i is rarely known, but the result for $i = 90^\circ$ yields a lower mass limit. For a statistical analysis it is useful to adopt the most probable inclination $i = 52^\circ$. We have plotted the single-lined systems with the resulting system mass in Fig. 6. Note that two binaries have probably combined masses in excess of the Chandrasekhar limit. However, the periods are rather long preventing merging within a few Hubble times.

Sometimes spectral features of both DD components are visible (Fig. 7), i.e. these are double-lined spectroscopic binaries (SB2). As an example for other double-lined systems we discuss here the DA+DA system HE1414-0848 (Napiwotzki et al. 2002). On one hand the analysis is complicated for double-lined systems, but on the other hand the spectra contain more information than

spectra of single-lined systems. The RVs of both white dwarfs can be measured, and the orbits of both individual components can be determined (Fig. 8). For our example HE1414-0848 we derived a period of $P=12^h25^m44^s$ and semi-amplitudes $K_1 = 127$ km/s and $K_2 = 96$ km/s. The ratio of velocity amplitudes is directly related to the mass ratio of both components:

$$M_2 / M_1 = K_1 / K_2 = 1.28 \pm 0.02. \quad (2)$$

However, additional information is needed before the absolute masses can be determined. There exist two options to achieve this goal in double-lined DDs. From Fig. 8, it is evident that the “system velocities” derived for components 1 and 2 differ by 14.3 km/s, much more than naively expected from the error bars. However, this is easily explained by the mass dependent gravitational redshift of white dwarfs, $z = GM/(Rc^2)$.

This offers the opportunity to determine masses of the individual white dwarfs in double-lined DDs. For a given mass-radius relation (e.g. from the cooling sequences plotted in Fig. 5) gravita-

tional redshifts can be computed as a function of mass. Since the mass ratio is given by Eq. 2, only one combination of masses can fulfil both constraints. In the case of HE1414-0828 we derived individual masses $M_1 = 0.55 \pm 0.03 M_\odot$ and $M_2 = 0.71 \pm 0.03 M_\odot$. The result for HE1414-0848 did not depend much (deviations not larger than $0.01 M_\odot$) on the particular choice of a mass-radius relation. The sum of both white dwarf masses is $M = 1.26 \pm 0.06 M_\odot$. Thus HE1414-0848 is a massive DD with a total mass only 10% below the Chandrasekhar limit.

If double-lined systems contain white dwarfs of low mass and/or similar mass the gravitational redshift differences are very small and this method cannot be used to determine absolute masses. Another method, which works in these cases as well, are model atmosphere analyses of the spectra to determine the fundamental parameters effective temperature and surface gravity, $g = GM/R^2$, of the stars. Because the HE1414-0848 system is double-lined the spectra are a superposition of both individual white dwarf spectra. A direct approach would be to disentangle the observed spectra by deconvolution techniques into the spectra of the individual components. Then we could analyse the spectra by fitting synthetic spectra developed for single-lined white dwarfs to the individual line profiles. Such procedures were successfully applied to main sequence double-lined binaries. However, they have not been tested for white dwarfs, for which the wavelength shifts caused by orbital motions are much smaller than the line

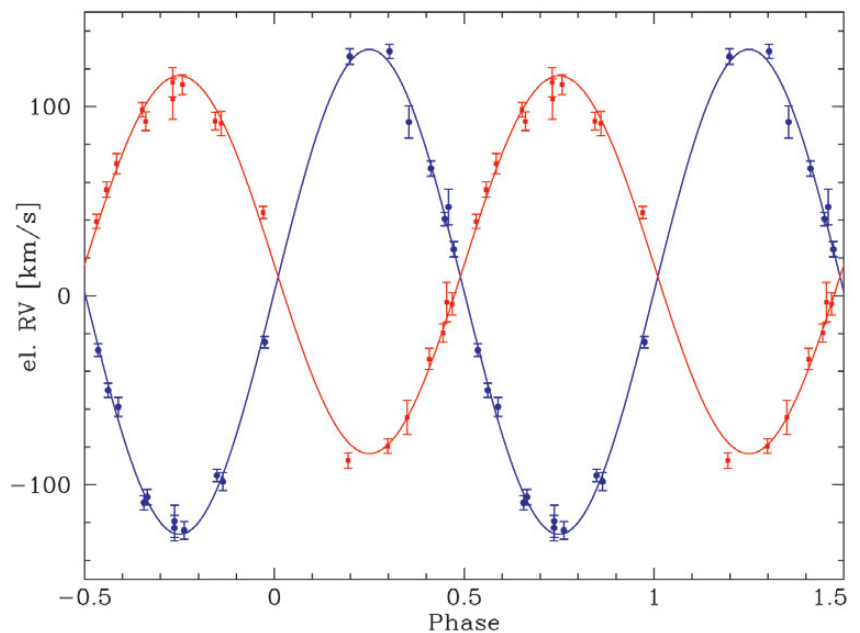


Figure 8: Measured RVs as a function of orbital phase and fitted sine curves for HE 1414-0848. Blue circles/red rectangles indicate the less/more massive component. Note the difference of the “system velocities” γ_0 between both components caused by gravitational redshift.

widths of the broad Balmer lines. Therefore we choose a different approach for our analysis of double-lined DD systems. We used the programme FITSB2, which performs a spectral analysis of both components of double-lined systems. It is based on a χ^2 minimization technique using a simplex algorithm. The fit is performed on all available spectra covering different spectral phases simultaneously, i.e. all available spectral information is combined into the parameter determination procedure.

The total number of fit parameters (stellar and orbital) is high. Therefore we fixed as many parameters as possible before performing the model atmosphere analysis. We have kept the radial velocities of the individual components fixed according to the radial velocity curve. Since the mass ratio is already accurately determined from the radial velocity curve we fixed the gravity ratio. The remaining fit parameters are the effective temperatures of both components and the gravity of the primary. The gravity of the secondary is adjusted according to the primary value during the fitting procedure. The surface gravities also determine the relative weight of the two model spectra from the radius, obtained from mass-radius relations. The flux ratio in the V-band is calculated from the actual parameters and the model fluxes are scaled accordingly. The individual contributions are updated consistently as part of the iteration procedure.

The results for HE1414-0848 are $T_{\text{eff}}/\log g = 8380 \text{ K}/7.83$ and $10900 \text{ K}/8.14$ for components 1 and 2. A sample fit is shown in Fig. 9. The derived $\log g$ values are in good agreement with the values corresponding to the masses derived from the RV curves: $\log g = 7.92$ and 8.16 , respectively.

We have plotted HE1414-0848 as well as our other results on double-lined systems in Fig. 6. Note that one double-lined system is probably a SN Ia progenitor. However, the RV curve of the hotter component is very difficult to measure causing the large error bars. Observing time with the far-UV satellite FUSE has been allocated, which will enable us to measure more accurate RVs.

Concluding remarks

The large programme part of SPY has now been completed with some observations underway to complete the observations of the white dwarfs with only one spectrum taken during the survey. We increased the number of white dwarfs checked for RV variability from 200 to 1000 and multiplied the number of known DDs by a factor of seven (from 18 to 139) compared to the results achieved during the last 20 years. Our sample includes many short period binaries (Fig. 6), several with masses

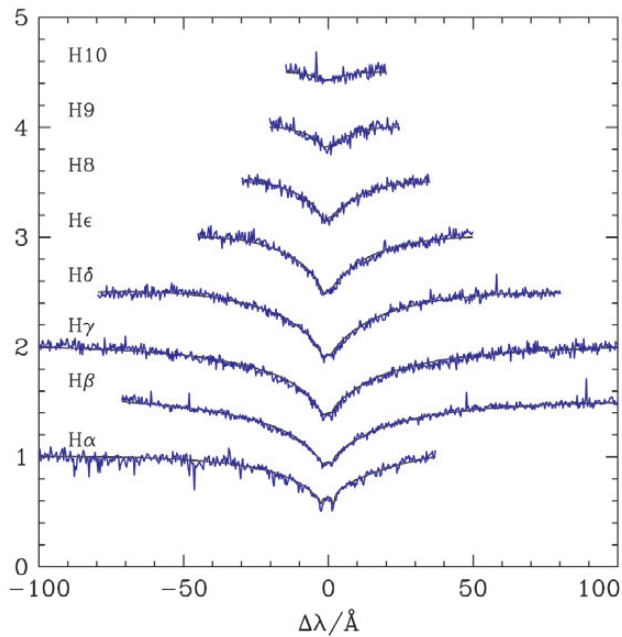


Figure 9: Model atmosphere fit of the Balmer series of HE 1414-0848 with FITSB2. This is only a sample fit. All available spectra, covering different orbital phases, were used simultaneously.

closer to the Chandrasekhar limit than any system known before, greatly improving the statistics of DDs. We expect this survey to produce a sample of about 150 DDs.

This will allow us not only to find several of the long sought potential SN Ia precursors (if they are DDs), but will also provide a census of the final binary configurations, hence an important test for the theory of close binary star evolution after mass and angular momentum losses through winds and common envelope phases, which are very difficult to model. An empirical calibration provides the most promising approach. A large sample of binary white dwarfs covering a wide range in parameter space is the most important ingredient for this task.

Our ongoing follow-up observations already revealed the existence of three short period systems with masses close to the Chandrasekhar limit, which will merge within 4 Gyrs to two Hubble times. Even if it will finally turn out that the mass of our most promising SN Ia progenitor candidate system is slightly below the Chandrasekhar limit, our results already allow a qualitative evaluation of the DD channel. Since the formation of a system slightly below Chandrasekhar limit is not very different from the formation of a system above this limit, the presence of these three systems alone provides evidence (although not final proof) that potential DD progenitors of SN Ia do exist.

Spin-off results

SPY produces an immense, unique sample of very high resolution white dwarf spectra. This database will have a large impact on many fields of white dwarf science. It will allow us for the first

time to tackle many longstanding questions on a firm statistical basis. Among those are the mass distribution of white dwarfs, the kinematical properties of the white dwarf population, surface compositions, luminosity function, rotational velocities, and detection of weak magnetic fields. A first part of the SPY sample was published in a recent paper of Koester et al. (2001), covering observations of about 200 white dwarfs of spectral types DA and DB. For all spin-off opportunities mentioned above the statistics will be dramatically improved by the final white dwarf spectra database. We are exploiting the SPY sample for two spin-off projects, which take advantage of the high spectral resolution: the kinematics of white dwarfs (Pauli et al. 2003) and their rotational velocities. A more detailed description of ongoing spin-off activity is given in Napiwotzki et al. (2001).

References

- Blöcker, T., Herwig, F., Driebe, T., Bramkamp, H., Schönberner D. 1997, in: White dwarfs, eds. J. Isern, M. Hernanz, E. Garcia-Berro, Kluwer, Dordrecht, p.57
- Iben, I. Jr., Tutukov, A. V., Yungelson, L. R., 1997, *ApJ*, **475**, 291
- Koester, D., Napiwotzki, R., Christlieb, N., et al., 2001, *A&A*, **378**, 556
- Livio, M., 2000, in: "Type Ia Supernovae: Theory and Cosmology", Cambridge Univ. Press, p. 33
- Marsh, T. R., 2000, *NewAR*, **44**, 119
- McCook, G. P., Sion, E. M., 1999, *ApJS*, **121**, 1
- Napiwotzki, R., Christlieb, N., Drechsel, H., et al. 2001, *AN*, **322**, 201
- Napiwotzki, R., Koester, K., Nelemans, G., et al., 2002, *A&A*, **386**, 957
- Nelemans, G., Yungelson, L. R., Portegies Zwart, S. F., Verbunt, F., 2001, *A&A*, **365**, 491
- Pauli, E.-M., Napiwotzki, R., Altmann, M. et al., 2003, *A&A*, **400**, 877

Abundances in Globular Cluster Dwarfs

R.G. GRATTON¹, P. BONIFACIO², A. BRAGAGLIA³, E. CARRETTA¹, V. CASTELLANI⁴,
M. CENTURION², A. CHIEFFI⁵, R. CLAUDI¹, G. CLEMENTINI³, F. D'ANTONA⁶,
S. DESIDERA^{1,7}, P. FRANCOIS⁸, F. GRUNDAHL⁹, S. LUCATELLO^{1,7}, P. MOLARO²,
L. PASQUINI⁸, C. SNEDEN¹⁰, F. SPITE¹¹, O. STRANIERO¹², M. ZOCCALI⁸

¹Osservatorio Astronomico di Padova, INAF, Italy; ²Osservatorio Astronomico di Trieste, INAF, Italy; ³Osservatorio Astronomico di Bologna, INAF, Italy; ⁴Dipartimento di Fisica, Università di Pisa, Italy; ⁵Istituto di Astrofisica Spaziale, CNR, Italy; ⁶Osservatorio Astronomico di Roma, INAF, Italy; ⁷Dipartimento di Astronomia, Università di Padova, Italy; ⁸European Southern Observatory; ⁹Department of Astronomy, University of Aarhus, Denmark; ¹⁰The University of Texas at Austin, USA; ¹¹Observatoire de Meudon, France; ¹²Osservatorio Astronomico di Collurania, INAF, Italy

Globular Clusters are huge, very compact aggregates of hundreds of thousands of stars (see Figure 1). There are about 150 such systems in our Galaxy, the closest being about 10,000 light years from us; some of them are visible with the naked eye (ω Centauri, 47 Tucanae), and many others are spectacular objects visible with small telescopes.

Globular Clusters play an important role in modern astrophysics mainly because they are the oldest objects in our Galaxy and in the whole Universe that we can accurately date. Provided that their distances are known, ages of Globular Clusters can in fact be determined quite precisely from the luminosity of the turn-off stars, that is the stars that are exhausting Hydrogen at their centre. The oldest Globular Clusters are so old that they formed when the Universe was very young, and very different from what it appears now. Accurately dating them is then basic to constraining the early epochs of formation of our own Galaxy, and even the age of the Universe. This last is important for cosmology: combined with estimates of the Hubble constant, it may tell us about the presence and nature of the mysterious dark energy, whose presence is suggested by the apparent decline of the luminosity of type Ia supernovae at high redshifts (Perlmutter et al. 1999), and by the characteristics of the X-ray emission of galaxy clusters (see the review by Rosati et al. 2002).

Observations of external galaxies indicate that Globular Clusters form during epochs of strong dynamical interactions. The lack of young Globular Clusters in our Galaxy can then be connected to the presence of the thin disc: in fact the thin disc would have been destroyed by strong dynamical interactions. The oldest components of the thin disc formed about 10 Gyr ago. While a substantial fraction of the Galactic Globular Clusters seems to be coeval and extremely old, there is a group of clusters that appears to be slightly younger (Rosenberg et al. 1999), although still older than the oldest com-

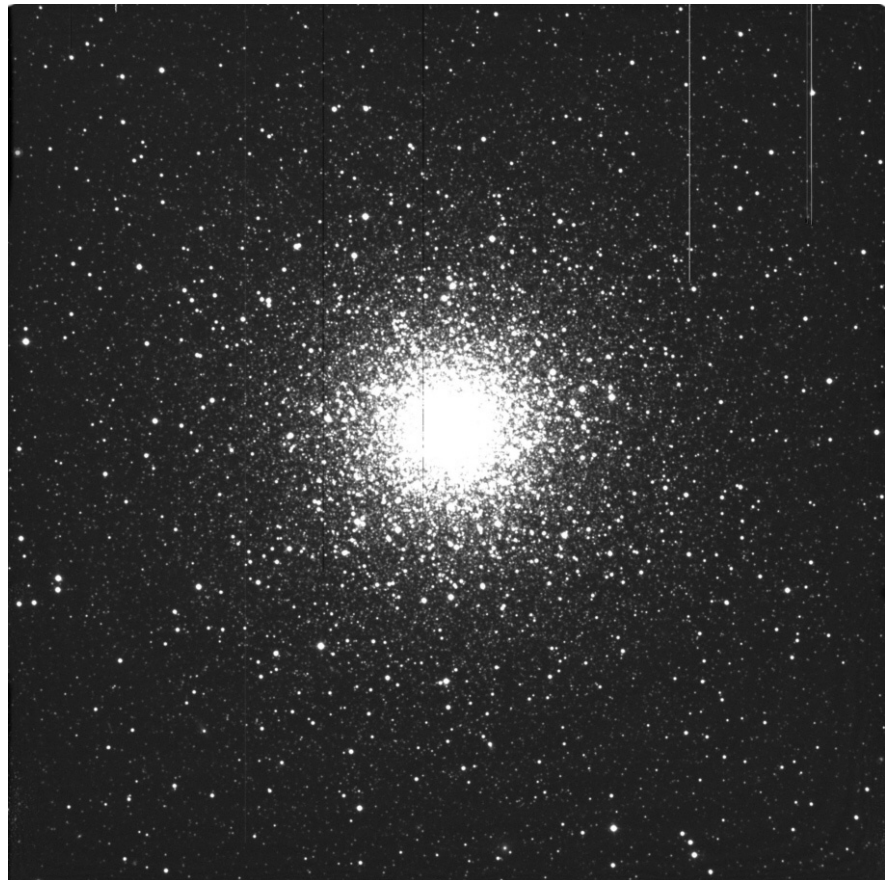


Figure 1: Image of a typical Globular Cluster (NGC 5024)

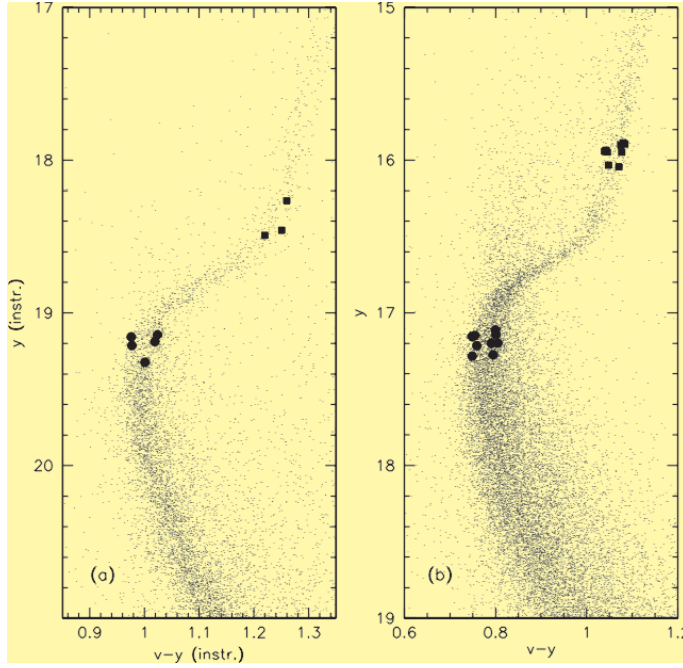
ponents of the thin disc. These “younger” Globular Clusters differ systematically from the oldest ones: they are more metal rich, and more concentrated toward the centre of the Galaxy. This second group of clusters is probably related to the thick disc, and perhaps to the bulge. Comparison between the chemical composition of the thick and thin disc stars suggests that there was an interval of low star formation between these two phases of the history of our Galaxy (Gratton et al. 1996). This hiatus in the star formation might be due to the accretion of a gas rich satellite, which may have caused the heating of the pre-existing disc, a burst of star formation, and possibly a galactic wind

that temporarily cleaned our Galaxy of gas from which stars could form. This strong dynamical interaction may be the site for the formation of the group of “younger” Globular Clusters. Precisely dating them can help to fix the scenario of the early evolution of the Galaxy.

Globular Cluster distances

Dating Globular Clusters requires knowledge of their distances. Globular Clusters are too far for direct distance estimates using trigonometric parallaxes with the presently available instrumentation, although in the next decade accurate distances will be likely obtained with GAIA. However, distances

Figure 2: Location in the colour magnitude of the stars observed in our programme in the Globular Clusters NGC6397 and NGC6752 (from Gratton et al. 2001)



to Globular Clusters can be obtained with various more indirect techniques. In the next few years, high precision distances will probably be obtained by comparing internal proper motions measured by HST with extensive radial velocity measurements obtained with the stellar multi-object spectrograph GIRAFFE fed by FLAMES at KUEYEN (VLT Unit Telescope 2). In the meantime, the best known method is the so-called Main Sequence Fitting. In this method, local subdwarfs whose parallaxes have been accurately measured by the ESA HIPPARCOS astrometric satellite are used as standard candles. Assuming that these stars are identical to main sequence stars in Globular Clusters, distances may be derived by the difference in the apparent magnitude. Since the luminosity of main sequence stars depends on temperature and metallicity, we need to know these quantities for both field and cluster stars. Note that these quantities must be derived differentially: what is important is that temperature and metallicities for field and cluster stars are on the same scale; absolute values have a much smaller impact. Up to now, all data about cluster abundances were based on giant stars; these values might not be consistent with those derived from dwarfs. Furthermore, temperatures are derived from colours; such a derivation is sensitive to the value adopted for interstellar reddening, but it is not demonstrated whether the reddening scale used for Globular Clusters is the same as for local subdwarfs, because the local subdwarfs lie within the dust absorbing layer, while Globular Clusters are much farther. This leads to about 6% uncertainty in the adopted distances. While this may appear as a small value, it translates into uncertainties of almost 2 Gyr in the ages.

On the other side, temperatures and metallicities can be derived, independently of concerns related to reddening, from high resolution spectra. In this case, temperatures may be derived e.g. from the strength of the Balmer lines (good temperature indicators for stars warmer than about 5000 K), and metal

abundances from weak metallic lines. In principle the method requires extraction of these parameters for the same field and cluster stars used to derive distances, that is, unevolved stars that are still on the main sequence. However, these stars are very faint even in the closest Globular Clusters. Slightly evolved stars near the turn-off can still be used: these are accessible in the case of the closest Globular Clusters using UVES at KUEYEN. If this technique is used, uncertainties in the distances are reduced to about 3%, allowing determinations of ages with errors of only about 1 Gyr. Such an accurate determination allows much more critical tests for both cosmology and Galaxy evolution.

UVES at the VLT is particularly suitable for a number of reasons: first, it is a very efficient spectrograph providing enough spectral resolution and S/N on faint sources ($V \sim 17$) such as Turn-Off stars in Globular Clusters; second, the wide spectral coverage observable in a single exposure allows simultaneous observation of $H\alpha$ and of a suitable number of metal lines in the blue portion of the spectra (the stars at the turn-off of metal-poor Globular Clusters have spectra with very few measurable lines). Third, the location of Paranal gives access to the closest Globular

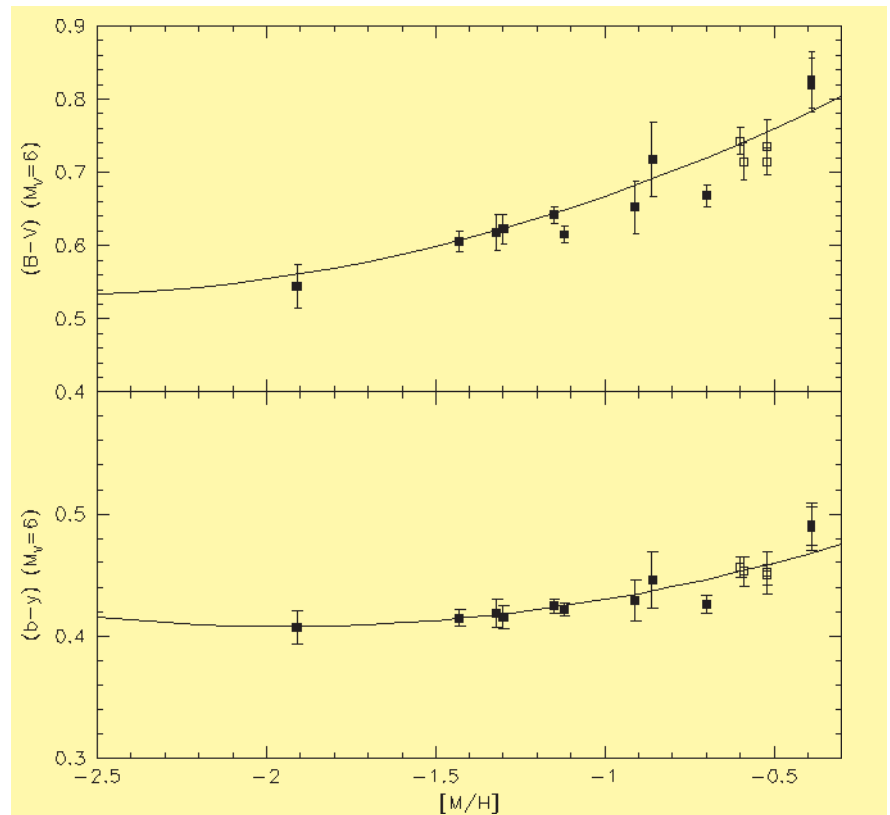


Figure 3: Observed colours of the Main Sequence at $M_v = 6$, as derived from local subdwarfs with accurate parallaxes from HIPPARCOS and metal abundances $[M/H]$ determined in our programme. Filled symbols are stars actually used in the distance derivations; open symbols are control stars. The upper panel shows the run with metallicity for the Johnson B-V colour; the bottom panel is for the Strömgen b-y colour. Superimposed are the predictions by models by Straniero et al.

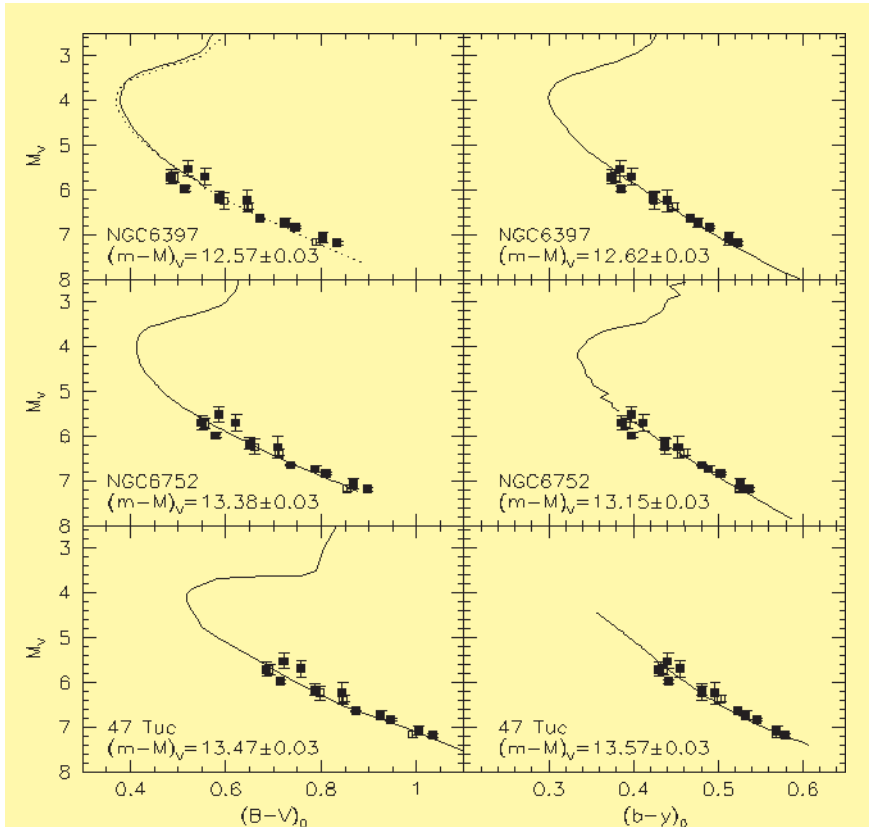


Figure 4: Fit of the Main Sequences of the program Globular Clusters NGC 6397, NGC 6752 and 47 Tucanae, with local subdwarfs. Left panels are for Johnson $B-V$ colours; right panels are for Strömgen $b-y$ colours

band Johnson $B-V$ and the intermediate band Strömgen $b-y$ colours. The agreement between observations and theoretical predictions is excellent, with only a small offset for $B-V$. Note however that these relations are only used to correct colours, i.e. differentially, so that this small offset has no impact in our analysis.

Figure 4 shows the fits we obtained for the three clusters, in both the Johnson (V , $B-V$) and Strömgen (V , $b-y$) colour-magnitude diagrams. There are small differences in the results obtained with different colours that can be attributed to small errors in the colour transformations from observed to standard sequences in the used photometry. However, the agreement is on the whole very good: distances estimated with this procedure have errors as small as 3.5%, and they are the best estimates currently available for these three clusters.

Clusters that are all located in the Southern hemisphere.

We addressed this issue in an ESO Large Programme. UVES high resolution spectra were obtained for about 15–20 stars in each of the Globular Clusters NGC6397, NGC6752 and 47 Tucanae. These three Globular Clusters were selected for observations because they are the closest to the Sun, except M4, which however has a variable foreground reddening, making it less suitable for precise dating. These three clusters cover a wide range in metal abundance, from very metal-poor ($[Fe/H] \sim -2.0$: NGC6397) to rather metal-rich ($[Fe/H] \sim -0.7$: 47 Tucanae). NGC 6397 and NGC6752 belong to the group of old clusters, while 47 Tucanae is likely slightly younger (Rosenberg et al. 1999). In each of these clusters, we selected for observations two groups of stars, one near the turn-off, and the second one at the base of the subgiant branch (see Figure 2). This choice allowed us to make further tests on the program stars, described in the next Sections. In order to ensure that the analysis of the stars in these clusters is strictly identical to that of field subdwarfs, we also acquired spectra of about thirty such stars, selected to have good Hipparcos parallaxes.

The analysis of the spectra of all these stars was done using the same procedures: effective temperatures were derived from the wings of $H\alpha$, using the same precepts for both field and cluster stars. From these analyses, we derived effective temperatures with errors of about 150 K for each star. Most of this

error stems from uncertainties in the flat fielding procedure, so that the error is fairly independent of the actual S/N of the spectra. However, averaging results from all stars, we were able to constrain the temperatures for the stars in a cluster to within 30 K. This in turn translates into unprecedented accuracies of about 0.005 mag in the estimates of the interstellar reddening $E(B-V)$, and of about 0.04 dex in the metal abundance $[Fe/H]$. Furthermore, we derive the abundances of important elements like O, Mg, Si, Ca, and Ti, so that appropriate values of the overall metal abundance could be obtained for each star.

Once reddening and metal abundances for both field stars and Globular Clusters were derived, distances could be obtained by fitting the main sequence of the Globular Clusters to the location occupied by the field subdwarfs. Only unevolved stars (that is stars with an absolute magnitude $M_V > 5.5$) were considered, in order to avoid possible concerns due to differences between the ages of field and cluster stars. However, before this fitting is done, the temperature (colours) of the field stars should be corrected to take into account the difference in metallicity between the field and the Globular Cluster stars. This was done using theoretical relations by Straniero et al. (1997): in Figure 3 we compare the prediction for the colour of the main sequence at $M_V = 6$ obtained with these models with the observed colours of the field subdwarfs used in the distance derivations. We considered two independent colours for each star: the broad

Globular Cluster Absolute Ages and their impact

The ages of the three Globular Clusters that can be obtained from the luminosity of the turn-off point using these distances are 13.8 ± 1.1 Gyr for NGC6397, 13.7 ± 1.1 Gyr for NGC 6752, and 11.2 ± 1.1 Gyr for 47 Tuc. This last cluster turns out to be about 2.5 Gyr younger than the other two, in excellent agreement with the age difference obtained by Rosenberg et al. (1999) using relative dating methods.

Leaving aside 47 Tucanae, the age of the two other clusters (that are coeval to the oldest Globular Clusters, according to Rosenberg et al. 1999) is $13.7 \pm 0.8 \pm 0.6$ Gyr, where the first error bar accounts for internal errors, and the second one for systematics, including uncertainties in the stellar models. This estimate for the age of Globular Clusters coincides with the age of the Universe determined by the WMAP group for a standard Λ_{CDM} model (Spergel et al. 2003). This indicates that, in the framework of a standard Λ_{CDM} model, the Galactic Globular Clusters began to form very early, within 1.4 Gyr from the Big Bang. Alternatively, this age estimate, combined with the estimate of the Hubble constant given by the HST Key Program (Freedman et al. 2001) and the WMAP experiment (Spergel et al. 2003) can be used to constrain the value of the matter density Ω_M in a flat Universe $\Omega_{tot} = \Omega_M + \Omega_\Lambda = 1$, as determined by the spectrum of perturbations of the microwave background (Spergel

et al. 2003). This estimate is independent from results provided by type Ia SNe and clusters of galaxies. The results of this exercise are shown in Figure 5: Ω_M is constrained to be $\Omega_M < 0.57$ (and $\Omega_\Lambda > 0.43$) at the 95% level of confidence. This confirms the need for some form of dark energy ($\Omega_\Lambda \neq 0$) providing the observed acceleration in the expansion of the Universe.

Our distance estimates can also be used to derive the luminosity of the horizontal branch (a benchmark for distance scales, as well as for theoretical models). When coupled with estimates of the apparent magnitudes of RR Lyrae stars in the LMC (e.g. using the derivation of Clementini et al. 2003 based on photometric data acquired with the Danish 1.5 m telescope and metallicities derived from FORS spectra), they can be used to derive the distance to the closest satellite to our Galaxy, the first step in the extragalactic distance scale. The value we obtain is 50 ± 4 Kpc, the same value adopted in the HST Key Project to derive the Hubble constant.

No evidence for element sedimentation in Globular Cluster stars

The most important theoretical uncertainty in the evolution of solar type stars concerns the impact of element sedimentation due to microscopic diffusion. Microscopic diffusion is a basic physical mechanism; it needs to be included in the solar models in order to predict correctly the very accurate and detailed run of the sound velocity within the interior of the Sun provided by helioseismology. Microscopic diffusion is a slow process and its effects may take billion of years to show up. Element sedimentation causes two important effects: first, Globular Cluster ages computed from models that include the effect of microscopic diffusion are about 1 billion years smaller than those obtained neglecting this effect. Second, the abundances of heavy elements for metal-poor stars near the turn-off should be quite different from those obtained for stars at the base of the subgiant branch, where the inward deep penetration of the outer convective envelope should have cancelled the sedimentation effects due to microscopic diffusion. This may have important consequences, e.g. on the interpretation of the observed abundances of Lithium (see below). Detailed predictions that takes into account partial ionisation and the effects of radiation pressure have been presented by Richard et al. (2002): these authors found that Fe is expected to be overabundant (and Li underabundant) by quite a large factor in turn-off stars with an initial value of $[\text{Fe}/\text{H}] = -2$ and an age of 12–14 Gyr.

Our observations of turn-off and sub-

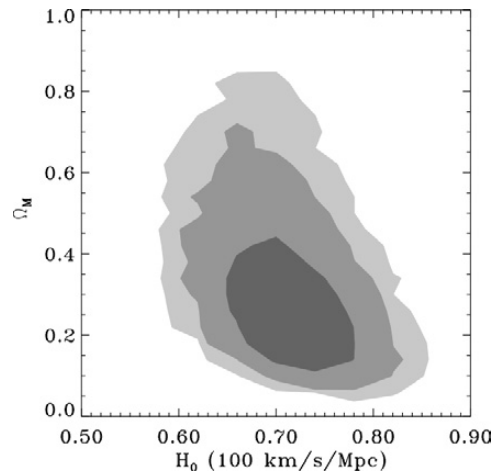


Figure 5: Allowed values of Ω_M as a function of H_0 derived using our estimate for the age of the oldest Globular Clusters (13.7 ± 1.4 billion years), for a flat Universe ($\Omega_{\text{tot}} = 1$)

giants of NGC6397 (a metal poor cluster with $[\text{Fe}/\text{H}] = -2.0$) may be used to test the effects of sedimentation. We found that there is no appreciable difference between the abundances of Fe and several other elements (Gratton et al. 2001). This severely constrains the impact of diffusion. The most reasonable explanation for the lack of evidence of sedimentation in stars of NGC6397 is that there is a region at the base of the outer convective envelope mixed up by turbulence that cancels the effects of sedimentation. Richard et al. (2002) showed that such a mixing effectively reduces the impact of microscopic diffusion on both the ages of Globular Clusters and on the depletion of the primordial Lithium abundances. This makes both ages and the interpretation of the Lithium abundances much sounder.

A second generation of stars in Globular Clusters?

Precise dating is not the only reason why Globular Clusters are interesting. They are also very dense stellar environments and this may cause systematic differences with respect to stars in the general (low density) field. A very intriguing difference concerns the anticorrelation between abundances of elements like O and Na that the Lick-Texas group (Kraft, Sneden and co-workers: see Kraft 1994) found among the stars they observed in Globular Clusters (close to the tip of the red giant branch). Figure 6 illustrates this anticorrelation: within Globular Clusters, stars that are rich in Oxygen are poor in Sodium, and vice versa. Such an anticorrelation is not present among stars in the general field and thus seems a peculiarity of Globular Clusters (Gratton et al. 2000).

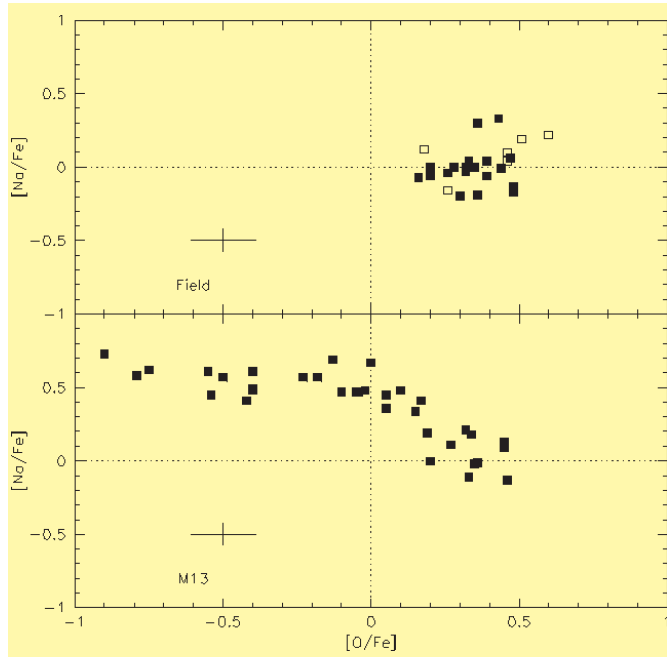
The Oxygen-Sodium anticorrelation is a sign of the presence of material processed throughout the complete CNO cycle. In fact, at high temperatures, Hydrogen is burnt into Helium through a chain that includes as inter-

mediate steps the participation of Carbon, Nitrogen, and Oxygen atoms. When the temperature is low (a few million degrees), as in the central regions of main sequence stars like the Sun, only part of this cycle is active, due to the large Coulomb barrier of Oxygen nuclei: practically, only Carbon and Nitrogen nuclei participate, and most of the original Carbon is transformed into Nitrogen because Nitrogen has a much smaller cross section for proton capture and then tends to accumulate. However, at the higher temperatures of a few tens of millions of degrees K that may be reached in the H-shell burning of Red Giants, Oxygen nuclei also participate in the cycle, and they are effectively transformed into Nitrogen nuclei too, because the cross section for proton capture is much larger than that for proton capture on Nitrogen. Hence, material coming from this region is depleted in Oxygen. However, at the same temperature, proton capture on Neon nuclei effectively produces Sodium; hence this material will be rich in Sodium.

It is not easy to bring material processed through the complete CNO cycle to the surface of small mass red giants like those in Globular Clusters. The structure of the star in fact prevents such a phenomenon, unless some deep mixing not predicted by standard models (i.e. normal non rotating stars) occurs. The reason is the large jump in entropy due to the variation of the molecular weight left over in the star by the maximum extension of the central convective region when the stars left the main sequence. Only when this molecular weight barrier is cancelled by the outward shift of the H-burning shell of the star evolving along the red giant branch is deep mixing allowed. This result is fully confirmed by observations of the field stars (see Figure 7). Why then do stars in Globular Clusters behave differently?

The critical observation is that of dwarfs in Globular Clusters. In fact, the central temperature of these stars is still

Figure 6: Run of the ratio between the abundances of Na and Fe, against the ratio between the abundances of O and Fe, for stars in the Globular Cluster M13 (lower panel), and in the field (upper panel). Note that an extended O-Na anticorrelation is present only among Globular Cluster stars (from Gratton et al. 2000).



too low for complete CNO burning. If then the O-Na anticorrelation is observed also in these stars, the deep mixing hypothesis is untenable. We performed this test using the turn-off stars we observed in NGC6752, a cluster that shows a clear O-Na anticorrelation among its giants. We found (see Figure 8) that the O-Na anticorrelation is present also among dwarf stars, where it is actually very similar to what is observed in giants (Gratton et al. 2001). It is then clear that the O-Na anticorrelation is not due to deep mixing.

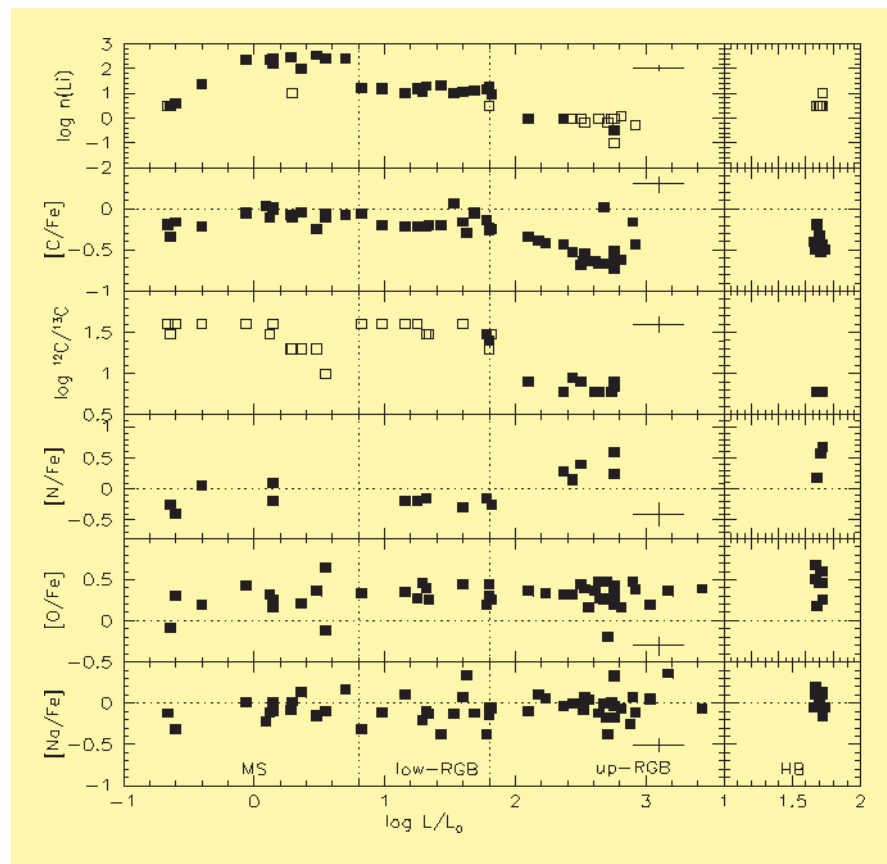
What is then the source of the CNO processed material we see in a large fraction of the Globular Cluster stars? The most probable sources are now extinct massive AGB stars (stars with masses of 4–5 solar masses), where large amounts of material processed through the complete CNO cycle at the

base of the outer convective are brought to the surface, and then lost at low velocity by the slow wind blowing from these stars. The escape velocity from Globular Clusters is typically a few tens of km/s, so that this material may be retained by these massive, concentrated objects, explaining the difference between cluster and field stars. Detailed computations show that massive metal-poor AGB stars may do the job. In some way, this material should arrive where it

is observed, that is in much smaller unevolved stars. This requires a transport mechanism: the most likely is that the O-poor, Na-rich stars belong to a second generation, born from the ejecta of these massive AGB stars. These stars should be a bit younger than the others: however, the age difference that corresponds to the lifetime of 4–5 solar masses stars is tiny (only 100 or 200 million years), compared with the age of the clusters (about 13 billion years). Such a small age difference would go undetected as far as the magnitude and colour of the turn-off in the colour-magnitude diagram are concerned.

This fascinating scenario for the evolution of clusters may help to understand one of the mysteries of Globular Clusters, the so-called second parameter. This concerns the horizontal branch of Globular Clusters, the phase where Globular Cluster stars burn helium at their centres. Theory predicts that the colour of stars along the horizontal branch should be essentially determined by their metal content. In the sixties, Sandage, van den Bergh and others noticed that there are pairs of Globular Clusters with apparently the same metal content, but very different colours of stars on the horizontal branch: the most famous pair includes M3 and M13. This anomaly indicates that there is a second parameter (other than metallicity) that determines the colour of the horizontal branch. This mystery has gone unsolved for over 35 years. The differences in colours are

Figure 7: Overabundances of various elements with respect to Fe vs. stellar luminosity in field metal-poor stars. Stars evolve increasing their luminosity, that is, from left to right in these diagrams. The elements shown are Li, C, N, O, and Na, as well as the $^{12}\text{C}/^{13}\text{C}$ isotopic ratios. Two mixing episodes occur in these stars: 1) the first dredge-up at the base of the giant branch is due to the inward expansion of the outer convective envelope, in zone where incomplete CN H-burning has occurred during the main sequence. It only causes variations in the abundances of C and N (and their isotopes), and a decrease in the Li abundance. 2) A second episode occurs later, when the H-shell burning reaches the point of maximum penetration of the convective envelope (RGB bump); again, it only changes the abundances of C, N, and Li. Surface Na and O abundances are not modified during the evolution of small mass stars (from Gratton et al. 2000).



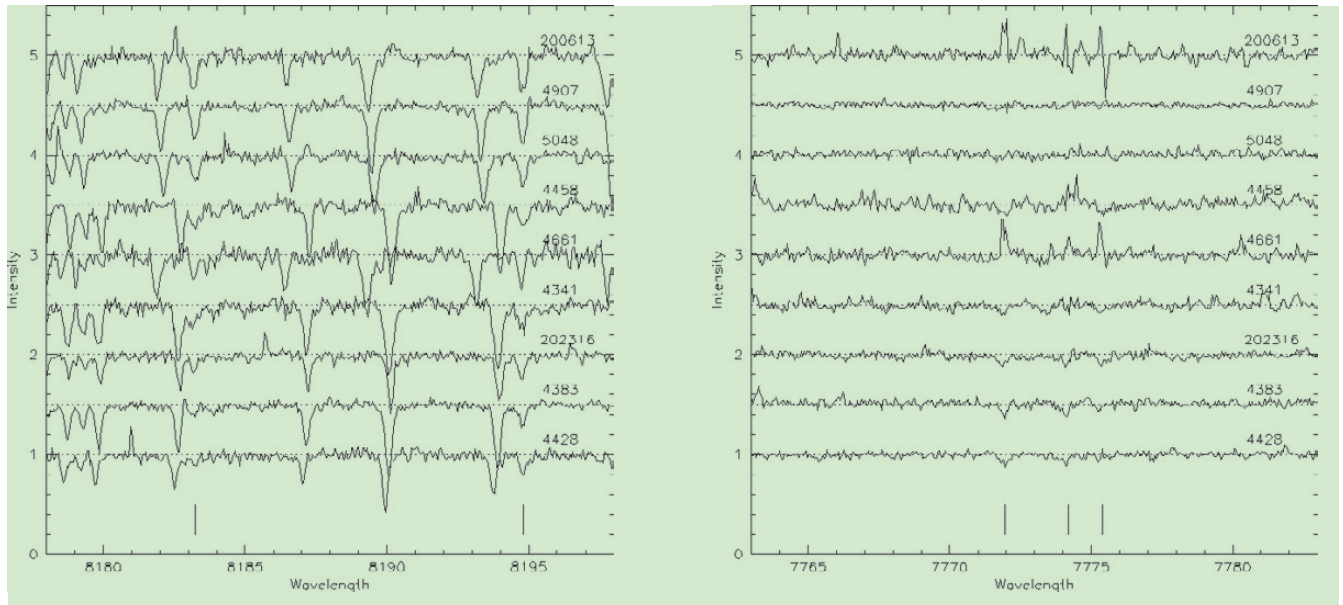


Figure 8: Plots of spectral regions including Na lines (panel a) and O lines (panel b) in dwarfs of the Globular Clusters NGC6752. The stars have virtually identical temperatures and chemical composition: the only difference is in the abundances of CNO elements and Na. Note that the strengths of the Na and O lines are anticorrelated each other: this trend is similar to that found in giants. Since the temperatures at the centres of these stars are not large enough for complete CNO cycle, the Na-rich, O-poor stars must contain material processed elsewhere (from Gratton et al. 2001).

essentially due to differences in masses of the stars on the horizontal branch: however, the reason for these different masses is not clear. In some cases, a difference in age may be the explanation. However, it has been shown by several authors that M3 and M13, for examples, have the same age.

A second generation born from the material expelled from massive AGB stars might explain the anomalous blue horizontal branch of clusters like M13, that has indeed a large population of O-poor, Na-rich stars. In fact this second generation of stars should also be enriched in Helium, produced by the H-burning. Stars richer in Helium evolve faster than normal stars: stars currently on the red giant branch would then be less massive, by a few hundredths of a solar mass. Not a large amount, but well enough to justify a very different colour when these stars are on the horizontal branch. Note however that M13 has virtually no star on the red side of the horizontal branch, so that this effect alone cannot solve the second parameter problem.

Of course many more observations are required to confirm this scenario. FLAMES, using both UVES and GIRAFFE spectrographs, is particularly well suited for such observations. ESO telescopes will likely play a basic role in future observations of Globular Clusters.

Globular Clusters and Ω_b

Besides Ω_M , Globular Clusters may be useful to determine the value of the baryonic component of the density of the Universe, Ω_b . In its first three min-

utes, the Universe was hot and dense enough to undergo nuclear reactions that formed ^2H , ^3He , ^4He and ^7Li . Production of heavier nuclei was not possible because of the rapid cooling of the Universe. According to Standard Big Bang Nucleosynthesis (SBBN), in the presence of three massless neutrinos, the primordial abundance of these light nuclei depends only on the baryon to photon ratio in the Universe, i.e. on the number of baryons, since the number of photons is known from the temperature of the cosmic microwave background (CMB). Therefore a determination of the primordial abundance of the light nuclei allows us, in principle, to determine Ω_b . Spite & Spite (1982) found that the warm metal-poor halo dwarf stars show the same lithium abundance independent of temperature or metallicity, the most straightforward explanation being that the lithium observed in these stars is the primordial lithium. This view may be challenged since the Li abundance in these stars might have been decreased by various stellar phenomena (stellar winds, convective and/or rotational mixing, diffusion, destruction in deep layers) and possibly increased by production through cosmic rays. Theories that predict Li depletion in metal poor stars imply the existence of a dispersion in Li abundances and the existence of a small number of highly depleted stars, as observed among halo field stars. In this respect a Globular Cluster is an ideal testing ground for such theories, since it allows us to observe a population of the same age and metallicity. However, the full power of the VLT is required to obtain high quality spectra of the faint TO

stars even in nearby Globular Clusters. Our analysis of the Li abundance in the TO stars of NGC 6397 showed that they share the same Li abundance (within errors), and there is very little room for dispersion above the observational errors. Out of the 15 TO stars so far observed in this cluster none has been found to be strongly Li depleted. This result therefore supports the primordial nature of the Li observed in these stars. From this value we determined a value of the baryonic density that is consistent at 1.3σ with the value determined from the WMAP experiment.

References

- Bonifacio P. et al. 2002, *A&A*, **390**, 91
- Clementini, G., Gratton, R.G., Bragaglia, A., Carretta, E., Di Fabrizio, L., & Maio, M. 2003, *AJ*, **125**, 1309
- Freedman, W.L. et al. 2001, *ApJ*, **553**, 47
- Gratton, R.G., Carretta, E., Matteucci, F. & Sneden, C. 1996, in *Formation of the Galactic Halo... Inside and Out*, H. Morrison & A. Sarajedini eds., ASP Conf Ser. **92**, 307
- Gratton, R.G., Sneden, C., Carretta, E., & Bragaglia, A. 2000 *A&A*, **354**, 169
- Gratton, R.G. et al. 2001, *A&A*, **369**, 87
- Kraft, R.P. 1994, *PASP*, **106**, 553
- Perlmutter et al. 1999, *ApJ*, **517**, 565
- Richard, O., Michaud, G., Richer, J., Turcotte, S., Turck-Chieze, S., & Vandenberg, D.A. 2002, *ApJ*, **568**, 979
- Rosati, P., Borgani, S., & Norman, C. 2002, *ARA&A*, **40**, 539
- Rosenberg, A., Saviane, I., Piotto, G., & Aparicio, A. 1999, *AJ*, **118**, 2306
- Spergel, D.N. et al. 2003, submitted to *ApJ* (astro-ph/030229)
- Spite M. & Spite F., 1982 *Nature*, **297**, 483
- Straniero, O., Chieffi, A., & Limongi, M. 1997, *ApJ*, **490**, 425

Intracluster Planetary Nebulae in the Virgo Cluster: Tracers of Diffuse Light

M. ARNABOLDI^{1,2}, O. GERHARD³, K.C. FREEMAN⁴

¹I. N. A. F., Osservatorio Astronomico di Torino, Turin, Italy; ²I. N. A. F., Osservatorio Astronomico di Capodimonte, Naples, Italy; ³Astronomisches Institut, Universität Basel, Binningen, Switzerland; ⁴RSAA, Mt Stromlo Observatory, ACT, Australia

Discovery of diffuse light in clusters

Stars are usually observed to form in galaxies (discs, dwarfs and starbursts). In nearby galaxy clusters, however, a diffuse intracluster stellar component has been detected from deep imaging and observations of individual intracluster stars.

Intracluster light (ICL) is potentially of great interest for studies of galaxy and galaxy cluster evolution. The dynamical evolution of cluster galaxies involves complex and imperfectly understood processes such as galactic encounters, tidal stripping and cluster accretion. Various studies have suggested that between 10% and 50% of a cluster's total luminosity may be contained in the ICL, with a strong dependence on the dynamical state of the cluster. The properties of the ICL may also be sensitive to the distribution of dark matter (DM) in cluster galaxies, as simulations have shown that the structure of DM halos in galaxies plays a central role in the formation and evolution of tidal debris.

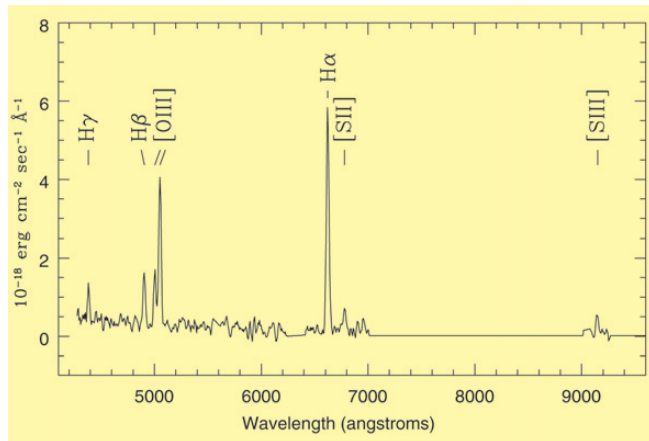
Recently progress has been made in the study of intracluster star light on several fronts. Individual intracluster stars, including planetary nebulae detected from the ground and red giants detected using HST, have been discovered in the Virgo cluster. These intracluster (IC) stars give the promise of studying in detail the kinematics, metallicity and age of the intracluster stellar population in nearby galaxy clusters, and thereby learning about the origin of this diffuse stellar component and the details of the cluster origin.

Direct observations of stars in Virgo field

Ferguson, Tanvir & von Hippel (1998) first looked for individual RGB stars in intracluster space. Using a HST deep F814W (*I*-band) image of a "blank" field located 45' east of the central Virgo Cluster galaxy M87, they were able to detect an excess of point sources relative to the HDF-north caused by the presence of IC red giants. Follow-up studies on a different IC field 41' north-west of M87 confirmed an excess of objects (with respect to background HDF-N and HDF-S fields) with $I \geq 27$.

Are these stars tidally stripped from galaxies during the early phases of

Figure 1: The emission spectrum of the compact Virgo cluster HII region obtained with UT4 and FORS2.



cluster collapse, or are they removed gradually over time via "galaxy harassment"? Do all of these stars have parent galaxies or do they form *in situ*? The recent discovery of an isolated compact HII region in the Virgo cluster (Gerhard et al. 2002) has shown that some star-formation activity can indeed take place in the outskirts of galaxy halos if not already in Virgo IC space. The spectrum of this isolated compact HII region is shown in Figure 1. This HII region is powered by a small star cluster of $\sim 400 M_{\odot}$, involving only 1 or 2 O stars, with an estimated metallicity of $Z = 0.4$. The age of this HII region is ~ 3 Myr and it will probably dissolve by internal processes in a few 10^8 yr: its stars and metals will then be added to the diffuse stellar population nearby. The location of this object in the Virgo field is shown in the ESO press release 02/03.

Intracluster Planetary Nebulae as tracers of cluster evolution

Intracluster planetary nebulae (IC PNe) have several unique features that make them ideal for probing intracluster starlight. The diffuse envelope of a PN re-emits 15% of the UV light of the central star in one bright optical emission line, the green [OIII] $\lambda 5007$ Å line. PNe can therefore readily be detected in external galaxies out to distances of 25 Mpc and their velocities can be determined from moderate resolution ($\lambda/\Delta\lambda \sim 5000$) spectra: this enables kinematical studies of the IC stellar population.

PNe trace stellar luminosity and therefore provide an estimate of the to-

tal IC light. Also, through the [OIII] $\lambda 5007$ Å planetary nebulae luminosity function (PNLF), PNe are good distance indicators, and the observed shape of the PNLF provides information on the line of sight distribution of the IC starlight.

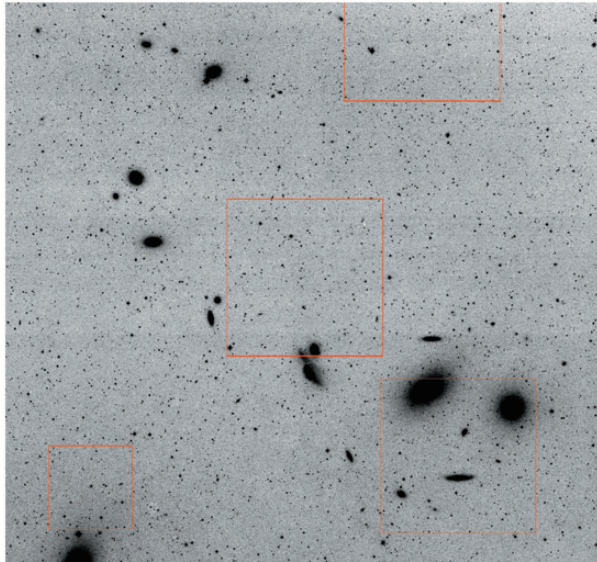
IC PNe are useful tracers to study the spatial distribution, kinematics, and metallicity of the diffuse stellar population in nearby clusters. Different cluster formation mechanisms predict different spatial distributions and velocity distributions for the IC stars. If most of the IC light originates in the initial cluster collapse, its distribution and kinematics should follow closely that of galaxies in the cluster. On the other hand, if the IC light builds slowly with time because of galaxy harassment and tidal stirring, then a fraction of IC light may still be located in long streams, and dynamically unmixed structures should be easily visible in phase space.

Narrow-band wide-field surveys

We have embarked on a narrow-band [OIII] imaging survey in the Virgo cluster (Figure 2), with the aim of determining the radial density profile of the diffuse light, and gaining information on the velocity distribution via subsequent spectroscopic observations of the obtained samples. Given the use of the PNLF as distance indicators, we also obtain valuable information on the 3D shape of the Virgo cluster from these IC PN samples (see also Feldmeier et al. 1998).

Wide-field mosaic cameras, such as the WFI on the ESO MPI 2.2 m telescope and the Suprime Cam on the

Figure 2: Our surveyed fields in the Virgo cluster. The two upper fields were obtained at the ESO MPI 2.2m telescope, and the lower-right field with the Suprime Cam at the 8.2 m Subaru telescope. The lower-left field is from Feldmeier et al. (1998) and was used to test the selection criteria on the spectroscopically confirmed IC PNe in Arnaboldi et al. (2002). Several more fields need to be surveyed to determine the large scale surface density distribution of the ICL in the Virgo cluster.



Subaru 8.2 m, allow us to identify the IC PNe associated with the extended ICL (Arnaboldi et al. 2002, 2003; Okamura et al. 2002). These surveys require the use of data reduction techniques suited for mosaic images, and also the development and refining of selection criteria based on colour-magnitude diagrams (CMD) produced with *SExtractor*.

Through this work, the on-band/off-band [OIII] imaging technique which has been used for PNe identification in Virgo and Fornax ellipticals has led to the following selection criteria for the most reliable detection of IC PNe candidates:

1. the source should be unresolved;
2. the source should have an emission line equivalent width (EW) larger than 100 Å. This is evaluated by measuring the ([OIII] - V) colour between a detected object in the on-band [OIII] image and the signal in the corresponding position in the off-band V image. The EW criterion corresponds to a filter-dependent colour excess relative to field stars;
3. there should be no source detected in the V-band image at the position of the detected [OIII] source.

The requirement on EW greatly reduces the contamination from [OII] starburst emitters at $z \sim 0.35$. The colour selection must take into account the photometric errors in the final on-image, via simulation of unresolved sources.

Spectroscopic confirmation and first results

The spectroscopic observations of the Feldmeier et al. (1998) Virgo IC PNe sample, carried out by our group using 2dF and the AAT, showed that most of the emission line sources in this sample are indeed IC PNe, because the combined spectrum of all the “sharp line” emitters clearly showed the [OIII] 4959/5007 Å doublet. In 2002, a high S/N spectrum for a single IC PN in the Virgo cluster (Figure 3) was obtained for

the first time at the VLT-UT4 with FORS2 by Arnaboldi et al. (2003). We conclude that the existence of IC PNe in the Virgo cluster is now beyond doubt.

Why then did the spectroscopic study by Kudritzki et al. (2000) find only background galaxies? The answer lies in examination of the luminosity function (LF) of their objects. The LF of the candidates studied by Kudritzki et al. (2000) follows closely the LF of field Ly- α emitters at $z = 3.1$; see Figure 4.

We can compare the LF for the Ly- α emitters with the LF for the 16 spectroscopically confirmed IC PNe of the Feldmeier et al. (1998) sample. These confirmed IC PNe are mostly brighter than the brightest of the Ly- α emitters shown in Figure 4. The brightest of the emission line candidates studied by Kudritzki et al. (2000) is 0.5 mag fainter than the bright cut-off in the PNLF for M87, and 0.8 mag fainter than the bright cut-off for the spectroscopically confirmed IC PNe in the Virgo cluster. Most of the current IC PN candidates in Virgo are within 1 mag of the bright cut-off in the PNLF. This is the reason why Kudritzki et al. did not find IC PNe. Their sample was dominated by the Ly- α emitters which are more abundant at fainter magnitudes. (See also Arnaboldi et al. 2002).

The bright cut-off of the LF for the Virgo IC PNe is about 0.3 mag brighter than for the PNe in individual Virgo galaxies. This is believed to be due to the elongated structure of the Virgo cluster, as previously found for the distribution of Virgo spiral galaxies using

the Tully-Fisher relation.

What is the fraction of Ly- α emitters in the first magnitude of the LF for the Virgo IC PNe samples? When we compute the fraction of Ly- α emitters which can contaminate the ICPN candidate sample selected as outlined in section 2.1, it amounts to about 15% of the observed sample. This estimate is supported by the empty field survey of Castro-Rodriguez et al. (2003).

Properties of the diffuse light in Virgo cluster

A primary goal is to estimate the fraction of light from intracluster stars in the surveyed region of the Virgo cluster. In our 0.25 deg² field at a distance of 1° from the cluster centre, the IC PNe sample indicates a total associated luminosity of $5.8\text{--}7.5 \times 10^9 L_{B,\odot}$, which corresponds to a surface luminosity of $0.33\text{--}0.57 L_{B,\odot}/\text{pc}^2$ or a surface brightness of $\mu_{B,*} = 28\text{--}27.7 \text{ mag}/\text{arcsec}^2$. As discussed by Arnaboldi et al. (2002), over the range of radii probed by the survey fields, the luminosity surface density of galaxies in Virgo decreases by a factor of ~ 3 , while that for the IC PNe is nearly constant. Therefore, from the data available so far, the IC PNe in Virgo are not centrally concentrated; however we need to investigate fields at larger radii to constrain the total amount of IC light.

One needs to compare the luminosity derived for the diffuse population with the luminous contribution from Virgo galaxies. If IC PNe are produced by phenomena acting locally, as the structure in the IC PNe distribution shown in Okamura et al. (2002) seems to support, then the fraction of diffuse light with respect to the computed light in galaxies in the field is about 10%. On the other hand, comparing the IC surface brightness with the smoothed out surface brightness of galaxies from Bingelli et al. (1987) gives an upper limit of about 40%.

Is the diffuse light in the Virgo cluster

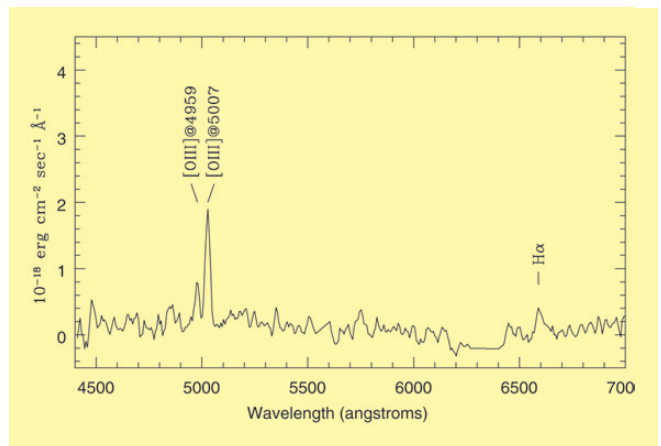
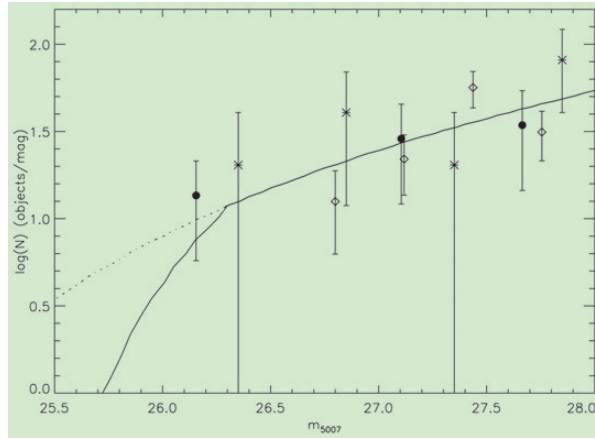


Figure 3: Spectrum of the confirmed intracluster PN in the Virgo cluster. The [OIII] doublet and the H α emission are visible in this high S/N spectrum from UT4 and FORS2.

Figure 4: The solid line shows the expected LF of the field Ly- α population at redshift $z = 3.1$ for objects with $V < 24.73$. The faint dotted line shows the expected Ly- α LF without any magnitude constraints in the V band. Asterisks indicate the LF of spectroscopically confirmed Ly- α emitters from Kudritzki et al. (2000). Filled dots and diamonds show the LF of Ly- α emitters in two other blank-field surveys. These are all consistent; from Castro-Rodriguez et al. (2003).



distributed uniformly? Recent discoveries of low surface brightness arcs in other nearby clusters, significant field-to-field variations in the number density of Virgo IC PNe, and the remarkably inhomogeneous distribution of IC PNe in the field surveyed by Okamura et al. (2002) (see Figure 5) have demonstrated that intracluster stars are not distributed uniformly.

An emission line survey carried out on an empty field in the Leo group, using the same selection criteria as adopted for the Virgo cluster survey, gives an upper limit on the diffuse surface luminosity of $4.4 \times 10^{-3} L_{B, \odot}/pc^2$, corresponding to a surface brightness limit $\mu_{B,r} > 32.8 \text{ mag/arcsec}^2$ (Castro-Rodriguez et al. 2003). This empty field survey, observed at the peak of the HI distribution in the Leo intragroup cloud, gives an upper limit on the fraction of diffuse light in this intra group field of $< 1.6\%$. The evidence coming from the Leo group is very interesting because it shows that the fraction of diffuse light vs. light in individual galaxies that we find in Virgo is related to the Virgo cluster and its evolution. It does not appear to be a general physical property of the local universe.

A high resolution simulation of a Virgo-like cluster in a LCDM cosmology was used to predict the velocity and the clustering properties of the diffuse stellar component in the intracluster region at the present epoch (Napolitano et al. 2003). The simulated cluster builds up hierarchically and tidal interactions between member galaxies and the cluster potential produce a diffuse stellar component free-flying in the intracluster medium. We find that at $z = 0$ the intra-

Figure 5: Deep [OIII] image in the Virgo central core region. The IC PN candidates are marked by circles. Envelopes of bright galaxies have been subtracted. The overdensity in the upper right quadrant of this field is highly significant. The majority of candidates in this field seem to be related to the M86-M84 region of the Virgo cluster, supporting a local origin for the IC PNe.

cluster stellar light is mostly dynamically unmixed and clustered in structures on scales of about 50 kpc at a radius of 400–500 kpc from the cluster centre. The simulations predict the radial velocity distribution expected in spectroscopic follow-up surveys. When we compare the spatial clustering in the simulation with the properties of the Virgo IC stellar population, we find a substantial agreement.

Conclusions

The results obtained so far from IC PNe samples have shown that *i*) the fraction of the diffuse light in the Virgo cluster amounts to 10%-40%; *ii*) the intracluster stars of Virgo are not centrally condensed and not uniformly distributed and *iii*) the front edge of the Virgo cluster is about 20% closer to us than M87. A high-resolution collisionless N-body simulation of a Virgo-like cluster at $z = 0$ predicts strong substructure in phase space, so our next goal will be to look for substructure in the radial veloc-

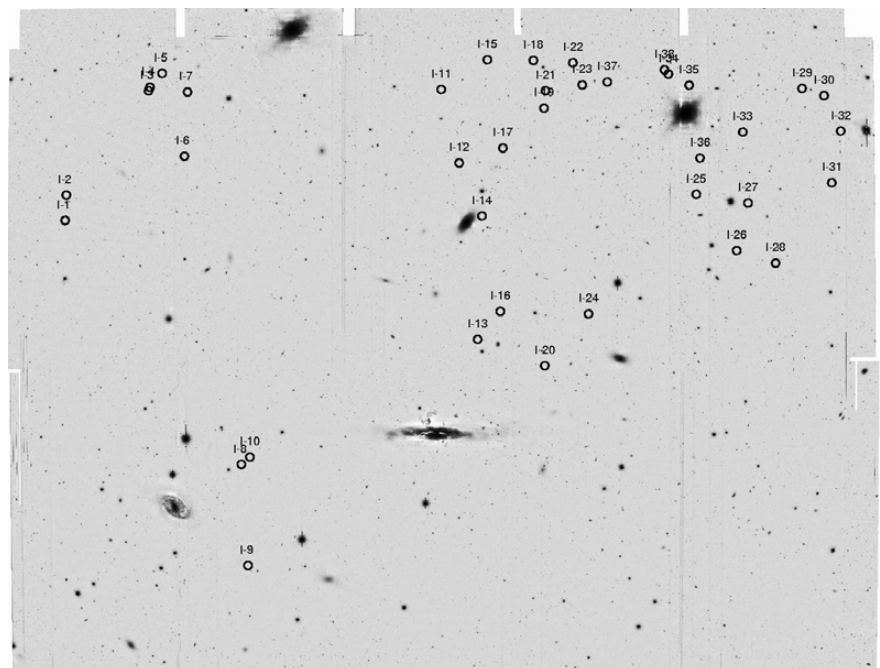
ity distribution of IC PN candidates in Virgo. The VLT instruments, FLAMES and VIMOS, will be most important in giving us the radial velocity distribution of the stars in the diffuse component, identifying individual streams, and providing us with samples of the phase space for the diffuse component at different cluster radii. These observational results will be compared with N-body high resolution cosmological simulations and in this way we should be able to determine how old dynamically the diffuse light is.

Acknowledgements

The authors wish to thank ESO for the support of this project and the observing time allocated both at La Silla and Paranal telescopes. We are grateful to the ESO 2.2 m telescope team for their help and support during observations, in particular E. Pompei and H. Jones. M. A. and O. G. thank R. Scarpa for efficient help at UT4. We would also like to thank all our collaborators. This work has been supported by the Schweizerischer Nationalfonds and by INAF.

References

- Arnaboldi, M., et al. 2002, *AJ*, **123**, 760
- Arnaboldi, M., et al. 2003, *AJ*, **125**, 514
- Binggelli, B., Tammann, G. A., Sandage, A. 1987, *AJ*, **94**, 251
- Castro-Rodriguez, N. et al. 2003, *A&A*, in press (astro-ph/0304057)
- Ferguson, H., Tanvir, N., von Hippel, T. 1998, *Nature*, **391**, 461
- Feldmeier, J. J., Ciardullo, R., Jacoby, G. H. 1998, *ApJ*, **503**, 109
- Gerhard, O. et al., 2002, *ApJ*, **580**, L121
- Kudritzki, R.-P., et al. 2000, *ApJ*, **536**, 19
- Napolitano, N. R., et al. 2003, *ApJ*, in press (astro-ph/0305216)
- Okamura, S. et al. 2002, *PASJ*, **54**, 883



The Red-Sequence Cluster Survey

FELIPE BARRIENTOS¹, MICHAEL GLADDERS², HOWARD YEE³, ERICA ELLINGSON⁴, PATRICK HALL^{1,5}, LEOPOLDO INFANTE¹

¹P. Universidad Católica de Chile; ²Observatories of the Carnegie Institution of Washington; ³University of Toronto; ⁴University of Colorado; ⁵Princeton University

Galaxy clusters are the largest and most massive discrete structures in the Universe. They represent the endpoint of gravity's influence on the growth and collapse of the Universe's large scale structure. Mass in the Universe, as traced by galaxies, is distributed in sheets surrounding large, nearly empty spherical voids. At the intersection of these sheets, at places referred to as filaments, the density of the universe is even larger. At the intersection of filaments, sitting much like spiders in a 3-D cosmic web, are galaxy clusters. Clusters are extremely dense, with central densities ~ 1000 times that of their surroundings. As the Universe ages, galaxy clusters are thought to become larger and larger, as mass drains along the filaments into the central clusters. Galaxy clusters are extremely important laboratories for the study of a number of questions in astronomy, and will be one of the most important targets for observations by both ground-based and space observatories in the coming years.

The Red-Sequence Cluster Survey is an ambitious project designed to identify a large sample of galaxy clusters over a wide range of redshifts (distances). The resulting sample of galaxy clusters will yield answers about the way in which structures formed and grew in the Universe, and will facilitate a number of other projects. The survey is the largest area survey ever conducted on 4-m class telescopes, and as such will yield

important new insights on hitherto poorly measured or unknown phenomena. Despite the large area of the survey (90 square degrees of sky - roughly 500 times the apparent area of the full Moon) a very efficient observing strategy allowed this unprecedented area to be covered in only 25 nights of observing time. Two telescopes were used to complete the project (the Canada-France-Hawaii 3.6 m telescope for the northern hemisphere, and the Cerro Tololo Inter-American Observatory 4 m telescope for the southern hemisphere). The survey began in mid-1999, and observations were finished by late 2001. We are currently using the powerful ESO VLT telescopes for following up some of the highest redshift clusters in the sample.

The method

In conjunction with the extensive data from the RCS project, we have devised a new algorithm for finding clusters in two-filter survey data. This algorithm exploits the fact that all clusters so far observed have a central population of old red galaxies. While the properties of the overall cluster galaxy population do evolve with redshift (i.e. the fraction of blue or actively star-forming galaxies is generally higher at higher redshift), in all well-formed significant clusters so far observed there is a red population. In essence, we define a cluster as an overdensity in both position and colour. The distribution of galaxy clusters, even in systems with a large fraction of blue galaxies, represents a colour distribution not generally found in the field (i.e. non-cluster) galaxy population. Additionally, the filters used for the RCS survey provide a particularly deviant (and hence readily identified) colour for clusters at modest to very high redshifts. Thus, simple colour cuts allow us to select 2-D groupings of red galaxies, which are very likely to be real 3-D clusters of galaxies at high redshifts. We have tested this method extensively using both real redshift survey data, and using complex and thorough simulations, and find that it works extremely well (a detailed description of the method can be found in Gladders & Yee 2000).

Clusters and Cosmology

The number density of galaxy clusters as a function of their mass and red-

shift, $N(M,z)$, is strongly dependent on the cosmological parameters Ω_m and σ_8 . Ω_m describes the matter density of the Universe, and σ_8 describes the amplitude of the early fluctuations in the Universe, which seed the growth of structures on the physical scale of galaxy clusters. In an expanding low-density universe (small Ω_m), structures like galaxy clusters must form relatively early, when the universe was still compact and relatively dense. Only in this setting does such a universe have sufficient mass density to cause large structures to collapse under the influence of gravity, and even then only if the initial fluctuations which seed the growth of structure are relatively large (high σ_8). Conversely, in a universe with much greater mass content (large Ω_m) structure continues to form as the universe expands and ages, even when the seed fluctuations are relatively modest (low σ_8).

We have known for a long time that the local universe contains many galaxy clusters. These clusters could result from either a low matter density, large fluctuation cosmology, or a high matter density, small fluctuation cosmology. However, as described above, the past history of this local cluster population is wildly different in these two cosmologies, and so studies of clusters at great distances (which, due to light travel-time effects also corresponds to the distant past) offer a powerful constraint on cosmological models. The RCS seems to contain many high-redshift, massive clusters, and hence initial results strongly favour a low Ω_m and high σ_8 universe. However, this conclusion depends critically on correct mass estimates for these systems, and our ongoing spectroscopy with the VLT+FORSS2, for which the first data have just been taken, represents a critical step in confirming this initial result. A summary of the first clusters with confirmed redshifts is shown in Figure 1.

Cluster Galaxy Evolution

Clusters of galaxies also provide us with natural laboratories to study galaxy evolution, since we find a number of galaxies in a relatively small region of the universe that can be traced to high redshift, or equivalently to an epoch when the universe was much younger.

Our studies are focussed on measuring properties such as the galaxy luminosity function (LF), blue fraction, and

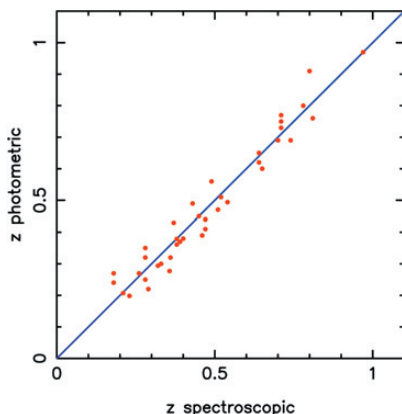


Figure 1: Spectroscopic confirmation of the first clusters found in the RCS. The measured spectroscopic redshift for the clusters in this sample agrees very well with the estimates obtained from the photometric data alone. We are currently working with the VLT and FORSS2 to populate this diagram in the region at $z > 0.9$.



Figure 2: IJK colour composite image of the field centred on RCS0439.6-2905. North is up and East to the left. This image shows approximately the central 1.1×1.1 Mpc.

the CMR (colour-magnitude relation, i.e. red sequence), for clusters over a range of richnesses and redshift (individually for rich clusters, in redshift bins for poor clusters). These data will allow investigations of the evolution of cluster galaxies, and will constrain their formation time and process through a detailed analysis of the evolution of the slope, scatter and colour of the CMR. As the sample will be volume limited for rich clusters over a large portion of the redshift range, we will be able to trace cluster galaxy evolution without strong selection biases.

RCS0439.6-2905: A Cluster Galaxy Evolution Case Study

As an example of such studies we present in Figure 2 an image of RCS0439.6-2905, one of the most massive distant clusters found in the RCS. Recent spectroscopy confirms that RCS0439.6-2905 is at $z = 0.97$ making it more distant than all but a handful of known galaxy clusters. The *I*, *J* and *K*-band colour composite in Figure 2 (*I*-band taken at Magellan and *J* and *K*-bands at the VLT) shows numerous galaxies with similar colours that presumably are cluster members.

Figure 3 shows the colour-magnitude relation for the galaxies in the field of this cluster. The quality of the images taken with the VLT was very good, with a seeing of ~ 0.4 arcsec, and this allows us to perform a morphological study by applying galaxy image fitting tech-

niques. The galaxies selected as elliptical or lenticular galaxies (E/S0s) on the basis of their 2-D light profiles are shown as red circles. Clearly these galaxies define a tight colour sequence in this cluster. The red sequence as it would appear at the distant redshift for the E/S0 galaxies in the Coma cluster, a nearby cluster of galaxies and the canonical example of a rich cluster, is shown as the blue broken line. The galaxies in RCS0439.6-2905 appear intrinsically slightly bluer than those in the Coma cluster, consistent with these galaxies being like those seen in Coma, but at a much younger age.

The excellent image quality of the VLT not only allowed us to segregate the E/S0 galaxies in this cluster at $z = 0.97$ but also to determine the size of the galaxies. The size of the galaxies, accounting for the seeing profile, is given by the effective radius, the radius that encloses half of the light of the galaxy, and is shown in Figure 4 as a function of their absolute magnitude. The red

symbols are the galaxies in the cluster at $z = 0.97$ and the blue crosses are their equivalent in local clusters of galaxies. The red solid line and the broken blue line are the best fit for the galaxies at $z = 0.97$ and for those in local clusters, respectively, keeping the same slope for both sets of galaxies. The offset between the lines is approximately 1.2 magnitudes. This brightness shift can be interpreted as the galaxies at $z = 0.97$ following a similar size-magnitude relation than those in local clusters but being 1.2 magnitudes brighter than their local counterparts. Much like the colour evolution, this is consistent with models of early formation of the stellar population in these galaxies, with subsequent fading and reddening as they age.

Strong-Lensing Clusters

The large area and depth covered by the RCS provides large samples of galaxy clusters spanning a wide range of properties. A particularly interesting subsample is the strong-lensing clusters, which due to gravitational effects act as lenses magnifying and distorting the images of distant objects background to the cluster. We have so far found 8 new strong lensing systems in the RCS, some of them with the presence of multiple giant arcs (Gladders et al. 2003). The incidence of such a large number of strong lensing clusters in the surveyed area is discrepant with current theoretical predictions (standard expectations are 0-1 such clusters in a survey the size of the RCS).

The first studied RCS lensing cluster, RCS0224.5-0002, is shown in Figure 5. Spectroscopy of this cluster was acquired using the 8.2 m Kueyen Telescope and FORS-2 in Director's

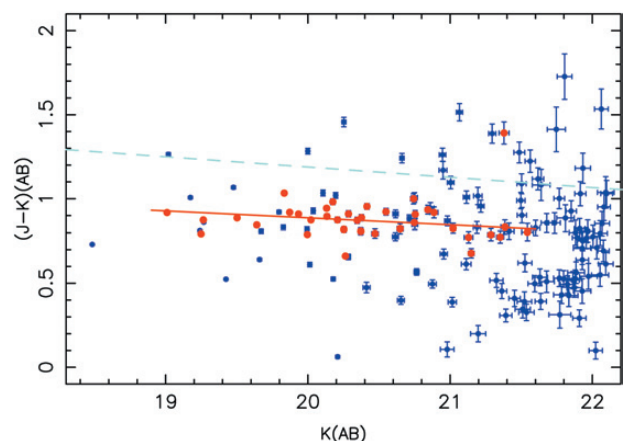


Figure 3: IR colour-magnitude diagram in the field of RCS0439.6-2905. All the objects are included and shown as filled circles. The morphologically selected E/S0 galaxies are shown as open circles. These galaxies define a tight sequence, similar to that found in local clusters. The solid line shows the best fit to the sequence of E/S0 galaxies in the cluster. The broken line corresponds to the colour-magnitude relation for the E/S0 galaxies in Coma cluster redshifted to $z = 0.97$.

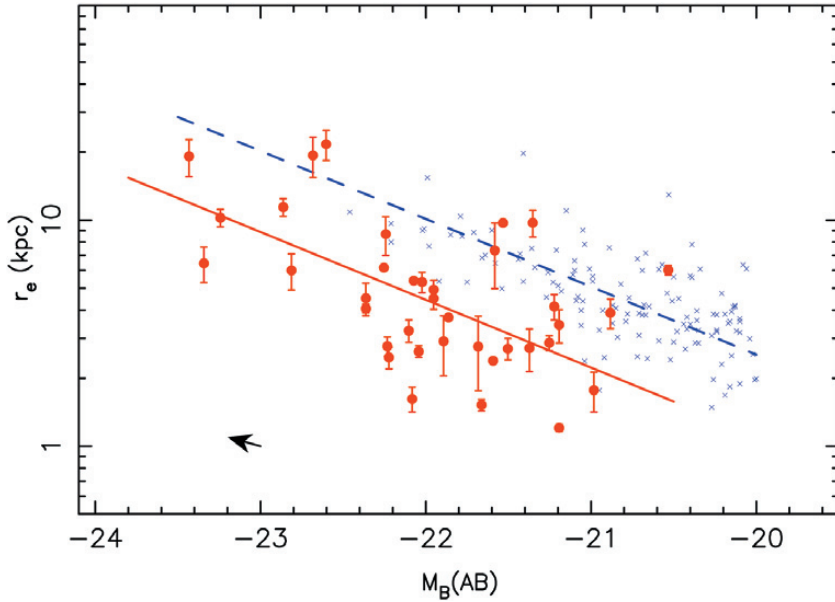


Figure 4: Size-magnitude diagram for the E/S0 galaxies (filled circles) in the field of RCS0439.6-2905. The size has been obtained from the 2-D galaxy light profile fitting algorithm. For comparison the E/S0 galaxies in local clusters are shown as crosses, including the best linear fit to these galaxies (broken line). The solid line corresponds to the fit for the galaxies in RCS0439.6-2905, constrained to have the same slope as that for the local E/S0 galaxies. There is an offset for the fit at $z = 0.97$ from the local relation that amounts to $\Delta M_B(AB) = -1.20 \pm 0.09$.

Discretionary Time, soon after the cluster was discovered. This initial spectroscopy demonstrated that the cluster was at $z = 0.773$, and showed that one of the arcs (the arc labelled 'C', visible in Figure 5) was extremely distant, at a redshift of 4.8786 (Gladders et al. 2002). The FORS spectrum of this arc at Ly- α is shown in Figure 6, along with the images of the arc in the R and I bands. The Ly- α emission (shown by both the spectrum and the R -band light), with an equivalent width of several hundred Angstroms, is spatially extended compared to the UV continuum just to the red of Ly- α (shown by the I -band light). At the time of discovery, RCS0224.5-0002 was the most distant cluster known with such spectacular strong lensing, and the high redshift arc was one of only two known giant arcs at such great distances, the other being an arc at $z = 4.92$ formed around the $z = 0.33$ cluster CL 1358+62 (Franx et al. 1997). Notably, the distant arc in RCS0224.5-0002 appears rather different in detail; it is spatially smooth with an extended Ly- α halo surrounding a compact star-forming core, and shows no velocity structure, whereas the in CL 1358+62 is knotty in appearance and shows velocity structure of ~ 300 km/s.

Since the discovery of RCS0224.5-0002 we have found several other spectacular multiple-arc strong lens clusters. Of the total of 8 strong-lens systems, 2 more are comparable to RCS0224.5-0002. This high proportion of multiple arc systems argues that there must exist a class of "super-lenses" which, for some yet undetermined reason, act as particularly powerful lenses. Notably, the strong lens clusters in the RCS are all at $z > 0.64$, and it thus seems likely that the source of this lensing boost is associated with early times when clusters are still forming, and that whatever is responsible for the lensing boost evolves away as clusters age (Gladders et al. 2003).

Additional Projects: Clustering and Evolution of Small Galaxy Groups

The wide area, depth and homogeneity of the RCS data allow us to pursue other relevant problems in galaxy evolution, such as the study of the formation and evolution of structure in the Universe, ranging from clusters, groups, pairs of galaxies to individual galaxies.

As is well known, the distribution of galaxies in the universe is believed to be different from the distribution of dark matter; the distribution of galaxies is a biased tracer of the matter. To understand the clustering pattern of galaxies through a good interpretation of observational data and to compare them to current predictions of cosmological models, this bias has to be understood.

In simulations, pairs, triples, small groups, groups and clusters of galaxies

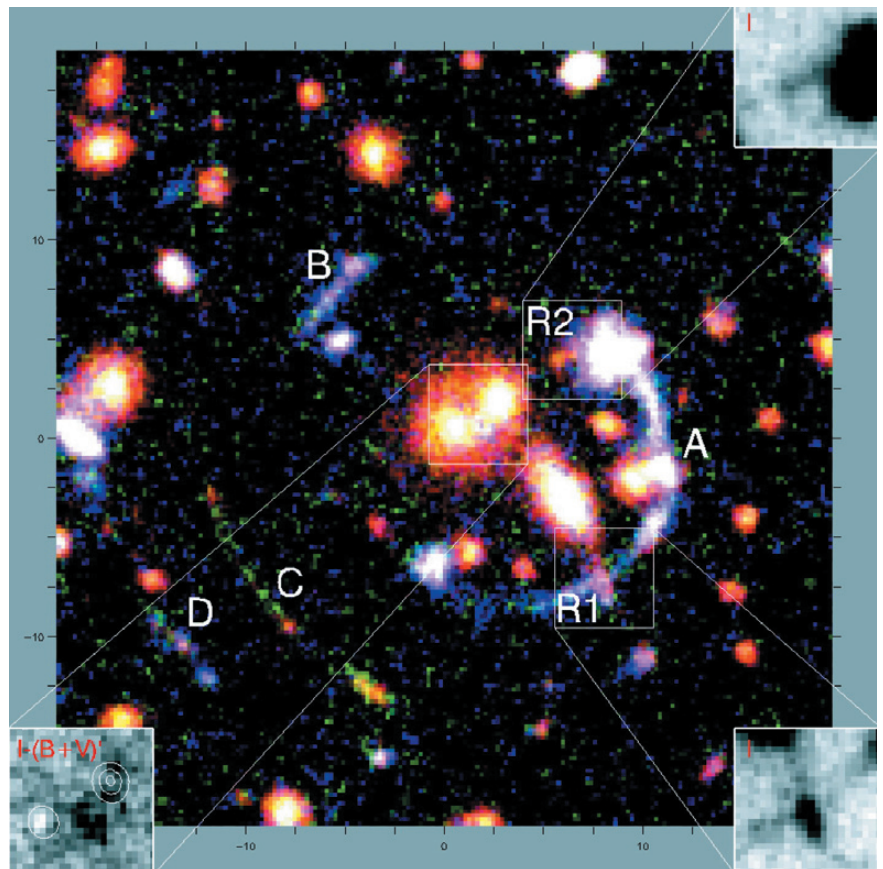


Figure 5: This $40'' \times 40''$ image is a colour composite of $zI+R+BV$ images of RCS0224.5-0002. Various features – two candidate radial arcs, and excess blue light in the cluster centre – are highlighted in grey-scale inserts. Arc C is at $z = 4.8786$. (Adapted from Gladders et al. 2002)

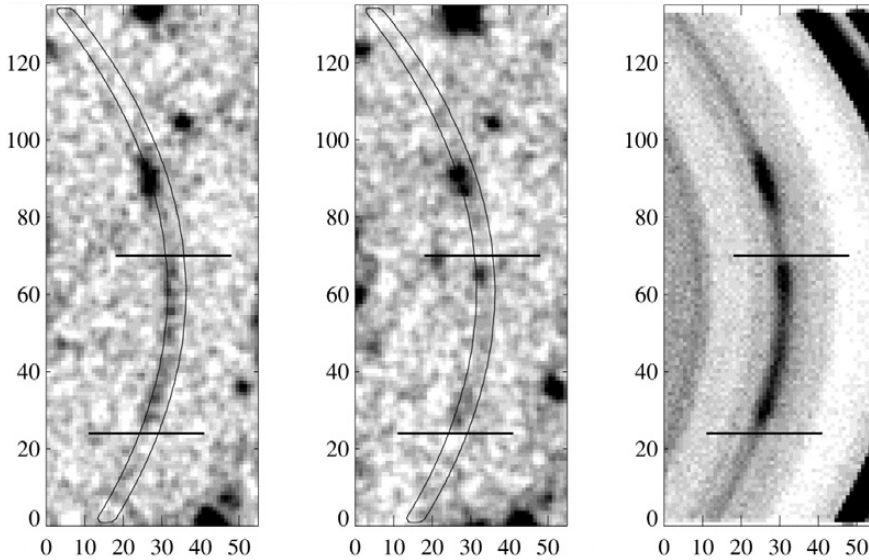


Figure 6: Arc C in R band (left), I band (middle), and in Ly emission (right). The spectral image has not been sky subtracted. The position of the slit as reconstructed after the FORS observations, is also indicated in the broadband images. (Adapted from Gladders et al. 2002)

are fully characterized by their corresponding halo dark matter mass. If so, how can observations be used to measure the “bias”? Theoretically, there is a

strong relation between the dark matter halo mass and the number of members with similar luminosities in clusters, cluster number richness, m . In the ob-

servational plane, the measured quantities are $N(z, m)$ and the two-point correlation function, $\xi(r, m)$.

No clustering studies of small galaxy groups with $m > 3$ have been carried out, basically because of small survey area, bad number statistics and lack of deep homogeneous data. To find groups at different redshifts, deep wide field imaging is needed. In this project, SDSS and RCS provide the low and high- z groups, to $z < 0.7$ respectively. A number of groups have been detected on the RCS data. In order to measure the spatial clustering properties, inversion of 2-dimensional data is required. Currently, redshifts of group members selected from SDSS and RCS are being measured.

References

- Gladders, M. D., & Yee, H. K. C. 2000, *AJ*, **120**, 2148
 Gladders, M. D., Yee, H. K. C., & Ellingson E. 2002, *AJ*, **123**, 1
 Gladders, M. D., Hoekstra, H., Yee, H. K. C., Hall, P. H., & Barrientos, L. F. 2003, *ApJ*, in press
 Franx, M., Illingworth, G. D., Kelson, D. D., van Dokkum, P. G., & Tran, K.-V. 1997, *ApJ*, **486**, L75

Long Period Variables in the Giant Elliptical Galaxy NGC 5128: the Mira P–L Relation at 4 Mpc

M. REJKUBA^{1,2}, D. MINNITI², D. R. SILVA¹, T. R. BEDDING³

¹ESO, Garching, Germany; ²Department of Astronomy, P. Universidad Católica, Chile; ³School of Physics, University of Sydney, Australia

In a stellar population older than a few hundred Myr, the near-infrared light is dominated by red giants. Among these, the stars lying on the red giant branch (RGB) are the brightest among the metal poor stars older than 1–2 Gyr. In intermediate-age populations (~ 1–5 Gyr old) numerous bright asymptotic giant branch (AGB) stars are located above the tip of the RGB. However, also among old populations like Galactic globular clusters with $[\text{Fe}/\text{H}] \geq -1.0$ and in the Galactic bulge, bright stars have been detected above the tip of the RGB implying the presence of bright AGB stars in metal-rich and old populations. All of the bright giants above the RGB tip in globular clusters seem to be long period variables (LPVs; Frogel & Elias 1988). Old populations of lower metallicity are known not to have AGB stars brighter than the RGB tip.

Long period variables are thermally pulsing asymptotic giant branch (TP-AGB) stars with main sequence masses between 1 and 6 M_{\odot} . They have variability with periods of 80 days or longer, and often the longest period variables show variable or multiple periods. Two main classes of LPVs are Mira variables (Miras) and semi-regular variables

(SRs). SRs usually have smaller amplitudes as well as shorter and more irregular or even multiple periods. They are sometimes divided into subclasses (SRa, SRb) depending on the regularity and multiplicity of their periods and shape of their light curves. The separation between Miras and SRs is not always very clear. The classical definition requires that Miras have V-band amplitudes larger than 2.5 mag and regular periods in the range of 80–1000 days. Mean K-band amplitudes of Miras are typically 0.6 mag. SRs show more irregular variability, as their name indicates, and have smaller amplitudes.

So far, LPVs have been studied in the Milky Way, Magellanic Clouds and a few other Local Group galaxies. However, the Local Group lacks the important class of giant elliptical galaxies. At the distance of about 4 Mpc (Harris et al. 1999), NGC 5128 (Centaurus A) is the closest giant elliptical galaxy, the closest active galactic nucleus (AGN), one of the largest and closest radio sources and a classical example of a recent merger. It is the dominant galaxy of the nearby Centaurus Group of galaxies. Rejkuba et al. (2001) presented optical-near-IR colour-magnitude diagrams

(CMDs) of two fields in the halo of this giant elliptical galaxy (Figure 1). These CMDs show broad giant branches indicating a large spread in metallicity. The RGB tip is detected at $K \sim 21.3$.

A large number of sources are observed brighter than the tip of the RGB. These can belong to one of the three categories: (i) intermediate-age AGB stars with abundances similar to those found in Magellanic Clouds, (ii) old and metal-rich AGB stars similar to those found in the Galactic Bulge and metal-rich globular clusters, or (iii) blends of two or more old first ascent giant branch stars. While Rejkuba et al. (2001) have shown with simulations that only a small part of these sources can be ascribed to blends, a definite proof that these bright red giants belong to the AGB population in NGC 5128 is through the detection of variability of these sources. Furthermore, the near-IR properties of long period AGB variable stars can be used to investigate the presence or absence of an intermediate-age component in the stellar populations of this giant elliptical galaxy. This has important consequences for the formation and evolution of giant elliptical galaxies.

Using the multi-epoch K-band pho-

tometry we investigated the nature of bright giants observed above the tip of the RGB (Figure 1) in two halo fields in NGC 5128. Field 1 is located in the north-eastern halo of the galaxy and it coincides with the prominent diffuse stellar shell, presumably a remnant from a recent merger. Field 2 is in the southern halo of the galaxy. The data were taken in the *K*-band over three years with ISAAC at the VLT. As a result of this long term program, which required repetitive observations of the same halo fields, we have discovered more than 1000 long period and large amplitude red variable stars confirming the presence of an AGB population in this giant elliptical galaxy halo.

ISAAC photometry

We obtained a total of 20 epochs of *K*-band photometry in Field 1 and 24 epochs in Field 2 in the time interval between April 1999 and July 2002. The data were obtained in service mode with ISAAC at the VLT, except one Field 2 epoch, which was secured on an observing run in February 2000 with SOFI at the NTT under exceptional seeing conditions. The exposure times for different epochs varied due to changes in seeing and sky conditions, but on average one hour of observation was taken per epoch for each field. The total exposure times amount to 19.7 and 21.1 hours for Fields 1 and 2, respectively. These are the deepest near-IR images taken so far in the halo of an elliptical galaxy.

Data reduction included dark subtraction, flat-fielding and sky subtraction. For each epoch, a single image was obtained combining individual

frames obtained with short (60 sec) exposures that were dithered in an automatic pattern in order to allow the sky subtraction in this stellar field. Each of these 60-sec exposures was already an average of six 10-sec exposures. It is necessary to average a large number of such very short exposures due to high background emission of the sky in near-IR wavelengths. The PSF fitting photometry was done for each single-epoch image individually. The final photometric catalogue contains 13,111 stars in Field 1 and 16,435 stars in Field 2, which have been detected on at least 3 *K*-band frames as well as in *J* and *H*-band images.

A combined colour image for Field 2 of *J*, *H* and the best-seeing epoch in *K*-band is shown in Figure 2. Figure 3 shows a small portion of this field, along with five *K*-band epochs in which several large amplitude stars can be seen. Most of these correspond to red sources on the colour image.

Long period variable stars

Variable stars were identified using a procedure similar to the one described by Stetson (1996). First, we selected all the stars with mean photometric errors given by ALLFRAME smaller than 0.2 mag. We then required each star to be detected on more than 5 frames and constructed variability indices which measure time-dependent correlation of magnitude residuals. In other words, given a mean magnitude and taking into account photometric errors, variability indices show how much a stellar brightness varies between different observations. With these indices, we found that 601 stars in Field 1 and 903 stars in

Field 2 have periodic variations. Of these, 536 and 878 had at least 10 measurements with individual errors smaller than 0.5 mag, and for these we constructed light curves.

A Fourier analysis of the *K*-band light curves was used to search for the periodic signal in the data. The period obtained from the frequency with largest power corresponds to the most probable sinusoidal component. It was further improved with a non-linear least-square fitting of the sine-wave. From this, the best-fitting period (*P*), amplitude, mean magnitude and phase were obtained. In optical passbands Miras often have asymmetric light curves, usually steeply rising to the maximum and with a shallower decline. In the near-IR the variations are more regular and nearly sinusoidal. Hence a sine-wave is a good approximation to most of the LPVs.

For 99 variable stars in Field 1 and 169 in Field 2, no acceptable periods could be obtained because of the non-sinusoidal variations, large errors combined with small amplitudes, multiple periods, presence of irregular period or cycle-to-cycle variations typical for Miras and semi-regular variables, or absence of period (e.g. microlensing, background AGN or SN). In Figure 4, we show a sample of good light curves folded with the periods that are indicated in each panel. Note that each point is plotted twice to emphasize the variability.

The mean amplitude of all the variables for which we could measure periods is 0.7 mag, and the majority have periods in the range of 150 to 500 days. With 24 or fewer measurements per star obtained over an interval of 1,197 days, and with observations distributed in 3–6 month intervals interspaced by ~6 months gaps, there may be some period aliasing. However, most of the determined light curves are of good quality (see Figure 4). For some of the variables the best fitting periods were longer than 600 days and these need to be confirmed with observations over a longer time baseline. The amplitudes and periods of the LPVs are characteristic of Mira variables and are similar to those found in the LMC, SMC and Galactic Bulge. These are the most distant Miras for which periods have been measured and the first in an elliptical galaxy.

The NGC 5128 distance with the Mira P-L relation

A well-defined period-luminosity (P-L) relation has been found for Miras in the Large Magellanic Cloud (Glass & Lloyd Evans 1981, Wood 1999), the Small Magellanic Cloud (Cioni et al. 2003), the Galactic Bulge (Glass et al. 1995), the solar neighbourhood (van Leeuwen et al. 1997) and in Galactic globular clusters (Feast et al. 2002).

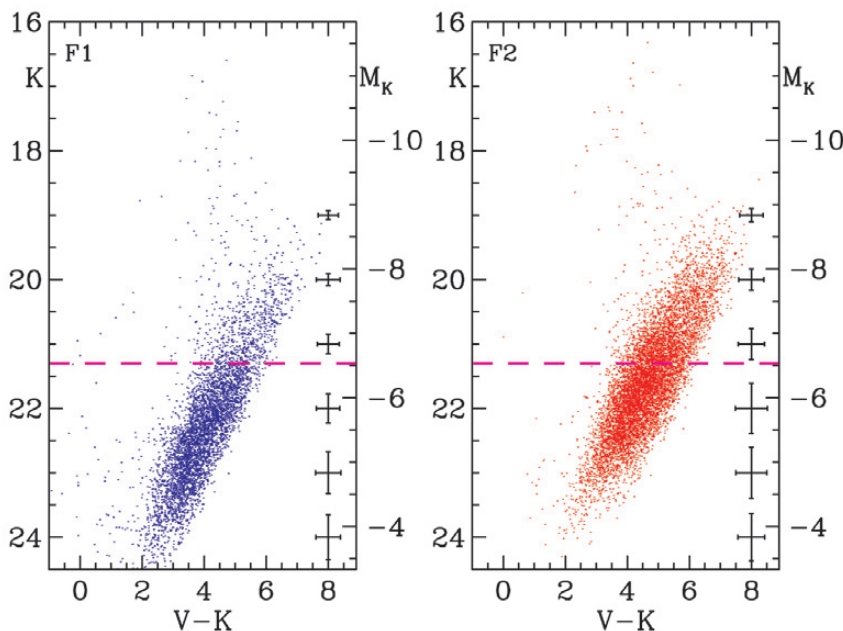


Figure 1: Optical-infrared CMD for 5630 stars in the NGC 5128 shell field (F1; left) and 9001 stars in the NGC 5128 halo field (F2; right), based on ISAAC+FORIS1 images of a region covering $2'5 \times 2'5$ (Rejkuba et al. 2001). A large number of stars brighter than the tip of the RGB, $K \leq 21.3$ (magenta dashed line), are LPVs.

The relation holds for both M_{bol} and M_K . Since Miras are very luminous, their tight P-L relation makes them interesting for distance determination to other galaxies.

Our data are not sufficient to discriminate Mira from SR variables on the basis of the regularity of their light curves. Hence, to select the most probable Miras we made a selection on period ($2 < \log P(d) < 2.6$) and on amplitude ($0.5 \text{ mag} < \Delta K < 1.5 \text{ mag}$). The mean magnitudes derived from the non-linear sine-wave fit were corrected for extinction by subtracting $A_K = 0.039$, corresponding to $E(B-V) = 0.11$. The period-luminosity diagram is displayed in Figure 5. Field 1 variables are plotted with blue and Field 2 variables with red symbols. Variables with better determined periods based on the significance parameter from Fourier fitting algorithm are plotted with larger symbols.

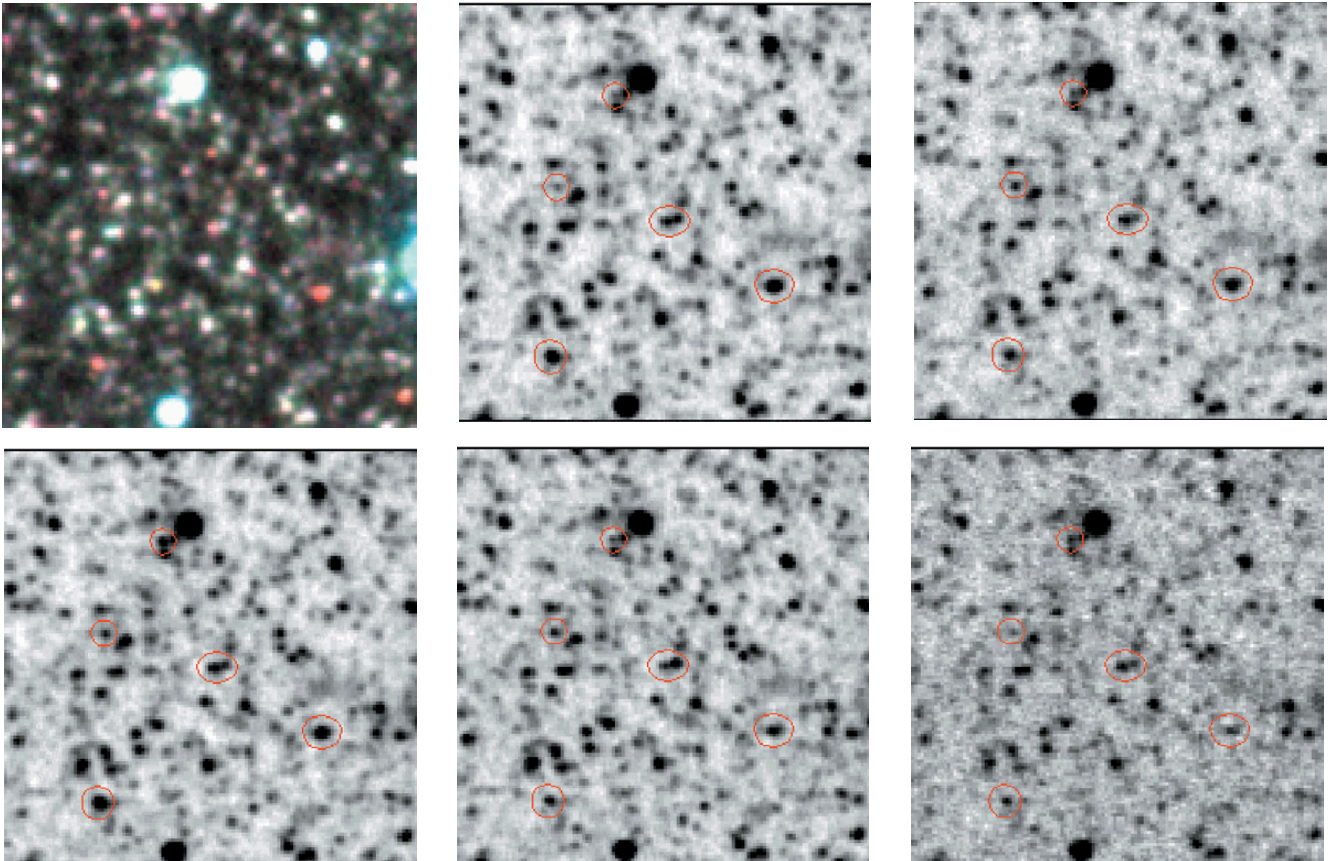
Most of these Mira variables are located where expected, along a well populated sequence in the P-L diagram. This is the first time a Mira P-L relation has been observed in a galaxy outside the Local Group.

Calibration of the P-L relation relies on the LMC P-L relation for Miras. Feast et al. (1989) fit to the LMC Mira P-L relation is: $M_K = -3.47 \log P + \beta$. The zero



▲ Figure 2: A combined color image for Field 2. The J-band is coded in blue, the H-band is green and the K-band image is red. This field is located roughly $9'$ (corresponding to 10.5 kpc at the distance of 4 Mpc) south of the centre of the galaxy. The total exposure time for each band is 1 hour and the field of view is $2'.0 \times 2'.07$. North is up and east to the right. Note the large number of red sources – most of these are long period variable stars.

▼ Figure 3: Zoom of a $131 \times 131 \text{ pix}$ ($19''.4 \times 19''.4$) region showing variable stars in Field 2. Most of the red stars are variable. There is a pair of stars in the centre of this field that varies in counter-phase with similar periods.



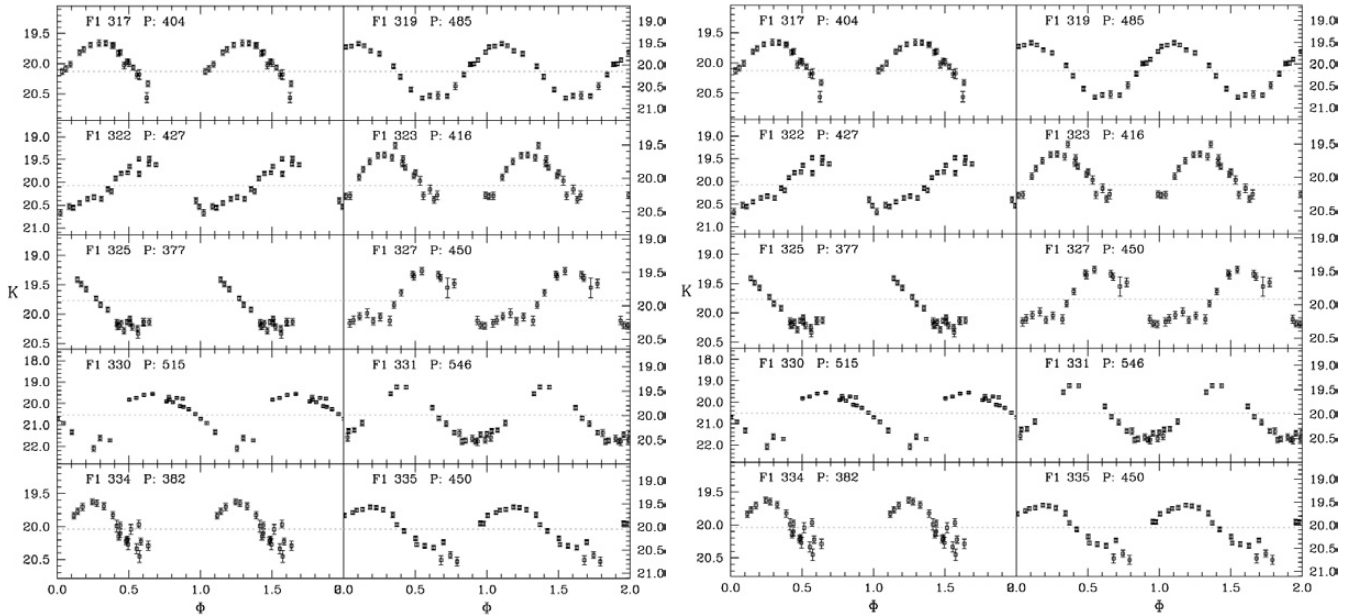
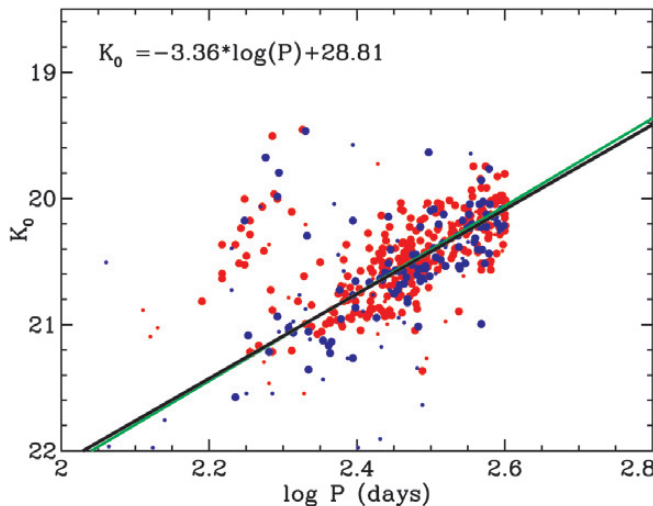


Figure 4: A sample of phased K-band light curves from both fields. Periods (P) are indicated in each panel. Each point is plotted twice to emphasize the variability.

Figure 5: Period-Luminosity diagram in NGC 5128 for long period ($2 < \log P(d) < 2.6$) and large amplitude ($0.5 < \Delta K < 1.5$ mag) variables. Large symbols are used for Miras with more significant periods. Field 1 variables are blue and Field 2 are red. The black line is our best fit to the Mira sequence. The green line is the best fit to the Mira sequence adopting the slope of -3.47 (Feast et al. 1989).



point $\beta = 0.88 \pm 0.10$ has been recently derived using *Hipparcos* parallaxes for Miras in the solar neighbourhood and in well-studied Galactic globular clusters (Feast et al. 2002). With such a calibration, the Large Magellanic Cloud distance modulus is 18.60 ± 0.10 .

A least-squares fit to the Mira sequence in NGC 5128 is:

$$K_0 = -3.36 (\pm 0.13) \log P + 28.81 (\pm 0.32).$$

This fit is overplotted as a solid black line in Figure 5. The 1σ scatter around the fit is 0.19. Fixing the slope to be -3.47 , the best fitting zero point is 29.09 ± 0.32 (solid green line in Figure 5), with the same RMS of the fit.

Finally, the derived distance modulus to NGC 5128 is 28.21 ± 0.32 , assuming a LMC distance modulus of 18.60. If 18.5 is preferred (e.g. Alves et al. 2002), the distance modulus to NGC 5128 would be 28.11 ± 0.32 , in good agreement with that derived from the RGB tip (Harris et al. 1999).

Conclusions

ISAAC multi-epoch K-band photometry of two fields in the halo of NGC 5128 was used to detect variable stars. We derived periods for most of these variables via Fourier analysis of the K-band light curves and sine-wave fitting. Their magnitudes indicate that they are in the AGB phase and their periods and amplitudes are consistent with being LPVs.

The long-period ($400 \geq P \geq 100$ d) large-amplitude ($0.5 < \Delta K < 1.5$ mag) Mira variables were used to determine the distance of NGC 5128 from a P-L relation. Adopting a LMC distance modulus of 18.50, we derive the distance modulus of 28.1 ± 0.3 , corresponding to $D = 4.2 \pm 0.6$ Mpc.

In closing, we would like to note that such programs that require numerous (>10) and relatively short (~ 1.5 h per Field) observations benefit greatly from the availability of service mode obser-

vations. All the images were taken in excellent seeing conditions, ranging from $0''.35 - 0''.65$, enabling us to detect variable stars in a giant elliptical galaxy for the first time and construct the first Mira period-luminosity diagram outside the Local Group. The catalogue with light curve parameters and near-IR photometry of all the variable stars is available through Astronomy & Astrophysics (Rejkuba et al. 2003).

Acknowledgements

We are indebted to many ESO staff astronomers who took the data presented in this paper in service mode operations at Paranal Observatory. DM is sponsored by FONDAF Center for Astrophysics 15010003.

References

- Alves, D.R., Rejkuba, M., Minniti, D., Cook, K.H., 2002, *ApJ*, **573**, L51
- Cioni, M.-R.L., et al., 2003, *A&A*, *in press*, astro-ph/0304143
- Feast M.W., Glass, I.S., Whitelock, P.A., Catchpole, R.M., 1989, *MNRAS*, **241**, 375
- Feast M.W., Whitelock, P.A. & Menzies, J., 2002, *MNRAS*, **329**, L7
- Frogel, J.A. & Elias, J.H., 1988, *ApJ*, **324**, 823
- Glass, I.S., Lloyd Evans, T., 1981, *Nature*, **291**, 303
- Glass, I.S., Whitelock, P.A., Catchpole, R.M., Feast, M.W. 1995, *MNRAS*, **273**, 383
- Harris, G.L.H., Harris, W.E. & Poole, G.B., 1999, *AJ*, **117**, 855
- Rejkuba, M., Minniti, D., Silva, D.R. & Bedding, T., 2001, *A&A*, **379**, 781
- Rejkuba, M., Minniti, D. & Silva, D.R., 2003, *A&A*, *in press*
- Stetson, P.B., 1996, *PASP*, **108**, 851
- van Leeuwen, F., Feast, M.W., Whitelock, P.A., Yudin, B., 1997, *MNRAS*, **287**, 955
- Wood, P. R. et al. 1999, in *IAU Symp.* 191: Asymptotic Giant Branch Stars, p. 151

The Dynamics of Dwarf Elliptical Galaxies

H. DEJONGHE¹, S. DE RIJCKE¹, W. W. ZEILINGER², G. K. T. HAU³

¹*Sterrenkundig Observatorium, Ghent University, Belgium;*

²*Institut für Astronomie, University of Vienna, Austria;* ³*ESO, Santiago, Chile*

A short history

Dwarf elliptical galaxies (dEs) are small diffuse galaxies with smooth elliptical isophotes. One of the most nearby examples is NGC 205 (M110), a satellite of the Andromeda galaxy. From the days of the great comet-hunter Charles Messier up to well into the 20th century, this was the only known object of the class that we now call dEs. In 1944, Walter Baade confirmed NGC 147 and NGC 185 as members of the Local Group by resolving them into individual stars, a feat which was only possible because these dEs are very nearby galaxies. No new Local Group dEs have been discovered since then. In the 1950s, dEs were also discovered in the nearby Fornax and Virgo clusters, offering the possibility to study their photometric properties on larger samples: a dE is a rather gregarious species, spotted abundantly in dense environments such as clusters and groups of galaxies. Spectroscopy of such low-surface-brightness galaxies is challenging however, and had to wait until the early 1990s. At that time, 4 m-class telescopes, CCD cameras, in combination with long exposure times, could start to explore the kinematics and stellar populations of the central regions. Only now however, with large telescopes such as

the VLT, do astronomers have the possibility to obtain spectroscopic information out to large radii, opening up the study of the spatial variations of the stellar populations and the determination of the orbital structure and dark matter content of dEs.

Models for dE Evolution

Although similar to normal ellipticals (Es) at first sight, dEs are quite different from their larger brethren. To begin with, dEs are much more diffuse objects with exponentially declining surface-brightness profiles (Es on the contrary are well described by the more centrally concentrated de Vaucouleurs law). Moreover, and again contrary to Es, dEs become noticeably redder towards larger radii. Current paradigm has it that star-formation proceeded most vigorously in the dense centres of Es, leading to a central population of metal-rich stars. These have many strong absorption lines in the blue part of the spectrum and thus make the centres of Es appear reddish. Finally, up to recent times, most of the dEs for which kinematic information was available turned out to rotate very slowly if at all. This sets them apart from the low-luminosity Es that are generally fast-rotating objects. This is the so-called “kinematic dichotomy” between Es and dEs. Wrapping this up, the photometric and kinematic differences between dEs and Es make it unlikely that ellipticals and dEs share a common origin or a similar evolution. Two currently popular models attempt to explain the properties of dEs (see Figure 1).

formation is enhanced at larger radii, dEs are more diffuse than Es (which have higher escape velocities and hold on to their gas more strongly) and have higher metallicities at larger radii, explaining the observed outward reddening of dEs. Since the stars are born out of gas that is moving outwards, the orbital distribution of the stars will favor radial orbits and rotation will be slow. There is a problem with this model however: standard cosmological models predict that small density fluctuations are less clustered than larger ones, from which the Es grow, contrary to the observed clustering properties of dEs.

The **harassment model** explicitly takes into account the fact that dEs are very clustered objects. N-body simulations have shown how a late-type (Sc-Sd) disc galaxy that orbits in a cluster or around a massive galaxy can be destabilized by gravitational interactions. The small disc galaxy develops a bar that transports angular momentum to the halo and to stars at larger radii which are lost as tidal tails. Gas is funneled in towards the centre by torques exerted by the bar where it is converted into stars, forming a nucleus. The originally rotationally flattened disc galaxy is heated and transformed into an anisotropic, slower rotating dE. The way a dwarf galaxy is affected depends on its orbit and some dEs may still contain some memory of their disk origin. Thus, these simulations not only offer a natural explanation for the clustering properties of dEs and the central luminosity spike (or “nucleus”) observed in many bright dEs, but they also accommodate a number of recently discovered key observational facts: the existence of fast-rotating dwarfs, dEs that still contain gas and dEs with an embedded stellar disc.

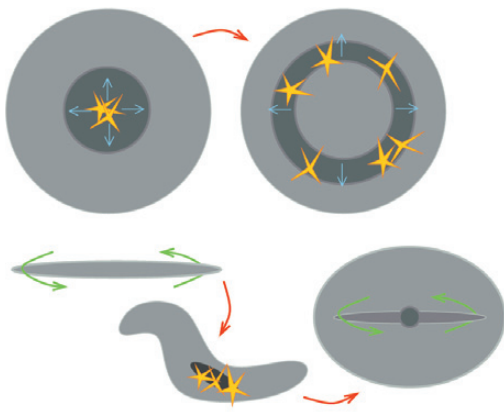


Figure 1: dE formation scenarios. Top : the wind-model. Supernovae blow away a dense gas shell (blue arrows) in which new stars are born. Subsequent supernovae further accelerate the shell and enrich it with metals. Bottom : the harassment scenario. A dE is initially a fast rotating (green arrows) small disc galaxy, destabilized by gravitational interactions. A bar develops and the disc is vertically heated. After a new equilibrium has been reached, the galaxy has a much rounder shape and slower (but still significant) rotation. Some relics of its previous state, e.g. a stellar disc, might survive the turmoil.

According to the **wind model**, dEs are primordial objects that formed from average-amplitude cosmological density fluctuations. Supernova explosions heat the interstellar medium (ISM) to velocities exceeding the galaxy’s escape velocity and cause a supersonic outflow of gas from the galaxy, blowing away most, if not all, of the ISM. Stars form in this expanding shell and subsequent supernova explosions further accelerate its expansion and enrich it with metals. Since star-

An ESO Large Programme

We embarked on a Large Programme to obtain deep, high resolution spectra along the major and minor axis from a varied and sizeable sample of group and cluster dEs to study their internal dynamics and stellar populations. The goals of this program are (1) to assemble a large, homogeneous data-set of photometry, kinematics and dynamics of dEs of unprecedented high quality, (2) to model the dynamics of dEs ranging from dE0 to dE6, including dS0s, to check whether the kinematic dichotomy between Es and dEs is real and whether dEs become more rotationally

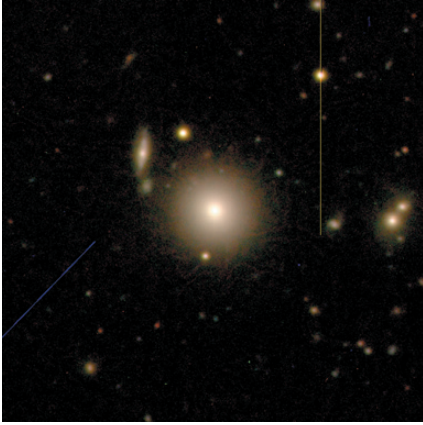


Figure 2: A VRI color composite image of FS76, a NGC5044-Group dE1. North is up, east is to the left.

supported as one goes to more flattened specimens, (3) to check the relation between the mass-to-light ratio and luminosity predicted by the wind model and whether a cuspy dark-matter density is required to fit the kinematic data (thus, dynamical models serve as a check on CDM cosmological models of galaxy formation), (4) search for dEs with peculiarities such as embedded discs, fast rotation, ionised gas, kinematically decoupled cores... that would support the harassment scenario, (5) measure line-strengths in the wavelength region $\lambda\lambda 790\text{--}930$ nm in order to study the stellar populations of the sample dEs.

We used FORS2, equipped with the very efficient volume phased holographic grating GRIS_1028z+29. This combination gives both a high throughput and high spectral resolution ($\sigma_{\text{instr}} = 30$ km/s with a $0.70''$ wide slit), allowing us to accurately measure velocity dispersions as low as 20 km/s, which we verified by extensive Monte Carlo simulations. The exposure times were fine-tuned so as to reach $1.5\text{--}2 R_e$ with a signal to noise ratio $S/N \approx 15$ per bin for the brightest dEs of our sample ($15 < m_B < 16$). For fainter objects ($m_B \geq 16.5$), we go out to $1\text{--}1.5 R_e$ at the same noise level. The standard data reduction procedures were performed with ESO-MIDAS. The individual spectra were bias-subtracted and flat-fielded. Cosmic ray events were removed and the spectra were binned to a linear wavelength scale (rectifying the emission lines of the arc spectra to an accuracy of 1 km/s FWHM). The sky background was subtracted very carefully. Using blank sky-spectra we corrected the spectra for variations of the slit-transfer function which resulted in a perfectly flat sky background that could be removed very accurately. The ubiquitous bright OH Meinel emission bands are undersampled at the high spectral resolution we are working at and proved much harder to remove completely. Fortunately, only a few galaxies had absorption lines that were affected by

these emission lines. Finally, the spectra were flux-calibrated and co-added.

In the following, we will discuss the extraction of kinematic information from galaxy spectra and our dynamical modeling method, and present our results so far (De Rijcke et al. 2001, 2003a, 2003b).

Determining kinematics

The absorption lines in a galaxy spectrum are Doppler broadened due to the motions of the stars along the line of sight and their precise shape depends on the line-of-sight velocity distribution (LOSVD) of the stars. The LOSVD is approximated as a fourth-order Gauss-Hermite series, condensing the kinematic information to the mean velocity v_p , the velocity dispersion σ_p and two coefficients, h_3 and h_4 , that quantify respectively asymmetric and symmetric deviations from a Gaussian LOSVD. These kinematic parameters can be obtained by fitting a weighted sum of stellar spectra, broadened with a parameterized LOSVD, to a galaxy spectrum. Doing this for each row of the galaxy spectrum yields the kinematics as a function of position along the slit.

Dynamical modeling

Kinematics along major and minor axis can be used to constrain the dynamics of a galaxy. A dynamical model consists of a gravitational potential and a distribution function. The potential generates the gravitational forces that bind the stars together, including the effects of the dark matter. The distribution function gives the number of stars on each orbit. From these two ingredients, all properties of a model can be calculated and compared to the observations. With our modeling technique, three-integral axisymmetric models are fitted to the kinematics. Since each model is given an absolute likelihood, a range of mass distributions that are compatible to the data at a given confidence level can be determined for each galaxy. This gives us detailed information about the orbital structures of the observed galaxies and allows robust

estimates of their masses and mass-to-light ratios to be made.

FS76, a rotationally flattened dE

The non-nucleated NGC5044-Group dE1 FS76 ($M_B = -16.70$ for $H_0 = 75$ km/s/Mpc) is a case study of a rotationally flattened dE (De Rijcke et al. 2001). Our observations were carried out in May, 2000 with FORS2 on Kueyen. Total integration time was 5 h for each position angle. The analysis of the surface photometry confirms the picture of FS76 as a normal dwarf elliptical (see Figure 2). No photometric peculiarities were noted: there is only a modest amount of isophote twist; also no significant deviations from ellipses were detected in the isophotes. Its heliocentric velocity, derived from the spectra, confirms FS76 as a member of the NGC5044 group.

The central velocity dispersion σ_p equals 46 ± 2 km/s. The maximum rotation velocity along the major axis is 15 ± 6 km/s. The asymmetry in the mean velocity and velocity dispersion profiles (see Figure 3) may signal that FS76 is currently undergoing an interaction with NGC5044 which is at a projected distance of only 30 kpc. The ratio of the mean velocity v_p to the velocity dispersion σ_p can be used as an indicator for the importance of rotation in the flattening of a stellar system. For an isotropic E1 galaxy, flattened by rotation, one expects $v_p/\sigma_p = 0.35$. The observed ratio of the peak velocity to the central velocity dispersion is $(v_p/\sigma_p)_{\text{obs}} = 0.33 \pm 0.15$, fully consistent with FS76 being an isotropic oblate rotator. Moreover, the best fitting dynamical model shows that the radial velocity dispersion varies only by a few km/s from the equatorial plane towards the rotation axis and therefore pressure differences play only a minor role in flattening this galaxy. Thus, the observed kinematics and detailed dynamical models unambiguously show that FS76 is indeed flattened by rotation and not by pressure. Since these findings were published, more dEs with significant rotation have been discovered, both by us and by others. These results

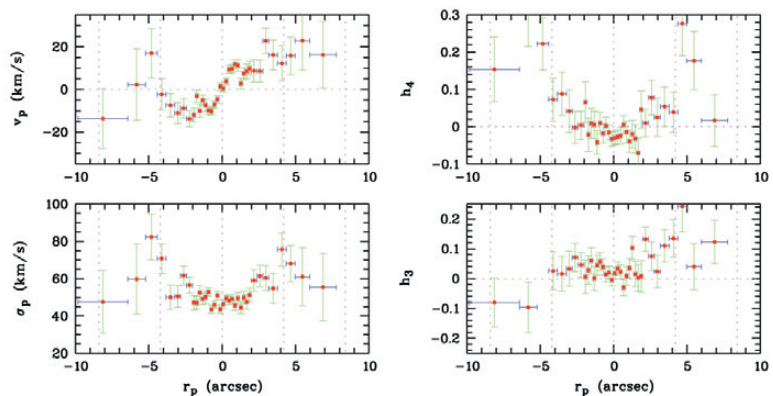


Figure 3: The major-axis kinematics of FS76. Left: mean velocity v_p and velocity dispersion σ_p . Right: Gauss-Hermite coefficients h_3 and h_4 , quantifying asymmetric and symmetric deviations from a Gaussian line-of-sight velocity distribution.

corroborate the prediction of the harassment scenario that fast-rotating dEs should exist.

dEs with embedded discs

We collected *R* and *I* band images of FCC204 (dE6, $M_B = -16.52$) and FCC288 (dE7, $M_B = -16.18$), two Fornax cluster dEs, with FORS2 on Kueyen in November, 2000 (De Rijcke et al. 2003b). Both galaxies have “disky” isophotes, so they are better classified as dwarf lenticular galaxies or dS0s. To check whether this diskiness is caused by the presence of a real stellar disc, we applied an unsharp masking technique. We smoothed the *R*-band image of each galaxy with the MIDAS command filter/med to replace each pixel by the median of a $6'' \times 6''$ surrounding box. This smoothed image is then subtracted off the original one, highlighting any fine structure. The original and residual images are presented in Figures 4 and 5.

The prominent disc in FCC288 can be traced out to 2 kpc. Clearly visible is the flaring and warping of the disc. The thickness of the disc remains more or less constant around 160 pc inside the inner kpc. Beyond that the disc thickens rapidly, reaching ≈ 500 pc at a radial distance of 2 kpc. FCC204 has a much less impressive disc, traceable to about 1.8 kpc and about 255 pc thick. Besides a large bulge, two brightness maxima at symmetric positions with respect to the nucleus are visible. A possible interpretation is that we are looking edge-on onto a bulge+bar system and that the two brightness enhancements constitute the edges of the bar or perhaps are even small spiral arms.

Spectra of FCC288 and FCC204 were obtained with FORS2 in November, 2000 on Kueyen and November, 2001 on Yepun, respectively. As an example, the major axis kinematics of FCC204 are plotted in Figure 6. Both galaxies are very rapid rotators. Still, they do not rotate fast enough to explain their apparent flattenings. This is most likely due to the fact that the observed kinematics also reflect the motions of the stars that make up the less flattened (i.e. slower rotating, more anisotropic) body of the galaxy. Inside the bulge of FCC204, the LOSVDs have a Gaussian shape. In the discs of both galaxies, the LOSVDs are more peaked and skewed. The edges of what we interpret to be a bar in FCC204 correspond to changes in the velocity dispersion and the rotation velocity. The very fast rotation and the correlation of the various kinematic parameters with the photometric features strengthen our interpretation based on the unsharp masking : both galaxies are seen practically edge-on and contain fast-rotating disc structures. Such embedded stellar discs may be relics from the pre-harassment era, according to the harassment scenario.

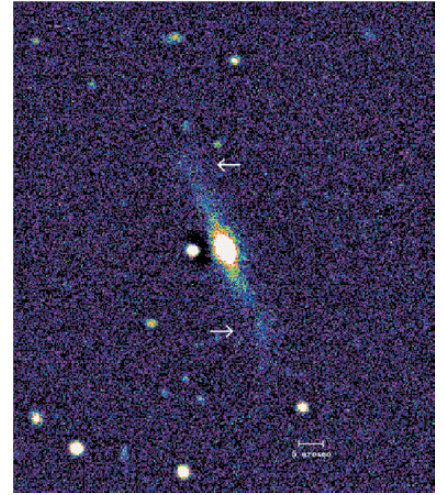
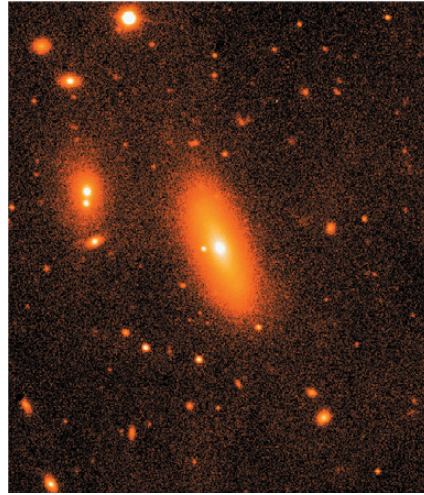


Figure 4: Left panel : 120 sec. R-band image of FCC204. Right panel : result of unsharp masking. At the outer edges of the disc, two brightness peaks are visible (marked by arrows). North is up, east is to the left.

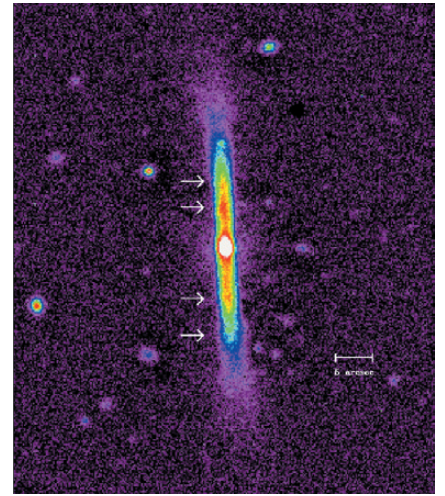
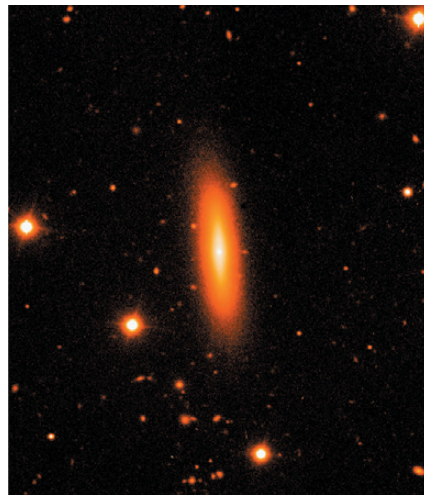


Figure 5: Left panel: 600 sec. R-band image of FCC288. Right panel: result of unsharp masking. The disc embedded in FCC288 runs practically across the whole face of the galaxy. The flaring of the disc and the brightness fluctuations in it (marked by arrows), which could be spiral arms, are clearly visible. North is up, east is to the left.

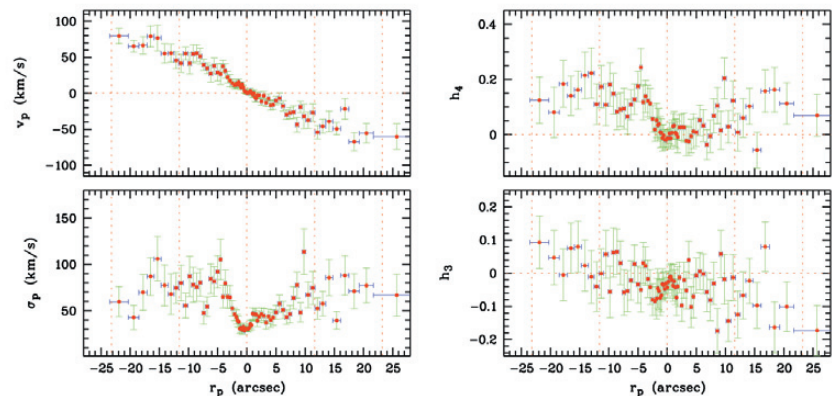


Figure 6: Major axis kinematics of FCC204. Left: mean velocity v_p and velocity dispersion σ_p . Right: Gauss-Hermite coefficients h_3 and h_4 , quantifying asymmetric and symmetric deviations from a Gaussian line-of-sight velocity distribution.

dEs with a warm ISM

We obtained *B*, *R*, and *I* broad-band images, $H\alpha + [NII]$ narrow-band images and spectroscopy of the nucleated dEs FCC046 (dE4N, $M_B = -15.29$) and FCC207 (dE2N, $M_B = -15.09$) in the

Fornax cluster in November 2000 and November 2001. FCC046 was classified as a non-nucleated dE4 so the presence of its very bright and blue nucleus came as a surprise. The nucleus is resolved under seeing conditions of

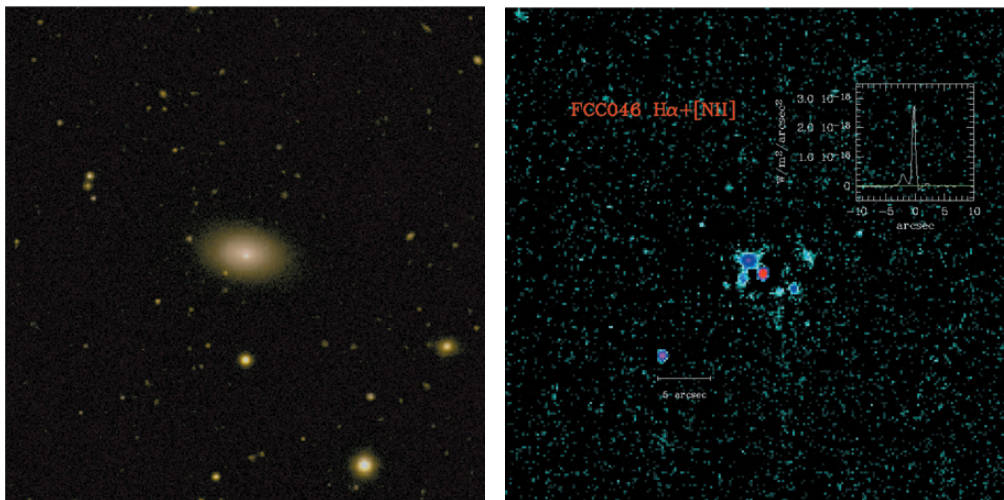


Figure 7: Left panel : a BRI colour composite image of FCC046. Note the off-centre nucleus. North is up, east is to the left. Right panel : $H\alpha+[NII]$ emission image of FCC046. Six emission clouds other than the nucleus can be discerned. The horizontal bar measures $5''$ on the sky. The inset shows a cut through the central emission region. The intensity is plotted in units of $W/m^2/arcsec^2$.

$0.8''$ FWHM and is offset by $1.1''$ to the south-west of the centre of the outer isophotes. It has a blue magnitude $m_B = 18.55$ mag ($M_B = -12.77$) and comprises about 10% of the total B -band luminosity of the galaxy. FCC046 shows a pronounced lopsided shape. Given that FCC046 is an isolated galaxy in the outskirts of the Fornax cluster, it is unlikely that an encounter caused this asymmetry. Based on broad-band colours, its disturbed shape and its very bright nucleus, FCC046 is akin to the class of amorphous dwarfs, the name coined by Allan Sandage for dwarf galaxies that have a disturbed appearance due to recent star formation and the presence of dust but are not irregular enough to be classified as Im (Magellanic-Cloud type irregulars). The nucleus of FCC207 has a distorted shape: it is more elongated than the bulk of the galaxy (E3 versus E2) and is somewhat kidney-shaped. This is probably due to dust-absorption to the north of the nucleus, noticeable in the $B-R$ color map. The $B-R$, $B-I$ colors stay essentially constant outside the nucleus. Based on published UBV colors and metallicities, it was concluded that FCC207 is too blue in $U-B$ ($U-B = 0.15$) and too metal-poor for its $B-V$ ($B-V = 0.78$) and this was interpreted as a consequence of the presence of a young stellar population. This motivated us to investigate both objects more closely.

We took 20 minute exposures of FCC046 and FCC207 with the $H\alpha/2500+60$ narrow-band filter with FORS2 on Yepun. R band images served as off-band images. The narrow-band filter only lets through the light of the $H\alpha$ 6563 \AA emission line of ionised hydrogen and two adjacent emission lines of ionised nitrogen, $[NII]$ 6548 , 6583 \AA and thus traces the presence of ionised gas. The standard data reduction procedures (bias subtraction, flat-fielding, cosmic removal, interpolation over bad pixels, sky subtraction) were performed with MIDAS. All science images were corrected for atmospheric

extinction using the R band extinction coefficient and interstellar extinction. The emission-images were converted to physical units (W/m^2) with the aid of the spectrum of a flux-calibration standard star.

Color images and pure $H\alpha+[NII]$ emission images of FCC046 are presented in Figure 7. The total emission luminosity of FCC046 is $L_{em}(FCC046) = 6 \times 10^{30} W$, about half of which is emitted by the central peak corresponding to the galaxy's nucleus. The total emission luminosity of FCC207 is somewhat higher: $L_{em}(FCC207) = 8 \times 10^{30} W$. The total mass in ionised hydrogen can be estimated assuming complete re-absorption of all Lyman photons and an electron density $N_e = 1000 \text{ cm}^{-3}$. We then find that for FCC046 $M_{HII} \approx 40-150 M_\odot$ and for FCC207 $M_{HII} \approx 60-190 M_\odot$, depending on the unknown contribution of the $[NII]$ lines to the $H\alpha+[NII]$ emission.

In FCC046, the emission is distributed over a bright central region and six fainter clouds, three of which are resolved. The diameters and luminosities of the resolved clouds are consistent with them being supernova-remnants but they are about 10 times larger than HII regions of comparable luminosity. Nebulae around Wolf-Rayet stars could be a plausible alternative and are found in many irregulars and have appropriate luminosities and diameters. The similarities of the broad-band colours of FCC046 to those of star-forming or amorphous dwarfs, its relatively strong core and the presence of emission clouds support the conclusion that FCC046 is actively forming stars, albeit at a very leisurely pace when compared to Blue Compact Dwarfs (BCDs) and amorphous dwarfs which are about a factor 1000 more luminous in $H\alpha$. The nuclear emission of FCC046 and FCC207 can be adequately accounted for by photo-ionisation by post-AGB stars although a contribution of $H\alpha$ emission from star-formation cannot be excluded. Only the emission from the

six clouds observed in FCC046 (supernova remnants, Wolf-Rayet nebulae) can be interpreted as unambiguous evidence for recent or ongoing star-formation.

Preliminary conclusions

In the course of this Large Program, we have assembled kinematics of unprecedented high quality of a sample of 15 dEs. All data have been reduced and analysed, and the last few objects are being modelled. Outstanding results based on selected objects have been published or are in press. More papers, in which we will present our conclusions based on the photometry, dynamics, and line-strengths of the full sample, will be submitted shortly.

Thanks to the high spatial and spectral resolution of our observations, we have uncovered the existence of dEs with complex behavior and internal structures (such as embedded stellar discs) that are hard to fit into a simple scenario in which dEs form through the collapse of primordial density fluctuations, like the wind model. Clearly, dEs are anything but small "island universes" that evolve in splendid isolation: their evolution appears determined, at least in part, by their environment. Thus, the harassment scenario offers an attractive explanation for many observed features that are hard to explain with the wind model.

References

- De Rijcke S., Dejonghe H., Zeilinger W. W., Hau G. K. T., 2001, *ApJL*, **559**, L21-L24
- De Rijcke S., Zeilinger W. W., Dejonghe H., Hau G. K. T., 2003, *MNRAS*, **339**, 225-234
- De Rijcke S., Dejonghe H., Zeilinger W. W., Hau G. K. T., 2003, *A&A*, **400**, 119-125
- Ferguson H. C., Binggeli B., *A&ARv*, **6**, 67-122
- Moore B., Katz N., Lake G., Dressler A., Oemler Jr. A., *Nature*, **379**, 613-616
- Mori M., Yoshii Y., Tsujimoto T., Nomoto K., *ApJL*, **478**, L21-L24
- Simien F., Prugniel P., *A&A*, **384**, 371-382

From Books to Bytes: Changes in the ESO Libraries over the Past Decade

UTA GROTHKOPF, ESO Library Garching, esolib@eso.org

Ten years in the lifetime of an astronomy library may not be much, but the past decade brought many changes, and it may be worthwhile to pause for a moment and look back. Ten years ago, we spent most of our time doing paper work, dealing with incoming invoices and processing new books. Our tasks centred on the publications physically located in the libraries.

Today, the physical library sites have decreased in importance, and the virtual library is about to take their place. The Internet has become the essential tool to retrieve information and provide rapid service to our users. Instead of making publications available in the library, it has become more important to provide access through the library so that astronomers can reach them conveniently from their desktops.

The Early 90s: Focus on the In-House Library Collection

During the early nineties, ESO maintained libraries in Garching and at La Silla as well as a smaller third library in La Serena. The main focus of our attention was on the resources physically available in the ESO libraries. Book acquisitions, journal issue check-in and other technical tasks demanded a large amount of time. After payment, all purchased items belonged to the library. The concept of "fair use" allowed us to photocopy journal articles for personal and research purposes as well as to send them to requesting libraries through inter-library loan. This assured (almost) equal and fair access to the scientific literature for researchers from rich and less fortunate institutes alike. Continued access to the astronomical literature was guaranteed because libraries archived publications of long-lasting interest.

Newsletters and reports from observatories around the world brought information about ongoing projects to the astronomers' attention. Occasionally, ESO scientists and engineers needed articles and books that were not available at ESO. Document delivery services were not yet in place, and obtaining publications from other libraries was a time-intensive process.

Many astronomers stopped by the library regularly to look at new journal issues, preprints and latest book acquisitions. Their visits provided ample op-

portunities for discussion about library matters and for suggestions and comments.

The Mid-90s: Electronic Journals

The Internet revolutionized communication and information access. In order to bring the library holdings to the astronomers' desktops, our catalogue became available online in 1992. At that time, access was via a non-graphical telnet interface that was replaced in 1996 by a more user-friendly web catalogue. A paradigm shift in information retrieval occurred in the mid-nineties with the advent of electronic publications. They opened a whole new world of challenges as well as concerns (see Table 1, top). Archiving electronic documents became one of the most heatedly discussed topics among librarians. E-publications cannot be stored once for good like paper documents, assuming that they will always be usable as they were at the time of their creation. Technology is changing rapidly; microfilm, microfiche, and the 5.25" diskette remind us how quickly storage media and the corresponding reading devices can become obsolete. In the early days of electronic publications, various archiving models were considered, ranging from off-line storage on CD-ROMs to simply discarding archives after some years. To date, a definitive solution is still pending.

We have spent a lot of time understanding, reviewing, and negotiating license agreements for electronic journals. Previously, copyright had determined for which purposes publications could be used, but these regulations were not extended to the electronic environment. Instead, contracts had to be signed which often reduced user rights and left questions, in particular regarding future access. What will happen if subscriptions end? Will we be allowed to access the volumes we already paid for after cancellation, or will we lose access to back issues? Will archives be maintained if a journal ceases publication or a publisher is sold to another company? Like many other observatory libraries, ESO does not belong to a university system where contracts are negotiated and signed by the central library for all affiliated branch libraries. This means that we have had to discuss any amendment directly with the pub-

lisher, trying to achieve the best possible conditions for our users. Some electronic journals were not subscribed because of unacceptable usage conditions or outrageous prices. During these years, communication and networking among astronomy librarians was invaluable. In 1988 the first conference on *Library and Information Services in Astronomy* (LISA) was held, and there was a strong wish among the community for another meeting. LISA II took place at ESO Garching in 1995; it provided an excellent opportunity for discussion about the changing world of libraries not only among librarians, but also with participating astronomers, publishers and computer specialists.

With the growing acceptance of the *arXiv.org* (astro-ph) e-print server since 1996, preprints were undergoing major changes. Electronic preprints allowed astronomers to distribute research results long before publication in journals, and observatories, in order to save on shipping costs, considered switching from paper to electronic format. This trend became obvious in our libraries when we started to receive lists of titles and authors instead of the actual preprints. Later, even these were substituted by pointers to the institutes' web pages where preprints were made available. It was a logical consequence to provide access to these web sites from our library pages. For the ESO libraries, the World Wide Web has always been an attractive way of providing information. Already in the early nineties, we began to explore its opportunities, and the library homepage was among the first at ESO. Since then, the content and layout have undergone several changes, and the number of pages has grown considerably. In particular for new users, the homepage often is the first point of contact with the library (www.eso.org/libraries/).

In 1994, the La Serena library was transferred to La Silla, the one at La Silla, in turn, moved to the Vitacura offices in Santiago. From that time onwards, the La Silla library was unstaffed except for occasional visits by the librarian. In the course of the years, its usage decreased, and book purchases were slowly reduced to reflect the changed user behaviour. Rising journal subscription costs, partly resulting from considerable extra fees for electronic access charged by some publishers,

were a constant matter of concern. In 1999, cancellations of less frequently used journals became necessary. This marked the beginning of a change from purchasing publications “just in case” to “just in time” – documents were no longer obtained because someone may eventually be interested, but only when they were actually requested. It was our responsibility to find the most cost-effective and efficient solution for each publication.

2000 Onwards: Virtual Libraries

Despite the increasing availability of electronic documents, print publications continue to arrive in our libraries as before. Up to now, electronic format hasn't replaced paper, but complements it. For most journals the print edition is still regarded as the reference version, and astronomy books are not even available yet in electronic format. Traditional library tasks like bookbinding, journal check-in, and book processing still demand their share of time. On the other hand, it is obvious that collection development in the digital age takes on a new face. The notion of all purchased publications being physically located within the four walls of our libraries has ceased to exist. Electronic books, once they are of importance in astronomy, will have to be integrated into our catalogue. Bibliographic records of electronic journals already contain hyperlinks to journal homepages so that users can access them seamlessly from the webcat. In 2002, ESO Management decided to establish an electronic-only library at the VLT telescope site at Paranal. The number of books purchased for Paranal will be kept at the very minimum and journals will be available in electronic format only. Also for the La Silla library, the emphasis will be on electronic access from now on. As a first step, existing print subscriptions including core astronomy journals were stopped for La Silla. The trend seems to be clear: astronomers retrieve publications electronically and print them locally. Figure 1 shows the number of *ApJ*, *AJ* and *PASP* article downloads from 2000 to 2002; the total number in-

	Early 90s	2000+
Print versus Electronic Publications		
Format	Print documents	Electronic (networked) documents
Material location	Library	Publishers' servers
Usage rules	Copyright	Contracts
Purchase concept	Library owns purchased publications	Access only for duration of contract
Archiving	Done by libraries	To be determined
Information Retrieval and Provision		
Information access	Locally in the library	From anywhere, at any time
Information resources	On paper	Interconnected databases; non-electronic resources become marginalised
Library visibility	Users are aware of the library and its services	Users bypass the physical library; library role becomes invisible
Past and present		
Library Mission and Role		
Mission statement	Fulfill the information needs of our users by selecting, collecting, preserving, and providing access to relevant resources	
Tools	Monitor, evaluate and, if appropriate, apply available information retrieval tools	
Interaction with users	Tailor library services according to the specific needs of users	
Mediation	Learn about requirements of library users; use results for service enhancement within the library and as feedback to publishers	

Table 1: What has changed and what hasn't: Library functions and role in the past decade.

creased by a factor of almost 2.6. Some questions remain though: How will astronomers cope with this approach in the long run? Will increased demand for electronic format result in even higher prices for e-journals? Will print-only resources be neglected completely in future?

During recent years, the library has become involved in bibliometric studies to measure scientific return from telescopes. Since the early nineties, we have compiled the bibliography of papers by ESO staff and visitors. While its initial purpose was to provide a complete list of publications for the ESO Annual Report, it has matured into a database on the use of ESO telescope data in refereed journal articles, including information on the instruments used for observations as well as observing programme IDs. These data may be linked to the AVO (Astrophysical Virtual Observatory) databases in the future.

The electronic age has been upon us for several years now. Astronomers have become used to interconnected resources being available from any-

where, at any time through the Internet, and they often bypass the library in their search for information. Our role in providing access to information resources has become invisible; many of the tasks we accomplish are not immediately noticed by the users, or are not attributed to libraries. The question may arise: do we still need libraries? The answer can be illustrated by an anecdote that dates from the time of LISA II. During program preparations, one of the organizers (not a librarian) suggested to change the full name of the conference to *Library and Information Systems in Astronomy*, but the librarians insisted that the S stands for Service, and the original name remained unaltered. Personalized service, tailored to the individual needs of the library users, distinguishes libraries from software tools. The “human factor” remains important also in the digital age, be it for “troubleshooting” if things go wrong or for tricky cases of information retrieval for which users appreciate assistance. Although many changes have occurred in library management and information provision during the past years, the library's mission and role are still the same (Table 1): we fulfil the information needs of our users by selecting, collecting, preserving, and providing access to relevant resources. We monitor, evaluate and, if appropriate, apply available information retrieval tools. By communicating with library users, we learn about their requirements and use the results for service enhancement within the library and as feedback to publishers and information providers. In this way, we sustain the traditional library functions and at the same time respond to the changes that occur in the way astronomers do their research today.

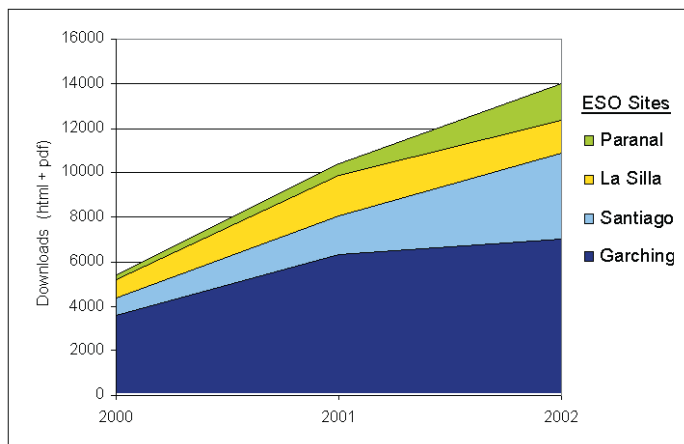


Figure 1: Article downloads from major astronomy journals, 2000 – 2002.

International Workshop on

First Decadal Review of the Edgeworth-Kuiper Belt: Toward New Frontiers

O. HAINAUT (ESO/Chile)

On March 11 to 14, 2003, an international conference on the Minor Bodies in the Outer Solar System was held in Antofagasta, Chile. The conference, which was organized by ESO and Universidad Catolica del Norte (UCN) of Antofagasta, gathered about 70 participants from 20 countries. Originally, it was supposed to take place on the UCN campus. However, a student strike forced us to relocate at the last minute to the Carrera Club Hotel. Thanks to the efforts of A. Lagarini, the conference secretary (and ESO/Chile Science secretary) and to the Hotel staff, this did not cause any disruption. The traditional group photo (opposite) was shot in front of the Geological Museum of UCN. This short summary highlights some of the results presented at this conference; the proceedings, which are currently being edited, will be published as a special issue of "Earth, Moon and Planets."

Just over 10 years ago, the first Trans-Neptunian Object (TNO), 1992 QB₁, was discovered by Jewitt and Luu (IAUC 5611). This was the first of about 700 TNOs known today. They are believed to be remnants of the proto-planetary nebula, the largest objects of the Edgeworth-Kuiper Belt (EKB), extending beyond ~ 30 AU from the Sun, which is also the reservoir of Short Period Comets.

Thanks to more and more detailed numerical simulations, which are supported by a continuously growing number of objects with well determined orbits, the broad lines of the dynamical history of these objects now begins to be fairly clear. Morbidelli presented a review of the latest results. The TNOs are distributed as follow:

- A large fractions are located in the main belt (the "Classical Objects"), which includes objects with fairly circular orbits of low inclination.

- Others have been trapped in stable motion resonances with Neptune, constituting the Resonant Population, also known as Plutinos (named after Pluto, the largest member). One of the very promising theories explaining the number of objects in these resonances involves the outward migration of Neptune, a migration caused by the ejection of proto-planetesimals by this planet, during the early days of the Solar System. In that process, the stable resonances swept the inner Kuiper belt, trapping the objects encountered,



and exciting their eccentricities and inclination.

- A third population is constituted by objects that have been ejected by interactions with Neptune. They are now on very eccentric and inclined orbits, constituting the "Scattered Disc."

One of the puzzling problems was that the "Classical Objects" appear to be distributed in a very dynamically cold population (low inclination), mixed with a secondary population of higher inclination. Gomez and Morbidelli demonstrated how this can be explained by interactions of objects of the inner edge of the Edgeworth Kuiper belt with Neptune, which would slightly "kick out" these objects. Malhotra and Kuchner further studied, from the theoretical point of view, the evolution of dust in the EKB, and compared it with other observed dust discs, suggesting some similarities.

Many other results were presented; for instance, Chiang performed extensive numerical simulations of the resonant objects, showing how they tend to cluster at preferred positions leading and trailing Neptune. Wyatt showed how similar effects could possibly be observed in extra-solar Edgeworth-Kuiper belts (also known as circumstellar discs). For instance, the disc around Vega displays some striking similarity with his simulations; if confirmed, this would imply the presence of (proto-) planet around that star. Fernandez, who is one of the founding fathers of the EKB as a reservoir of comets, made some promising connections between the Scattered Disc and the Oort cloud.

Koebert discussed the possibility of a perturbation in the EKB as the origin of the "Late Heavy Bombardment" that the inner planets suffered 3.8 Gyr ago. Jancart presented a generic model that considers dissipative force combined with the effects of the orbital resonances.

After a session full of numerical simulations of dynamical processes, the observers presented the results of ongoing surveys. While over the past years, many "generic" surveys discovered the bulk of the currently known objects, we see now a specialization of these surveys. Buie et al presented the "Deep Ecliptic Survey," which aims at discovering many TNOs of intermediate brightness, with special care in securing the orbits by carefully planned (and time consuming) follow up. This follow up is critical, as about half of the known objects do not have orbits reliable enough to ensure their recovery. Moody, and Trujillo and Brown performed extremely wide, shallow surveys aimed at discovering all the brightest TNOs. Unfortunately, they did not detect any new Pluto, although there is still a possibility to have a couple of objects of that size out there. The survey by Moody et al has the very sad peculiarity of having been terminated by the destruction of its telescope, at Mount Stromlo. Fortunately, the data are not lost. Kinoshita, Holman and Hainaut have performed some deep to extremely deep surveys (with Subaru, VLT and HST) in order to study the faint end of TNO luminosity function. Kinoshita, with his results down to mag ~ 27.7 reported a bent in

that luminosity function at mag ~ 24 . The two other surveys (which should be even deeper, possibly beyond mag 30 by combining 3 nights of data on 2 VLTs in parallel) will soon check and refine this result. Indeed, such a bend is expected, as the power-law luminosity function cannot extend down to dust size. Otherwise, the resulting dust cloud would have been detected by IRAS. The size at which it happens will give direct constraints on the importance of disruptive/aggregating collisions and accretion in the early solar system. Also, we hope that these deep surveys will reveal what lies beyond 45 AU, where absolutely no object has been discovered so far, while the protoplanetary nebula is expected to have extended out to several hundred AU, making this lack of distant objects one of the most puzzling questions of the field.

The observers continued with physical studies of TNOs. It is worth reminding the reader that TNOs are faint (typically in the 20–25 mag range) making their physical studies quite challenging, especially for spectroscopy, where the expected absorption features are very shallow. In order to get a grasp of the whole population, large photometric surveys have been performed, collecting colours of almost 100 objects in total. They reveal a broad distribution ranging from neutral (solar) to very red colours, the large majority of objects having a fairly linear reflectivity spectrum. Dorressoundiram and Boehnhardt presented such a survey, performed in the framework of a VLT large program (which was concluded during the conference). Dorressoundiram and Thebault analysed them by comparing them with a model of collisions affecting the TNOs. Indeed, collisions, by resurfacing the objects, are expected to have an effect on their colours. Fulchignoni split the objects in families using multivariate analysis of their colours, as done 30 years ago with the main belt asteroids, resulting in taxonomic families that were later related to the physical nature of the objects. Stephens (who presented a large HST-based colour survey) and Peixinho performed various statistical tests in order to reveal possible correlations between the colours of the objects and their other parameters (orbital elements, size, etc).

Sheppard, Jewitt and Ortiz have obtained light curves of several objects, which reveal their rotational periods and constrain their elongations. While most objects do not display significant magnitude variations (which is interpreted as almost spherical objects), about a quarter of them have light curves with full amplitude greater than 0.15 mag. Also, the measurements of 1995 SM₅₅ (by Sheppard and Jewitt) displayed a strong dispersion – a controversial result, to which a controversial interpretation is attached: this could be the evidence of cometary activity. Cometary activity, caused at these distances by the sublimation of super-volatile ices such as CO, should in theory be possible, but has never been observed. It would be an interesting process for resurfacing the objects, possibly explaining (part of) their colour diversity. In the same line, Meech obtained some extremely deep images of TNO 24952 with Subaru, in order to search for direct evidence of a coma surrounding the object; her results are negative. The first phase functions of TNOs were presented by Sheppard and Jewitt, and Rousselot; they observed a phase dependency of the brightness much steeper than expected for icy bodies. Bagnulo obtained the first polarimetric measurements of a TNO – another challenge for the VLT. The phase function (which describes the variation of brightness of the object with the solar phase angle) and the polarimetric characteristics of an object can be interpreted in terms of surface properties. Barucci, De Bergh and Dotto analysed spectra of TNOs, some of them revealing variable surface features on some objects.

Recently, binary TNOs have been discovered. While binary asteroids tend to be formed by a main body and a small satellite, binary TNOs appear as pairs of fairly similar objects. Noll summarized the general properties of these objects, while Kern, Osip and Takato presented physical studies of some pairs.

The surface of TNOs is expected to be composed by a mixture of dust and ices. In order to understand the observations, various groups are performing laboratory experiments involving the irradiation of ices by high energy particles, in order to simulate the effect of cosmic rays on the TNOs. Moore and

Brucato presented the latest results of such work. Cooper and Moroz presented their studies of irradiation of KBO surfaces; Cooper detailed the effects of the various high-energy particles that are expected to affect objects in the outermost parts of the Solar System. This “space weathering” is considered one of the most important processes explaining the diversity of colours observed in TNOs. Levasseur-Regourd has performed other laboratory experiments to study the formation of regoliths in microgravity.

Pluto, the largest TNO, caused some stellar occultations in 2002; these were the first ones observed since 1985 when its atmosphere was discovered. Roques (representing the European team, that was known as the “Pluto Flying Circus” because of its impressive deployment in South America) and Elliot presented the interpretations of these occultations, which demonstrate that the atmosphere of Pluto has significantly changed since 1985. A space mission to Pluto, which has already been cancelled several times for budgetary reasons, is now finally secured (under designation of New Horizon Mission), to be launched in 2006, for a Pluto/Charon fast fly-by around 2015. As it would be frustrating to go that far for only one (pair of) object, astronomers are now looking for suitable TNOs located on the track of the space probe. Unfortunately, these hypothetical candidates are now located in front of the Milky Way, appearing close to the galactic centre. The field crowding makes the discovery of TNOs in these regions very challenging. In the mean time, theoretical studies of that object continue: McKinnon presented models of the interior of Pluto and other large TNOs. The very small TNOs were also considered by Keller, who summarized the physical properties of cometary nuclei.

Future survey projects – including new methods – were discussed: Alcock, Cooray and Roques plan to discover objects by stellar occultations. While such an event is not very probably, observing many stars – or observing for a long time – should lead to many discoveries, leading to some information on the size and distance of the object. This is a very promising way to discover the smallest bodies of the EKB, and the



Panoramic view of the Monturaqui meteoritic crater. Photo by John Davies.

only way to observe comets in the Oort Cloud. Sekiguchi and Stansberry discussed the observations that will be possible with ASTE (the Japanese counterpart to APEX) and SIRTf (resp.). Jewitt presented a very ambitious project, Pan-STARRS, that will be installed on Mauna Kea and scan the whole sky on a weekly basis. This programme, originally targeted at Near Earth Objects, will discover and follow up all TNOs down to mag 24.

Having 70 astronomers in Antofagasta, a trip to the VLT was a must. Bus-loads invaded Paranal on the Saturday following the conference. Finally, on Sunday, 25 brave adventur-

ers went into the deep Atacama Desert, lead by L. Barrera from UCN, in order to inspect the Monturaqui meteoritic crater. This 300-m diameter crater is located South of the large Salar de Atacama, a 6 hours drive from Antofagasta.

Amazingly, none of the participants was lost on the way, which goes against the legend that astronomers cannot be disciplined when needed.

In 1998, a conference on the same topic was held at ESO/Garching. At that meeting, we were confident that we were on the way to understanding the TNO formation, evolution, composition, etc, with the enthusiasm of a field that was only a few years old. The broad

lines were traced, the general picture was in place. The feeling left by this new conference is that we have now enough information to reveal the weaknesses of this general picture, and that even some fundamental questions are still unanswered, such as the reason (or the reality) of a sharp edge terminating the EKB at 45 AU, or the nature of the processes leading to the observed colour distribution.

Finally, during the final discussion session, it was unanimously decided that the branch of science devoted to the study of the TNOs, also designated as Edgeworth-Kuiper belt Object, will be known as EKology.

Fellows at ESO

Stefano Etori



In October 2001, I started my fellowship in ESO, after 6 years spent at IoA in Cambridge (England) doing my PhD and first Post-Doc in the X-ray

Group headed by Andrew Fabian. My area of research is clusters and super-clusters of galaxies, with particular interest on the cosmological implications of their observed properties. To study these objects that are the largest virialized structures in the Universe, I look in the optical (with VLT) and X-ray (through XMM and Chandra) wavebands. These observations allow me to determine densities and temperatures of the hot plasma collapsed in the dark matter halo and to recover the cluster baryonic and gravitational masses. With my collaborators here at ESO, I do this at different redshifts from moderate $z = 0.3$, where the X-ray masses can be directly compared to those obtained from weak lensing analyses, up to 1.2 where few clusters are known through X-ray detection. Of these systems, I have recently used their baryonic mass fraction as cosmological tool to put stringent constraints on the energy constituents of the cosmos.

My duties at ESO are to support the release to the community of the ground based data of the Chandra Deep Field South as part of the Great Observatories Origin Deep Survey (GOODS) project, to represent the Fellows and Students in the Computer Co-ordination Group in Garching and to maintain X-ray software for the few of us that are interested in it.

I am really enjoying my time here: ESO is a perfect place to work both in

terms of hard/software assistance and of motivations, it promotes the interaction with other researchers with several lunch/tea talks, informal discussions and crowded offices (sic!) and is big enough to find anytime the right person to discuss with. For my family and myself, it was a debated question whether to accept this fellowship, but now, and also considering the difficulties in changing social life in a country with such a strange language (still originating from Ur-germanic but nothing to do with English...), we think we made the right choice.

Lisa Germany



Having arrived at ESO Chile in September 2000, I truly feel like one of the veterans of La Silla now. There has been an almost complete turnover of support astronomers since I

arrived, and I have met many of the visiting astronomers on several previous occasions! But this is part of the great thing about working at La Silla - you get to talk to astronomers from all over the world, learn about different areas of astronomy and instrumentation, build collaborations, and make new friends.

I came here straight from my PhD, which I completed at Mount Stromlo Observatory in Canberra, Australia. I was the 3rd person from Stromlo working here at ESO Chile in 2000/2001, and all three of us actually lived in the same house while we were students! I'm one of these Supernova people who, along with the Gamma Ray Burst people, are the bane of visiting astronomers (all those Targets of

Opportunity stealing valuable telescope time). My biggest claim to fame during my PhD is my contribution to the discussion about whether Supernovae and Gamma Ray Bursts are connected.

I am currently investigating the fields around apparently "hostless" supernovae (i.e. supernovae which did not appear to have a host galaxy) to look for faint hosts and, if they exist, investigate their properties. So far, all the supernovae do appear to have hosts, and in one case, we can still see the supernova itself three years after the event! For a supernova to be visible after such a long time is highly unusual, and makes this particular supernova a very interesting object to study – stay tuned for more on that one!

My other main interest is public outreach and taking science to the people. Before starting my PhD I completed a Graduate Diploma in Scientific Communication and have always wanted to pursue this further. To my great joy, ESO is developing an exhibition to go into the science centre here in Santiago, and I am very happy to be part of the team of people working on that.

Linda Schmidtbreick



When I performed my first observations in La Silla in February 1997, I immediately fell in love with the place and decided I wanted to work here someday. In September

2001 after finishing my PhD, working for a year at MPIA Heidelberg, and spending two years as a Postdoc in Padova, I indeed started as an ESO Fellow – with

duty station La Silla, of course. Although the place has sadly changed due to the closing of the smaller telescopes, I still like the work here very much. The team spirit is exceptional, the exchange with the visiting astronomers is very rewarding, and I like the practical and technical work of telescope and instrument maintenance as counterbalance to pure thinking and science.

For the scientific work I find plenty of time when off-duty. I have always been widely interested and hence touched several astronomic topics like interplanetary dust, comets, various types of individual stars, structure of the Milky Way, star formation, and some external galaxies.

More recently, I have focused on the study of the Galactic disc via stellar population analysis, and on Cataclysmic Variables, where I am mainly interested in the accretion process and the outburst mechanisms of the various subclasses. Together with collaborators in Chile and all around Europe, we recently recovered the old nova V840 Oph, which shows an enormously high Carbon content, we followed the dust production during novae outbursts in the sub-mm, and while studying the accretion disc of RR Pic, discovered evidence for a so far unique asymmetric wind.

Since I have originally studied to be-

come a teacher (Maths, Physics, and Philosophy) the educational work is something I miss at ESO. However, I try to propagate science in public talks and articles, I am working in the Museo Interactivo Mirador (Santiago) project (public astronomy exhibition and workshops) and will hopefully manage to give some lectures at Chilean Universities in the near future.

During my free time, I try to express myself in music and painting, I enjoy the great life in Santiago, especially in Nuñoa or Providencia, the part where I live, and you will always find me with a book close by.

Manuela Zoccali



I have been a Fellow at ESO Garching since September 2000. My three years at ESO are about to end, and in September I will start my second postdoc, the Andes Fellowship, at Universidad Catolica in Santiago (Chile) and Princeton University (USA). Before coming to ESO I was in Padova, where I obtained my PhD.

For my thesis I worked on an HST survey of Galactic Globular Clusters cores, looking for rare populations such as blue stragglers and extreme horizontal branch stars, meanwhile testing stellar evolution models. I also worked on the determination of the Initial Mass Function, and in the problem of absolute and relative GC ages obviously connected with the measure of distances. More recently I moved towards the study of the Galactic bulge, where I determined the stellar Initial Mass Function down to 0.15 solar masses: a power-law with an exponent significantly flatter than Salpeter. With extensive near-IR and optical photometry I recently set new constraints on both the age and metallicity distribution of the bulge.

Working at ESO also gave me the privilege to work for a new instrument: the VLT fibre spectrograph FLAMES. Joining the FLAMES team and sharing the excitement for its success has been fun. It also motivated me to move into high resolution spectroscopy, which, I believe, is going to represent the key tool for our understanding of resolved stellar populations.

In my little spare time I like to play guitar, and dream about living by the sea: swimming, scuba-diving, sailing and windsurfing, all the hobbies that I've been neglecting too much in the last years.

High Honour to Ray Wilson

RICHARD WEST, ESO

During a ceremony at the ESO Headquarters in Garching in the afternoon of 28 February 2003, the Order of the French Legion of Honour was bestowed upon Dr. Raymond N. Wilson, ESO staff member from 1972-1993.

The decoration was made by Professor Charles Fehrenbach, member of the French Académie des Sciences and Honorary Director of the Observatoire de Haute-Provence.

On behalf of the French government, the Acting French Consul in Munich, Mrs Annie Mari, presented Dr. Wilson with the official scroll. Other speeches were given by Dr. Catherine Cesarsky and Professor Lodewijk Woltjer, present

and former Director General of ESO. Many of Ray Wilson's friends and colleagues from the optical and astronomical communities in France and at ESO also witnessed the ceremony.

In his presentation, Professor Fehrenbach emphasised the enormous impact of the Active Optics concept on current astronomy and astrophysics – a fundamental invention made by Ray Wilson and his team at ESO in the 1980's and first implemented with great success in the 3.5-m ESO New Technology Telescope. This concept paved the way towards larger telescope mirrors, effectively overcoming century-old size and weight limitations. Most of the world's giant telescopes including ESO's own unique Very Large Telescope are based on this revolutionary concept.

Expressing words of thanks, Ray Wilson explained how this innovation was the most visible result of a long, productive and inspiring collaboration with many colleagues, es-



Dr. Wilson (left) receives his honour from Prof. Fehrenbach.



From left to right: Prof. L. Woltjer, Dr. C. Cesarsky, Dr. R. Wilson, Mrs. A. Mari and Prof. Fehrenbach.

pecially in the ESO Optics Group. It was a great reward for him to witness the unequalled success of the VLT and to sense the daring visions for new and powerful facilities now taking shape within ESO and elsewhere in the world. An article by Ray Wilson on these developments will appear in the September issue of *The Messenger*.

The May 7 Mercury Transit

H. BOFFIN and R. WEST, ESO

On May 7, 2003, the planet Mercury passed in front of the Sun. This transit, that occurs approximately once every 7 years, was visible from Europe, Africa and Asia and lasted more than five hours. European observers were particularly at their advantage to follow the event as the Sun was relatively high in the sky during the entire transit. And, luckily, the weather did cooperate over most of Europe.

On this occasion, ESO, in collaboration with the European Association for Astronomy Education (EAAE), the Institut de Mécanique Céleste et de Calcul des Éphémérides (IMCCE) and the Observatoire de Paris in France, set up a comprehensive web site which provided detailed information about the

event itself and also a lot of useful background information, including special sheets for students and teachers in no less than 12 languages. In addition, a live webcast was held with live images and a running commentary. Images obtained at observatories in Belgium, the Czech Republic, Denmark, Hungary, Italy and Spain were shown.

Astronomers at ESO weren't of course going to miss this opportunity and several telescopes were set-up. In particular, a Meade LX200 equipped with a solar filter, a Barlow lens and a Nikon D-100 camera was used as a "webcam" to provide live images on the web.

The event was very successful as shown by the load on the ESO website which reached an all-time record of

about 10,000 hits per minute! Many visitors therefore needed a little patience to see the images. On May 7, the ESO website experienced a total of about 3.5 million hits and about 50 Gigabytes of data, mostly images, were delivered. The great majority of these were from the "Mercury Transit" pages.

The May 7 transit of Mercury was a fine "prelude" to the much more rare event next year when, on June 8, 2004, the planet Venus will pass in front of the Sun. On this occasion, ESO plans to launch, with its educational partners, a major public programme that will allow all interested persons to participate actively.

More information can be found on <http://www.eso.org/outreach/eduoff/vt-2004/>.

ANNOUNCEMENTS

ESO Fellowship Programme 2003/2004

The European Southern Observatory awards several postdoctoral fellowships to provide young scientists opportunities and facilities to enhance their research programmes. Its goal is to bring them into close contact with the instruments, activities, and people at one of the world's foremost observatories. For more information about ESO's astronomical research activities please consult <http://www.eso.org/science/>

Fellows have ample opportunities for scientific collaborations. A list of the ESO staff and fellows, and their research interest can be found at <http://www.eso.org/science/sci-pers.html> and <http://www.sc.eso.org/santiago/science/person.html>. The ESO Headquarters in Munich, Germany host the Space Telescope European Coordinating Facility and are situated in the immediate neighbourhood of the Max-Planck-Institutes for Astrophysics and for Extraterrestrial Physics and are only a few kilometers away from the Observatory of the Ludwig-Maximilian University. In Chile, fellows have the opportunity to collaborate with the rapidly expanding Chilean astronomical community in a growing partnership between ESO and the host country's academic community.

In **Garching**, fellows spend beside their personal research up to 25% of their time on support or development activities of their choice in the area of e.g. instrumentation, user support, archive, VLT, ALMA, public relations or science operations at the Paranal Observatory. Fellowships in Garching start with an initial contract of one year followed by a two-year extension.

In **Chile**, the fellowships are granted for one year initially with an extension of three additional years. During the first three years, the fellows are assigned to either the Paranal or La Silla operations groups. They support the astronomers in charge of operational tasks at a level of 50% of their time (split into 80 nights per year on the mountain and 35 days per year at the Santiago Office). During the fourth year there is no functional work and several options are provided. The fellow may be hosted by a Chilean institution and will thus be eligible to apply for Chilean observing time on all telescopes in Chile. The other options are to spend the fourth year either at ESO's Astronomy Center in Santiago, Chile, or the ESO Headquarters in Garching, or any institute of astronomy/astrophysics in an ESO member state.

We offer an attractive remuneration package including a competitive salary (tax-free), comprehensive social benefits, and provide financial support in relocating families. Furthermore, an expatriation allowance as well as some other allowances may be added. The Outline of the Terms of Service for Fellows at <http://www.eso.org/gen-fac/adm/pers/fellows.html> provides some more details on employment conditions/benefits.

Candidates will be notified of the results of the selection process in December 2003/January 2004. Fellowships begin between April and October of the year in which they are awarded. Selected fellows can join ESO only after having completed their doctorate.

The closing date for applications is October 15, 2003.

Please apply by:

- filling the form available at <http://www.eso.org/gen-fac/adm/pers/forms/fellow03-form.pdf>
- and attaching to your application:
 - a Curriculum Vitae including a publication list (the latter split into refereed and non-refereed articles, please)
 - a summary of the current and thesis work (max. 1 page)
 - an outline of the research plans if you came to ESO (specify which facilities you foresee to use, whose interest might overlap with yours and what is your motivation to come to ESO (max. 2 pages)
 - an outline of your technical/observational experience (max 1 page)
 - three letters of reference from persons familiar with your scientific work.

All documents should be typed and in English.

The application material has to be addressed to:

European Southern Observatory
Fellowship Programme
Karl-Schwarzschild-Str. 2, 85748 Garching bei München, Germany
vacancy@eso.org

Contact person: Angelika Beller, Tel. +49 89 320 06-553, Fax +49 89 320 06-490, e-mail: abeller@eso.org

All material, including the recommendation letters, must reach ESO by the deadline (October 15); applications arriving after the deadline or incomplete applications will not be considered!

Call for Proposals for a Third Generation Instrument for the NTT

Introduction

The scientific mission of the La Silla Observatory is periodically reviewed (typically every 3 years) by special *ad-hoc* Committees, appointed by the ESO Director General and composed of members of the User's Committee (UC), the Scientific Technical Committee (STC), and ESO staff. The reports of these Committees have been presented to STC and Council and used in planning the long range strategy of ESO. The three successive La Silla Committee reports (LS2000, LS2000+, and LS2006+) have been widely distributed in the community, and one of them (LS2000+) is available on-line through the ESO web site (www.eso.org).

One of the key recommendations of the LS2006+ Committee (chaired by A. Cimatti of Arcetri Observatory) was to quickly replace one of the existing instruments at the NTT by a next generation one, in order to keep the telescope facility fully competitive beyond 2006. Present instruments in operation at the NTT are: 1) EMMI, a multi-mode spectro-imager in the Visible domain, installed in 1990; 2) SUSI, the SUpber-Seeing Imager installed in 1991 and upgraded to SUSI2 in 1998 and 3) SOFI—Son OF Isaac—a near-IR spectro-imager, which originated as an early spin-off from the development of ISAAC for the VLT and was put into operation also in 1998.

Five years into VLT operations and after 15 years of successful NTT operations, it is indeed timely—as proposed by the LS2006+ Committee and recommended by the STC—to reassess the scientific mission of the existing NTT instrumentation and how it could be partly or totally replaced with a new instrument and/or with easy access to a visitor focus. Any new instrument would have to physically replace either SOFI/SUSI or EMMI. It should offer to the community an end to end observing capability at the frontier of present astrophysical research, taking into account the medium size and ex-

cellent quality of the telescope and the superb observing conditions at La Silla. It should complement the VLT and other future facilities (VST, VISTA, ALMA), provide unique scientific results in its own merit and address the needs of a significant segment of the community. On the technical side, ESO would favor an instrument easy to operate and with a reasonable cost.

This Call is addressed to all past or potential users of the ESO telescopes. Any astronomer working in an ESO member country (including ESO staff) is warmly invited to provide his/her input. This can be in the form of a recommendation on how to proceed or as a formal letter of intent expressing the interest in developing a new instrument, as spelled out in the next two sections.

Survey on the observing modes to be offered at the NTT

ESO is interested in your properly justified view on these specific points:

(a) Which among the existing NTT instruments will be mostly needed beyond 2006 and with what mode(s);

(b) Which observing mode(s) currently not offered at the NTT would be most interesting to complement the VLT capabilities and make unique science.

(c) Whether an NTT focus for visitor instruments should be given high priority

Please add any other consideration relevant for the choice of future NTT instrumentation. In particular, you may comment on the need for a new general use capability or instead on some new facility dedicated for a large fraction of NTT time to a specific and challenging scientific goal (like the extensive exo-planet search with HARPS at the 3.6 m).

Your contribution should be sent by email to epompei@eso.org and sdodoric@eso.org.

As Subject, please enter: Survey on fu-

ture observing modes with the ESO NTT.

Deadline: August 31st, 2003

Intent to submit a proposal to build a new instrument for the NTT

ESO solicits proposals to build a new instrument for the NTT from Institutes or groups of Institutes. The project could be developed in collaboration with ESO, and in particular with the La Silla Observatory. The framework would be the one used in other VLT or La Silla collaborative projects, where the contribution by an external Consortium in manpower and/or cash is rewarded with guaranteed observing time.

In this case, the PI should forward (1) a conceptual description of the instrument he/she is proposing and of its scientific drivers and operating model; (2) the main Institute(s) which are expected to be associated to the project and the preliminary endorsement by the Director of the leading Institute and (3) the contribution expected from ESO.

For technical information on the NTT, please contact Emanuela Pompei (epompei@eso.org) at La Silla Observatory.

The above expression of intent should be forwarded by e-mail to gmonnet@eso.org and to jmelnick@eso.org. As Subject, please enter: Proposal to build an instrument for the ESO NTT.

The e-mails should be timely followed by a formal Letter of Intent addressed to:

Head Instrumentation Division
Attention: G. Monnet
Subject: New NTT Instrument
European Southern Observatory
K. Schwarzschild Str. 2
D- 85748 Garching b. München

E-mail deadline: August 31st, 2003

The proposals will be technically and managerially assessed by ESO and presented to the STC in October 2003 for a recommendation, together with the results of the survey in the community.

Kurt Kjär retires from ESO



After a long and dedicated service to ESO, Kurt Kjär is retiring from the post of Technical Editor which he has held during an unprecedented period of almost 30 years.

From the beginning, ESO has profited enormously from his solid technical expertise and thoroughness, great sense for form and content and, not least, impressive knowledge of languages. He has been deeply involved in and has put his personal stamp of quality on hundreds of ESO publications at all levels and scopes, ranging from the Annual Report, the ESO Messenger, ESO conference proceedings and scientific preprints to technical reports and brochures, etc. Much time and many resources have been saved thanks to his profound knowledge and enormous ex-

perience, especially visible during the all too frequent hectic periods to meet imposed deadlines. The European astronomical community has witnessed the steady progress of the ESO Messenger from the first thin issue in 1974 to the current, very comprehensive ones. This would not have been possible without a close and friendly, highly effective collaboration between Kurt Kjär and the various Messenger editors. As one of these, I am happy to testify here to the fantastic stimulus and help it has been to work with a person like Kurt. We are all deeply thankful to him.

Kurt Kjär will retire to live with his wife in Oberschleissheim, a few kilometres from the ESO Headquarters.

Richard West

The Instrumentation Division at the ESO Headquarters in Garching near Munich, Germany, offers the following job opportunity:

Head of the Instrumentation Division Career Path: VII

Assignment: The Head of the Instrumentation Division directs all ESO-activities pertaining to optical and infrared astronomical instrumentation and reports directly to the Director General. As a member of the ESO Management, the Head of Division contributes directly to the development of the overall policy, strategic planning and maintains professional contacts at highest level outside the Organisation. The Instrumentation Division consists of about 30 astronomers, physicists and engineers, who work in groups or teams developing infrared and optical instruments and detectors. They also receive extensive support from the ESO Technical Division e.g. in the areas of optical design, electronics hardware and software. The main tasks of the Division are:

- to develop, test and install state-of-the-art instruments, for both in-house projects and those involving collaborations with consortia of external suppliers or institutes;
- to support in the maintenance and upgrading of the instruments at the Observatories;
- to conduct a future advanced instrumentation programme through design studies, preparation of proposals, development and testing of critical components and subsystems.

As a Senior Astronomer the Head of the Instrumentation Division is a member of the ESO Science Faculty and is expected and encouraged to conduct active astronomical research.

Qualifications and Experience: Basic requirements for the position include a PhD in astronomy, astrophysics or physics or related fields, a proven record of scientific leadership, experience in international scientific collaborations and at least 10 years' experience in the design and use of astronomical instrumentation. Substantial management and leadership experience within a scientific organisation, preferably international, is required. Excellent communication skills and a very good knowledge of English are essential.

Duty station: Garching near Munich, Germany, with regular duty travels to Chile.

Starting date: as soon as possible

Remuneration and Contract: We offer an attractive remuneration package including a competitive salary (tax-free), comprehensive social benefits and financial help in relocating your family. The initial contract is for a period of three years with the possibility of a fixed-term extension. Serious consideration will be given to outstanding candidates willing to be seconded to ESO on extended leaves from their home institutions. Either the title or the grade may be subject to change according to qualification and the number of years of experience.

Application: If you are interested in working in a stimulating international research environment and in areas of frontline science and technology, please send us your CV (in English) **before 31 July 2003**

All applications should include the names of four individuals willing to give professional references.

For further information, please contact Mr. Roland Block, Head of Personnel Department, Tel +49 89 320 06 589, e-mail: rblock@eso.org. You are also strongly encouraged to consult the ESO Home Page (<http://www.eso.org>).

Although preference will be given to nationals of the Member States of ESO: Belgium, Denmark, France, Germany, Italy, The Netherlands, Portugal, Sweden, Switzerland and United Kingdom, no nationality is *a priori* excluded. The post is equally open to suitably qualified male and female applicants.

PERSONNEL MOVEMENTS

International Staff

(1 March – 31 May 2003)

ARRIVALS

EUROPE

ACCARDO, Matteo (I), Mechanics Technician
BOFFIN, Henri (B), Editor
BRAST, Roland (D), Electrical Engineer/Senior Technician
LUNDIN, Lars Kristian (DK), Data Analysis Specialist/Software Engineer
LYNAM, Paul (GB), Associate
MACKOWIAK, Bernhard (D), Associate
MEUSS, Holger (D), ALMA Archive Software Developer
NASS, Petra (D), Operations Support Scientist
NYLUND, Matti (S), Software Engineer
OBERTI, Sylvain (F), Assembly Integration and Testing Engineer
PUECH, Florence (F), VLT System Engineer
SCHILLING, Markus (D), ALMA Software Developer
SCHUHLER, Nicolas (F), Student
VOIRON, Samuel (F), Student

CHILE

DEL BURGO, Stephan (F), Optical Engineer
DEPAGNE, Eric (F), Fellow
GONCALVES, Nelson (P), Associate
JEHIN, Emmanuel (B), Operations Staff Astronomer
RANTAKYRÖ, Fredrik (S), VLT Astronomer

DEPARTURES

EUROPE

ALEXOV, Anastasia (USA), Science Data Analyst/Programmer

BRYNNEL, Joar (S), Electronic Engineer
CIASTO, Hubert (D), Senior Administrative Assistant
GALLIANO, Emmanuel (F), Student
HATZIMINAOGLOU, Evanthia (GR), Associate
HOFFMANN-REMY, Martin (D), Internal Auditor
KJÄR, Kurt (D), Technical Editor
MAINIERI, Vincenzo (I), Student
PIRZKAL, Norbert (F), Science Systems Analyst/Programmer

CHILE

FAURE, Cécile (F), Student
WOODS, Paul (GB), Student

Local Staff

(1 February 2003 – 31 May 2003)

ARRIVALS

ARANDA CONTRERAS, Ivan, Archival Technician
CID FUENTES, Claudia, Telescope Instrument Operator
CORTES CARVALLO, Angela, Telescope Instrument Operator
DONOSO MARIN, Reinaldo, Maintenance Mechanical Technician
GUAJARDO OBANDO, Patricia, Telescope Instrument Operator
SANZANA ROJAS, Lilian, Software Engineer

DEPARTURES

AMESTICA VALENZUELA, Rodrigo, Joint Software Group Leader
BAEZA ARAYA, Silvia, Software Engineer Developer
BARRIGA CAMPINO, Pablo, Instrumentation Engineer

ESO, the European Southern Observatory, was created in 1962 to "... establish and operate an astronomical observatory in the southern hemisphere, equipped with powerful instruments, with the aim of furthering and organising collaboration in astronomy..." It is supported by ten countries: Belgium, Denmark, France, Germany, Italy, the Netherlands, Portugal, Sweden, Switzerland and the United Kingdom. ESO operates at two sites in the Atacama desert region of Chile. The new Very Large Telescope (VLT), the largest in the world, is located on Paranal, a 2,600 m high mountain approximately 130 km south of Antofagasta, in the driest part of the Atacama desert where the conditions are excellent for astronomical observations. The VLT consists of four 8.2-metre diameter telescopes. These telescopes can be used separately, or in combination as a giant interferometer (VLTI). At La Silla, 600 km north of Santiago de Chile at 2,400 m altitude, ESO operates several optical telescopes with diameters up to 3.6 m and a submillimetre radio telescope (SEST). Over 1300 proposals are made each year for the use of the ESO telescopes. The ESO headquarters are located in Garching, near Munich, Germany. This is the scientific, technical and administrative centre of ESO where technical development programmes are carried out to provide the Paranal and La Silla observatories with the most advanced instruments. There are also extensive astronomical data facilities. ESO employs about 320 international staff members, Fellows and Associates in Europe and Chile, and about 160 local staff members in Chile.

The ESO MESSENGER is published four times a year: normally in March, June, September and December. ESO also publishes Conference Proceedings, Preprints, Technical Notes and other material connected to its activities. Press Releases inform the media about particular events. For further information, contact the ESO Education and Public Relations Department at the following address:

EUROPEAN
SOUTHERN OBSERVATORY
Karl-Schwarzschild-Str. 2
D-85748 Garching bei München
Germany
Tel. (089) 320 06-0
Telefax (089) 3202362
ips@eso.org (internet)
URL: <http://www.eso.org>
<http://www.eso.org/gen-fac/pubs/messenger/>

The ESO Messenger:
Editor: Peter Shaver
Technical editor: Henri Boffin

Printed by
Universitätsdruckerei
WOLF & SOHN
Heidemannstr. 166
D-80939 München
Germany

ISSN 0722-6691

ESO Workshop on Large Programmes and Surveys

S. WAGNER (OPC) and B. LEIBUNDGUT (ESO)

On 19 to 21 May, 2003, the scientific impact of Large Programmes was assessed at a workshop in Garching. Several members of the OPC and STC actively participated in the workshop.

Every PI of a Large Programme (LP) approved up to ESO Period 69 was invited to present the results of their project. All LPs but one were presented in half-hour talks. A two-hour discussion session was held to assess whether the current scheme of LPs is adequate or should be adjusted.

The general impression was that most LPs have produced excellent results and unique science, which would have been unachievable through regular programmes. They allowed European astronomers to directly compete with the best American groups, some of whom profit from significant access to large telescopes. The LPs have

had the effect of unifying the community in certain astronomical fields.

The effectiveness of the restriction of LPs to two years duration was cited as a good incentive to produce important results quickly, one major reason to originally introduce the LPs.

Overall the LPs are considered a success and should be continued. They provide European astronomers with the opportunity to achieve important results in a competitive and timely fashion.

The OPC discussed the outcome of the workshop at its meeting on June 2 and decided to continue with Large Programmes with P73. ESO will accept Large Programmes for this period again.

An article on the workshop providing more details will appear in the next issue of *The Messenger*.

Contents

TELESCOPES AND INSTRUMENTATION

C. Cesarsky: Progress with the Atacama Large Millimeter Array	2
F. Primas: The Science Verification of FLAMES	3
R. Arsenault et al.: MACAO-VLTI First Light: Adaptive Optics at the Service of Interferometry	7
Ch. Leinert et al.: MIDI Combines Light from the VLT: the Start of 10 μ m Interferometry at ESO	13
L. Germany: News from La Silla	18

REPORTS FROM OBSERVERS

G. Rudnick et al.: Studying High Redshift Galaxy Clusters with the ESO Distant Cluster Survey	19
R. Napiwotzki et al.: SPY — The ESO Supernovae Type Ia Progenitor Survey	25
R.G. Gratton et al.: Abundances in Globular Cluster Dwarfs	31
M. Arnaboldi et al.: Intracluster Planetary Nebulae in the Virgo Cluster: Tracers of Diffuse Light	37
F. Barrientos et al.: The Red-Sequence Cluster Survey	40
M. Rejkuba et al.: Long Period Variables in the Giant Elliptical Galaxy NGC 5128: the Mira P-L Relation at 4 Mpc	43
H. Dejonghe et al.: The Dynamics of Dwarf Elliptical Galaxies	47

OTHER ASTRONOMICAL NEWS

U. Grothkopf: From Books to Bytes: Changes in the ESO Libraries over the Past Decade	51
O. Hainaut: International Workshop on "First Decadal Review of the Edgeworth-Kuiper Belt: Toward New Frontiers"	53
Fellows at ESO: Stefano Etori, Lisa Germany, Linda Schmidtobreick and Manuela Zoccali	55
R. West: High Honour to Ray Wilson	56
H. Boffin and R. West: The May 7 Mercury Transit	57

ANNOUNCEMENTS

ESO Fellowship Programme 2003/2004	57
Call for Proposals for a Third Generation Instrument for the NTT	58
R. West: Kurt Kjær retires from ESO	58
ESO Vacancy: Head of the Instrumentation Division	59
Personnel Movements	59
ESO Workshop on Large Programmes and Surveys	60